

3.4 Cooperative Phenomena in Complex Macroscopic Systems

Tensor-network-based methods and their application to discrete lattice models

Naoki KAWASHIMA

Institute for Solid State Physics,

The University of Tokyo, Kashiwa-no-ha, Kashiwa, Chiba 277-8581

Tensor network (TN) is a useful concept in various fields, not only in the condensed matter theory, but also in data science and machine learning. Even in the condensed matter theory alone, the application of the TN concept is multi-fold. In variational principles calculation, the TN is used as a new type of variational wave function. In the real-space renormalization group (RG) theory, it serves as a natural representation of a renormalized system. In the pure mathematical physics, it is used as a new language for discussing the topological nature of the quantum states. In SY2019, we developed new algorithms for general TN-based computation [1], the boundary conformal-field theory [2,3], the classical dynamics [4], and variational optimization of topological quantum states. [5,6]

In [1], we proposed a new method for obtaining an efficient representation of a many-ranked tensor in terms of a ring network of smaller-ranked tensors. This kind of operations is vital both in TN application to the real space renormalization group and in data science. The central technical problem here is, how to avoid

the local-minima-trapping due to the formation of redundant entanglement loops. Our benchmark showed that the new method efficiently removes such loops when the target tensor has, at least approximately, the structure of the corner double line tensor, which is typical in TN-based RG calculations.

In [2,3], we developed the tensor renormalization group (TRG) algorithm for statistical systems with open boundaries. This allows us to investigate properties of boundary operators. We applied the method to several two-dimensional classical spin models with open boundaries. The boundary conformal spectrum was obtained and turned out consistent with the underlying boundary conformal field theories (BCFTs) for the Ising, tricritical Ising, and three-state Potts models.

In [4], we developed a method for tracing the time-evolution of the probability distribution function of a given dynamical systems, which is otherwise difficult. We studied (1+1)-dimensional directed percolation, a canonical model of a nonequilibrium continuous transition. We find a universal relaxation of Rényi entropy at the absorbing

transition point. We also detected a singularity in the "entanglement entropy" in the active (i.e., non-absorbing) phase. Although the absorbing states is exponentially rare in this phase, its rare appearance causes this singularity.

In [5], we studied the Kitaev model by the TN representation. We proposed a new wave function that is extremely simple in the TN representation but still shares many essential properties with the ground state of the Kitaev model, such as the quasi-long-range correlation, the short-range magnetic correlation, the flux-free property, the Z_2 gauge structure, and the 2D Ising universality. We call this state the "loop gas state" because of its mathematical equivalence to the loop gas model, one of the standard and solvable statistical physical models. We showed that the loop gas state is adiabatically connected to the ground state of the Kitaev model, indicating a similar role to the AKLT state for the $S=1$ AFH chain.

Later we extended our method to several other models: $S=1$ Kitaev model [6], and Kitaev-Gamma model [7,8]. In particular, in [8], we studied field-induced quantum phases in theoretical models of the Kitaev magnets, such as α - RuCl_3 for which the half quantized thermal Hall conductivity was discovered. Our TN calculation suggested that a field-induced

phase appears between the low field zig-zag magnetic order and the high field polarized state. We found that the chiral Kitaev spin liquid occupies an area in the phase diagram, smaller than predicted by other groups.

References

- [1] Hyun-Yong Lee and Naoki Kawashima: J. Phys. Soc. Jpn. **89**, 054003 (2020)
- [2] Shumpei Iino, Satoshi Morita, and Naoki Kawashima: Phys. Rev. B **101**, 155418 (2020)
- [3] Shumpei Iino, Satoshi Morita, and Naoki Kawashima: Phys. Rev. B **100**, 035449 (2019)
- [4] Kenji Harada and Naoki Kawashima: Phys. Rev. Lett. **123**, 090601 (2019)
- [5] Hyun-Yong Lee, Ryui Kaneko, Tsuyoshi Okubo, and Naoki Kawashima: Phys. Rev. Lett. **123**, 087203 (2019)
- [6] Hyun-Yong Lee, Naoki Kawashima, and Yong Baek Kim: arXiv:1911.07714
- [7] Hyun-Yong Lee, Ryui Kaneko, Tsuyoshi Okubo, Naoki Kawashima: Phys. Rev. B **101**, 035140 (2020)
- [8] Hyun-Yong Lee, Ryui Kaneko, Li Ern Chern, Tsuyoshi Okubo, Youhei Yamaji, Naoki Kawashima and Yong Baek Kim: Nature Communications **11**, 1639 (2020)

Kármán-Vortex Cavitation Around Circular-Cylinder Arrays

Yuta ASANO¹, Hiroshi WATANABE^{1,2}, and Hiroshi NOGUCHI¹

¹ *Institute for Solid State Physics, University of Tokyo,
Kashiwa-no-ha, Kashiwa, Chiba 277-8581, Japan*

² *Department of Applied Physics and Physico-Informatics, Keio University,
Yokohama, Kanagawa 223-8522, Japan*

Cavitation is a flow phenomenon accompanied by the formation, growth, and collapse of bubbles caused by local pressure changes in a liquid with the high flow velocity. Since cavitation has adverse effects on fluid machinery such as performance degradation, vibration and noise, and erosion, the elucidation of its mechanism is of great engineering importance. The cavitation inception is thought to be caused by the growth of small bubble nuclei in a low-pressure region for enough time to grow [1]. However, since it is extremely difficult to discuss the dynamics of microscopic bubble nuclei in a macroscopic flow field, the mechanism of cavitation generation is not well understood. In addition, because the phase transition has to be directly discussed in the flow field, it is extremely difficult to analyze the cavitation inception of the liquid in which no bubble nuclei are contained as in the case of flow in hydraulic machines.

In the present study, molecular dynamics (MD) calculations are performed to analyze cavitation around periodically aligned cylinders, and the formation and growth processes of

bubbles and their effects on the surrounding flow are investigated by MD calculations [2].

3-dimensional MD simulation is carried out to analyze the flow around the periodically aligned cylinders. The Lennard-Jones (LJ) interaction is used for the interaction between the fluid particles. The cylinder is modeled by fixing LJ particles on its surface. Periodic boundary conditions are used for all directions in the system, and two cylinders are arranged perpendicular to the flow to represent an infinite row of cylinders. In this way, interference of the vortices behind the upper and lower cylinders can be taken into account. The temperature and velocity are controlled by the Langevin heat bath at the downstream side of the cylinder. Fluids in the supercritical region are inflow. Cavitation is generated by a decrease in the local temperature of the inflow fluid.

Figure 1 shows a snapshot of the density (left panels) and vorticity (right panels) fields. At high temperature (temperature $T=2$), there are no bubbles and therefore non-cavitating flow is obtained. An anti-phase synchronized Kármán

vortex is generated behind the cylinder. It is also found that this synchronization amplifies the vibrations acting on the cylinder. At the lower temperature, $T=1.3$, bubbles are generated in conjunction with the shedding cycle of the Kármán vortex. The Kármán vortex remains synchronized in the anti-phase as in the non-cavitating flow. At $T=1.25$, a gas-phase region is formed behind the cylinder and the distance to the formation of the Kármán vortices increases. The phase of the Kármán vortices is slightly disturbed. As the temperature is further reduced to $T=1.2$, the gas-phase region behind the cylinder is further expanded and the upper and lower Kármán vortices become asymmetric. It is also found that this asymmetric structure is switched by a long period of time. In Newtonian fluids in which no phase transitions occur, no such

changes occur due to temperature changes.

The change in the vortex structure should change the characteristics of the vibrations excited by the vortex. It is found that the bubbles generated near the cylinder inhibit the propagation of the vibration associated with the ejection of the vortex, and the vibration amplitude decreases and eventually disappears.

In summary, the analysis from the molecular scale reveals that bubbles generated near the cylinder significantly change the properties of the lift and flow fields.

References

- [1] C. E. Brennen, *Cavitation and Bubble Dynamics* (Oxford University Press, 1995).
- [2] Y. Asano, H. Watanabe, and H. Noguchi: *J. Chem. Phys.* 152 (2020) 034501.

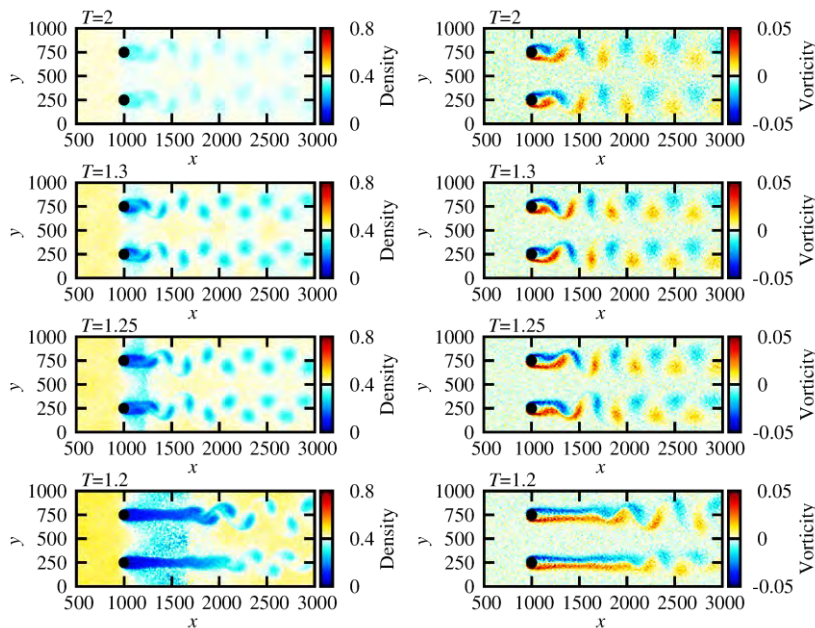


Figure 1: Snapshots of density (left panels) and vorticity (right panels) fields of LJ fluid. The black circles in the figure represent cylinders.

Detachment of fluid membrane from substrate by protein adhesion

Hiroshi NOGUCHI

Institute for Solid State Physics, University of Tokyo, Kashiwa, Chiba 277-8581

Lipid membranes supported on a solid substrate are considered as a model system for biological membranes and are extensively used to study protein functions and membrane properties. Recently, the membrane detachment from the substrate was reported by the adhesion of Ca^{2+} -dependent membrane-binding proteins annexin. The membrane rolling and blebbing have been observed. To understand the mechanism to form these membrane structures, we have performed meshless membrane simulations with the isotropic spontaneous curvatures. We focus on the generation of the spontaneous curvature by the protein adhesion here.

Before considering the detachment from the substrate, we investigated the closing transition from a membrane patch to a vesicle at a finite spontaneous curvature [1]. We have determined the theoretical condition of the closure and proposed the estimation method of the membrane Gaussian modulus from the curvature of the membrane patch.

Next, we added the attraction to a solid substrate by the Lennard-Jones potential. When a high curvature C_0 is imposed, a membrane disk is detached from the substrate, and vesicles are formed [see Fig. 1] [2]. The membrane edge is rolled up, and the edge undulation expands leading to the vesicle formation. The average vesicle size is several times larger than the minimum vesicle size formed by the membrane closure of a cup-shaped membrane patch.

With strong adhesion, the competition between the bending and adhesion energies determines the minimum value of the spontaneous curvature for the detachment. In contrast, with weak adhesion, a detachment occurs at smaller spontaneous curvatures due

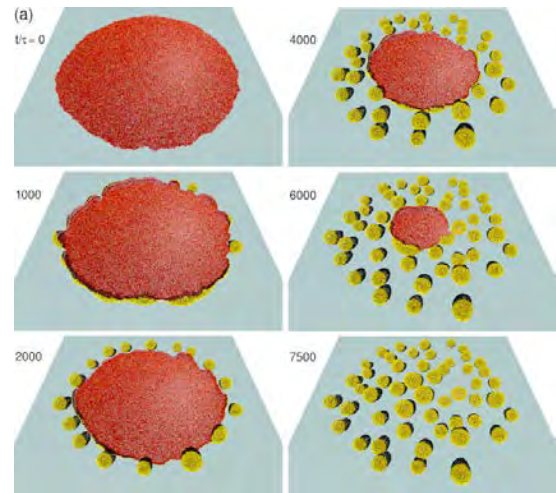


Figure 1: Sequential snapshots of the detachment and vesiculation of the disk-shaped membrane from a solid substrate.

to the membrane thermal undulation. When parts of the membrane are pinned on the substrate, the detachment becomes slower, and a remained membrane patch forms straight or concave membrane edges. The edge undulation induces vesiculation of long strips and disk-shaped patches. Therefore, membrane rolling is obtained only for membrane strips shorter than the wavelength for deformation into unduloid. This suggests that the rolling observed for the annexins A3, A4, A5, and A13, results from by the anisotropic spontaneous curvature induced by the proteins.

References

- [1] H. Noguchi: *J. Chem. Phys.* **51**, 094903 (2019).
- [2] H. Noguchi: *Soft Matter* **15**, 8741 (2019).

Brittle structure of semicrystalline polymers by large-scale coarse-grained molecular dynamics simulation

Yuji HIGUCHI

*Institute for Solid State Physics, University of Tokyo
Kashiwa-no-ha, Kashiwa, Chiba 277-8581*

We have studied mechanical properties of semicrystalline polymers [1, 2, 3] and double-network gels [4] via coarse-grained molecular dynamics simulations. Understanding the fracture process of the semicrystalline polymers at the molecular level is essential to increase its toughness against the stretching. This year, void formation and growth processes in the fracture process of semicrystalline polymers were studied on System B.

Figure 1 shows the fracture process of the lamellar structure consisting of 1.5×10^7 monomers. The lamellar structure consists of amorphous and crystalline layers. Voids are generated in amorphous layers, and then they grow parallel to the stretching direction cylindrically. This process is different from those in elastomers and glassy polymers. The void structures during their growth process at the molecular level are still debatable in experiments. The maximum length of voids along x , y , and z -directions are monitored during the stretching. At first, the maximum length of voids in x and y -directions, which are perpendicular to the stretching direction, is larger than that in z -direction, which is parallel to the stretching direction. Then, the length in z -direction becomes larger than those in x and y -directions. This result is consistent with that observed in the experiment [5]. Thus, the void generation and growth processes in the lamellar structure of crystalline polymers at the molecular level are successfully revealed.

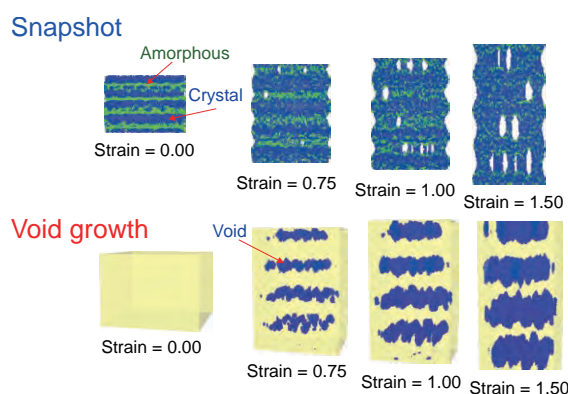


Figure 1: The deformation and fracture process of the lamellar structure. (a) Snapshot and (b) void generation and growth processes.

References

- [1] Y. Higuchi and M. Kubo: *Macromolecules* **50** (2017) 3690.
- [2] Y. Higuchi: *Polym. J.* **50** (2018) 579.
- [3] Y. Higuchi: *Macromolecules* **52** (2019) 6201.
- [4] Y. Higuchi, K. Saito, T. Sakai, J. P. Gong, and M. Kubo: *Macromolecules* **51** (2018) 3075.
- [5] S. Humbert, O. Lame, J. M. Chenal, C. Rochas, and G. Vigier: *Macromolecules* **43** (2010) 7212.

Topological Magnetization Plateau of Quantum Antiferromagnetic Spin Chain with Anisotropies

Tôru SAKAI^{1,2}, Hiroki NAKANO^{1,2}, and Tokuro SHIMOKAWA³,

¹*Graduate School of Material Science, University of Hyogo,
Kouto, Kamigori, Hyogo 678-1297, Japan*

²*Synchrotron Radiation Research Center, Kansai Photon Science Institute,
Quantum Beam Science Research Directorate,
National Institute for Quantum and Radiological Science and Technology (QST)
SPring-8, Kouto, Sayo, Hyogo 679-5148, Japan*

³*Okinawa Institute of Science and Technology Graduate University, Onna,
Okinawa 904-0945, Japan*

The symmetry protected topological phase[1, 2] is one of interesting topics in the strongly correlated electron systems. The recent study[3, 4] using the numerical diagonalization of finite-size clusters and the level spectroscopy analysis revealed that the symmetry protected topological phase appears in the $S = 2$ antiferromagnetic chain with the single-ion anisotropy D and the coupling anisotropy Δ . However, the region of this phase is quite small in the ground state phase diagram. Thus it would be difficult to discover in some real experiments. In the present study we focused on the symmetry protected topological phase in the magnetization plateau of the $S = 2$ antiferromagnetic chain, using the same numerical diagonalization and level spectroscopy analysis. As a result, it is successfully found that the symmetry protected topological phase appears in much larger region of the phase diagram of the $1/2$ magnetization plateau. In addition the biquadratic interaction is revealed to enhance this phase[5].

The $1/3$ magnetization plateau of the distorted diamond spin chain was also investigated using the numerical diagonalization and the finite-size scaling analysis. As a result it

is found that the magnetization plateau vanishes for sufficiently large XY -like coupling anisotropy. The phase diagram of the $1/3$ magnetization plateau was also obtained[6, 7].

As related topics to the magnetization plateau, we investigated the spin gap of the kagome-lattice antiferromagnet. We performed the large-scale numerical diagonalization of the spin gap and the magnetization curve of the system and tried to compare them with the recent experimental results[8, 9]

References

- [1] F. Pollmann, A. M. Turner, E. Berg and M. Oshikawa, Phys. Rev. B **81**, 064439 (2010).
- [2] F. Pollmann, E. Berg, A. M. Turner and M. Oshikawa, Phys. Rev. B **85**, 075125 (2012).
- [3] T. Tonegawa, K. Okamoto, H. Nakano, T. Sakai, K. Nomura and M. Kaburagi, J. Phys. Soc. Jpn. **80**, 043001 (2011).
- [4] K. Okamoto, T. Tonegawa and T. Sakai, J. Phys. Soc. Jpn. **85**, 063704 (2016).

- [5] T. Sakai, K. Okamoto and T. Tonegawa, Phys. Rev. B **100**, 054407 (2019).
- [6] Y. Ueno, T. Zenda, Y. Tachibana, K. Okamoto and T. Sakai, JPS Conference Proceedings **30**, 011085 (2020).
- [7] T. Zenda, Y. Tachibana, Y. Ueno, K. Okamoto and T. Sakai, JPS Conference Proceedings **30**, 011084 (2020).
- [8] H. O. Jeschke, H. Nakano and T. Sakai, Phys. Rev. B **99**, 140410(R) (2019).
- [9] R. Shirakami, H. Ueda, H. O. Jeschke, H. Nakano, S. Kobayashi, A. Matsuo, T. Sakai, N. Katayama, H. Sawa, K. Kindo, C. Michioka and K. Yoshimura, Phys. Rev. B **100**, 8722674 (2019).

Numerical Diagonalization Study on Spin Nematic Phase of Low-Dimensional System

Tôru SAKAI^{1,2}, Hiroki NAKANO^{1,2}, and Tokuro SHIMOKAWA³,

¹*Graduate School of Material Science, University of Hyogo,
Kouto, Kamigori, Hyogo 678-1297, Japan*

²*Synchrotron Radiation Research Center, Kansai Photon Science Institute,
Quantum Beam Science Research Directorate,
National Institute for Quantum and Radiological Science and Technology (QST)
SPring-8, Kouto, Sayo, Hyogo 679-5148, Japan*

³*Okinawa Institute of Science and Technology Graduate University, Onna,
Okinawa 904-0945, Japan*

The spin nematic phase has attracted a lot of interests in the field of the quantum spin systems. It was theoretically predicted to appear around the saturation magnetization in the magnetization process of the frustrated spin chain[1]. Our present study using the numerical diagonalization and the finite-size scaling analysis revealed that the spin nematic liquid phase appears in the $S = 1$ spin ladder system with the easy-axis single-ion anisotropy D even for a small magnetic field H . The phase diagram in the DH plane and the DH plane were obtained[2, 3].

The research of the three-leg spin tube with the ring-exchange interaction J_4 using the numerical diagonalization and the finite-size scaling analysis[4] indicated that the spin nematic liquid phase appears for sufficiently large J_4 . In addition the spin nematic liquid phase was also revealed to appear in the spin ladder system with the antiferromagnetic leg and the ferromagnetic rung exchange interaction in the present of the XXZ anisotropy[5].

References

- [1] T. Hikihara, L. Kecke, T. Momoi and A. Furusaki, Phys. Rev. B **78**, 144404 (2008).
- [2] R. Yamanokuchi, K. Okamoto and T. Sakai, Proceedings of 2018 16th International Conference on Megagauss Magnetic Field Generation and Related Topics (MEGAGAUSS) (2019) 8722674.
- [3] T. Sakai and K. Okamoto, JPS Conference Proceedings **30**, 011083 (2020).
- [4] T. Sakai, JPS Conference Proceedings **29**, 014004 (2020).
- [5] K. Okamoto, T. Tonegawa, M. Kaburagi and T. Sakai, JPS Conference Proceedings **30**, 011024 (2020).

Aggregation process of full-length amyloid-beta peptides studied by molecular dynamics simulations

Hisashi Okumura

*Exploratory Research Center on Life and Living Systems,
Institute for Molecular Science, Okazaki, Aichi 444-8585*

Alzheimer's disease is thought to be caused by aggregates of amyloid-beta peptides, such as oligomers and amyloid fibrils. Amyloid-beta peptide is a peptide consisting of 39-43 amino acid residues. The oligomer structure of the amyloid-beta peptides is not clear. We investigated the aggregation process of full-length amyloid-beta peptides by molecular dynamics simulations. Several amyloid-beta peptides were placed in explicit water, and their dynamics and structural changes were observed. As a result, aggregates with intermolecular beta-sheet structure was generated. During this oligomerization process, A β peptides are first aggregated by electrostatic force. Then, they are aggregated by hydrophobic interaction.

We also developed an improvement of the replica-exchange [1, 2] and replica-permutation methods [3], which we call the replica sub-permutation method (RSPM) [4]. Instead of considering all permutations, this method uses a new algorithm referred to as sub-permutation that contains transitions only to the adjacent temperatures. The RSPM can reduce the

number of combinations between replicas and parameters without the loss of sampling efficiency. For comparison, we applied the replica sub-permutation, replica-permutation, and replica-exchange methods to a β -hairpin mini protein, chignolin, in explicit water. We calculated the transition ratio and number of tunneling events in the parameter space, the number of folding–unfolding events, and the autocorrelation function to compare sampling efficiency. The results indicate that among the three methods, the RSPM is the most efficient in both parameter and conformational spaces.

References

- [1] K. Hukushima, K. Nemoto, *J. Phys. Soc. Jpn.* **65** (1996) 1604.
- [2] Y. Sugita, Y. Okamoto, *Chem. Phys. Lett.* **314** (1999) 141.
- [3] S. G. Itoh, H. Okumura, *J. Chem. Theor. Comput.* **9** (2013) 570.
- [4] M. Yamauchi and H. Okumura: *J. Comput. Chem. B* **40** (2019) 2694.

Monte Carlo study of the critical properties of noncollinear Heisenberg magnets: $O(3) \times O(2)$ universality class

Yoshihiro Nagano, Kazuki Uematsu and Hikaru Kawamura
Graduate School of Science, Osaka University, Toyonaka 560-0043

The critical properties of the antiferromagnetic Heisenberg model on the three-dimensional stacked-triangular lattice [1] are studied by means of a large-scale Monte Carlo simulation in order to get insight into the controversial issue of the criticality of the noncollinear magnets with the $O(3) \times O(2)$ symmetry [2]. The maximum size studied is 384^3 , considerably larger than the sizes studied by the previous numerical works on the model. Availability of such large-size data enables us to examine the detailed critical properties including the effect of corrections to the leading scaling. Strong numerical evidence of the continuous nature of the transition is obtained. Our data indicates the existence of significant corrections to the leading scaling. Careful analysis by taking account of the possible corrections yield critical exponents estimates, $\alpha = 0.44(3)$, $\beta = 0.26(2)$, $\gamma = 1.03(5)$, $\nu = 0.52(1)$, $\eta = 0.02(5)$, and the chirality exponents $\beta_k = 0.40(3)$ and $\gamma_k = 0.77(6)$, supporting the existence of the $O(3)$ chiral (or $O(3) \times O(2)$) universality class governed by a new 'chiral' fixed point [3,4]. We also obtain an indication that the underlying fixed point is of the focus-

type, characterized by the complex-valued correction-to-scaling exponent, $\omega = 0.1^{+0.4}_{-0.05} + i 0.7^{+0.1}_{-0.4}$. The focus-like nature of the chiral fixed point accompanied by the spiral-like renormalization-group (RG) flow [5] is likely to be the origin of the apparently complicated critical behavior. The results are compared and discussed in conjunction with the results of other numerical simulations, several distinct types of RG calculations including the higher-order perturbative massive and massless RG calculations and the nonperturbative functional RG calculation, and the conformal-bootstrap program.

References

- [1] H. Kawamura, *J. Phys. Condens. Matter* **10**, 4707 (1998).
- [2] Y. Nagano, K. Uematsu and H. Kawamura, *Phys. Rev. B* **83**, 103704 (2019).
- [3] H. Kawamura, *Phys. Rev. B* **8**, 4916 (1988).
- [4] A. Pelissetto, P. Rossi and E. Vicari, *Phys. Rev. B* **63**, 140414(R) (2001); **65**, 020403(R) (2001).hi
- [5] P. Calabrese, P. Parruccini and A.I. Sokolov, *Phys. Rev. B* **66**, 180403(R) (2002).

Multiscale analysis of polymeric fluids and solids

Takahiro MURASHIMA

*Department of Physics, Graduate School of Science,
Tohoku University, Aramaki-Aza-Aoba, Aoba-Ward, Sendai, Miyagi 980-8578*

Polymeric materials are used in many products and are now an integral part of our lives. In recent years, however, the use of microplastics has tended to be discouraged due to concerns about the damage they can cause to ecosystems. The development of new materials with less impact on ecosystems, such as biodegradable plastics, is expected.

In order to develop more functional materials, it is essential to control the physical properties on the molecular scale and to control the formability on the macro scale. The micro-scale properties of polymer materials and macro-scale mechanical properties are strongly correlated and cannot be treated independently, making their understanding difficult. Therefore, we have been developing multi-scale simulations that simultaneously combine micro-scale molecular simulations and macro-scale continuum simulations. In this project, we have developed a multi-scale simulation that combines molecular dynamics simulation and finite element simulation, and the results have been published in several papers[1-3].

The method of multi-scale simulation is as follows. The macro-scale cube is divided into

100 tetrahedral elements and the deformation of each element is calculated using the finite element method. Each element has a molecular simulation system and molecular simulation is carried out according to the deformation. The stresses are then obtained from the molecular simulation system and passed on to the macroscopic system. On the macro-scale side, the deformation occurs according to the determined stress field. The entire system is developed in time by alternating these macro- and micro-scale calculations. Multiscale simulations are now possible to include molecular features that are difficult to handle in conventional macro-scale simulations, and to calculate large deformations that are difficult to handle in conventional micro-scale simulations.

References

- [1] T. Murashima, S. Urata, S. Li: Euro. Phys. J. B **92** (2019) 221.
- [2] T. Murashima: CICSJ Bulletin **37** (2019) 87.
- [3] S. Li, S. Urata, T. Murashima: IACM Express. **46** (2020) 10.

Dynamical simulation of spin-orbit insulators

Hidemaro Suwa

Department of Physics, University of Tokyo
7-3-1 Hongo Bunkyo, Tokyo 113-0033

Dynamics of correlated quantum materials is a long-standing problem in condensed matter physics. The recent development of experimental techniques such as inelastic neutron and x-ray scattering has revealed dynamical properties and excitations with unprecedented precision. In particular, resonant inelastic X-ray scattering has revealed a lot of hidden features of high- T_c superconductors and spin-orbit insulators. It is of great interest to find novel quasi-particles and understand complex excitations in correlated materials.

Spin-orbit insulators emerge from $5d$ electron systems with strong spin-orbit coupling. Coulomb repulsion between electrons in $5d$ atomic orbitals is not strong enough to suppress charge degrees of freedom completely. As a result, the charge gap can be comparable to the magnon-band width, as experimentally measured in strontium iridates. Such electron systems can be described by the Hubbard model with an intermediate Coulomb repulsion, which is parameterized by U .

Strontium iridates, which can be approximated by a half-filled $J = 1/2$ single-band Hubbard model, provide an excellent playground of charge-spin-orbital entanglement. The dimensionality drastically changes the electronic property: the single layer material Sr_2IrO_4 is a Mott insulator with 400 meV charge gap, the bilayer material $\text{Sr}_3\text{Ir}_2\text{O}_7$ is an insulator in the intermediate coupling regime with 130 meV charge gap, and the three-dimensional material SrIrO_3 is a correlated metal. These systems provide one of the best opportunities to study the metal-insulator

transition. Particularly, the bilayer system is expected to show a characteristic excitation emerging in the crossover regime. Moreover, in the view of engineering, the magnetic energy scale enhanced in the crossover regime would be crucial to realistic devices.

To understand the dynamics of spin-orbit insulators, we have developed an efficient numerical approach that enables large-scale calculation of dynamical quantities at finite temperatures in a broad- U region of the Hubbard model. In our approach, sampling of the auxiliary vector fields from the Boltzmann distribution is combined with real time evolution of the self-consistent density matrix.

We used ISSP System B through class C projects (ID: H31-Ca-0057, H31-Cb-0047). Our code is implemented with MPI parallelization using GPUs. In particular, GPU programming is crucial to fast matrix-vector multiplication and diagonalization. Applying our approach to the bilayer iridate $\text{Sr}_3\text{Ir}_2\text{O}_7$, we have clarified excitonic excitations of the longitudinal or Higgs mode appearing in the dynamical spin structure factor. Interestingly, excitons exhibit a significant softening as the temperature approaches the magnetic transition temperature, while transverse magnons do not.

Our approach is applicable to a broad range of the Hubbard model without restrictions of the lattice, hopping parameters, and electron filling. The developed method is expected to push the boundary of dynamical simulation of correlated electron systems and lead to the identification of hidden excitations emerging from charge-spin-orbital entanglement.

Computational design of enzymes and ligand-binding proteins

Kazuhisa OHARA¹, Mio SANNO¹, Shunji SUETAKA¹, Nao SATO¹, Yoshiki OKA¹,
Koji OOKA², Yuuki HAYASHI¹, and Munehito ARAI^{1,2}

¹*Department of Life Sciences, Graduate School of Arts and Sciences, and*

²*Department of Physics, Graduate School of Science,*

The University of Tokyo, Komaba, Meguro, Tokyo 153-8902

Proteins have various functions, including binding and catalysis. Thus, proteins are potentially useful for industry and medicine if their functions are sufficiently improved or modified. However, because the protein folding problem remains unsolved, development of computational protein design strategies has been a great challenge. To solve this issue, here we attempted to use the Rosetta software suite to computationally design various proteins, including enzymes and ligand-binding proteins. The static version of the Rosetta 3.8 suite was used in the following calculations [1,2]. In addition, to solve the protein folding problem, we developed a statistical mechanical model of protein folding that can explain the folding pathways of multi-domain proteins.

(1) First, we aimed to rationally improve a catalytic activity of an enzyme. By optimizing the interactions between an enzyme, dihydrofolate reductase [3], and its ligands, we computationally designed many mutants of the enzyme that were expected to improve its catalytic activity. Subsequently, we selected 34

top mutants, created the mutant proteins experimentally, and measured their activities. We found that 20 out of 34 mutants had the activity higher than the wild-type protein. Moreover, for the top 2 mutants, we succeeded in improving the activity ~4-fold compared with the wild type. Thus, our strategies for rationally improving activity of an enzyme will be applicable to industrial use.

(2) Second, to develop a protein that can be used as an anti-allergy drug, we designed two types of proteins that inhibit the interaction of interleukin-33 (IL-33) with the ST2 receptor of type 2 innate lymphoid cells [4]. One template for the inhibitor design was a fragment of the ST2 protein. Rosetta calculation was used to reduce the number of disulfide bonds in the fragment, to make it easier to purify the protein that was expressed in *Escherichia coli*. As expected, we could obtain the mutant of the ST2 fragment having a reduced number of disulfide bonds as well as the ability to bind IL-33. Another strategy to design the IL-33–ST2 inhibitors was to make mutants of IL-33 that

binds tightly to one of the two IL-33 binding sites on ST2 but does not bind to another site. The calculations were already done, and the experimental verification is now under way.

(3) Third, we rationally designed inhibitors for the interactions between the KIX domain of a transcriptional coactivator CBP and transcriptional activators [5]. We designed and created the mutant fragments of the transcription activator MLL, which bind more tightly than the wild type. We also designed the KIX mutant that can bind more tightly to the transcription activator c-Myb than the wild-type KIX. Since the protein-protein interaction between KIX and c-Myb is responsible for the blood cancer, leukemia, our results may be useful for developing anti-cancer drugs.

(4) Fourth, we attempted to modify a substrate specificity of a ligand-binding protein using the Rosetta software. Here, an ATP-binding protein was designed to bind GTP instead of ATP. For experimental verification, we selected more than 20 mutants that were predicted by Rosetta to bind GTP more tightly than ATP. However, the experimental results showed that none of the mutants acquired a new function to bind a different ligand. It might be possible that dynamics of both the protein and ligand should be taken into account more extensively to accommodate the difference in the size and shape of ligands, although it requires much more calculations.

(5) Finally, to solve the protein folding problem, we developed a statistical mechanical model of protein folding. The WSME model has been known to be able to explain the folding pathways of small proteins and is considered to be a promising model to solve the protein folding problem [6]. However, the model could not be applicable to large, multi-domain proteins, and this problem has been unsolved for more than 20 years. By introducing a new Hamiltonian in the WSME model and computationally calculating the closed form of the partition function, we succeeded in predicting the folding pathways of multi-domain proteins. Thus, our model is promising for a unified theoretical description of protein folding mechanisms.

References

- [1] B.J. Bender, et al.: *Biochemistry*, **55** (2016) 4748-4763.
- [2] R. F. Alford, et al.: *J Chem Theory Comput.* **13** (2017) 3031-3048.
- [3] M. Arai, et al.: *J Mol Biol.* **410** (2011) 329-342.
- [4] X. Liu, et al.: *Proc Natl Acad Sci USA.* **110** (2013) 14918-14923.
- [5] R. N. De Guzman, et al.: *J Mol Biol.* **355** (2006) 1005-1013.
- [6] M. Sasai, et al.: *Biophys Physicobiol.* **13** (2016) 281-293.

Event-chain Monte Carlo method applied to non-equilibrium relaxation analysis

Y. Ozeki and Y. Osada

Graduate School of Informatics and Engineering, The University of Electro-Communications

The event-chain algorithm is investigated for its applicability to the nonequilibrium relaxation (NER) method and the estimation of the dynamical exponent z , which indicates an efficiency to perform Monte Carlo (MC) simulations. The event-chain method has introduced for the MC simulation with a multi-spin-flip algorithm [1,2]. It shows an efficient performance for the relaxation even in frustrated systems and gives estimation of the dynamical critical exponent $z \sim 1$ [1], which indicates a faster dynamics as compared with those with a single-spin-flip algorithm such as the the Metropolis one.

The NER method is an efficient numerical technique for analyzing equilibrium phase transition [3]. It provides the critical temperature and critical exponents accurately for second-order transition systems, and has been used successfully to study various problems, including frustrated and/or random systems. In the NER analysis, the equilibration step is not necessary. Simulation is made only up to steps when the asymptotic behavior indicates the equilibrium state. Thus, one can analyze large systems as compared with equilibrium simulations. This advantage becomes more effective for slow-relaxation systems.

We analyze the classical XY model in three dimensions;

$$\mathcal{H} = -J \sum_{\langle ij \rangle} \mathbf{S}_i \cdot \mathbf{S}_j, \quad (1)$$

where summation for $\langle ij \rangle$ is taken over all nearest-neighboring sites on a simple cubic lattice. The initial state of relaxation is prepared as the all-aligned state $(1, 0)$. Since the relaxation is much fast in the simulation with the event chain analysis, we cannot use the magnetization $\langle S_i^x \rangle$ as the dynamical order parameter, which is used in the NER analysis with the Metropolis algorithm. Thus, we estimate the relaxation of the absolute value of the magnetization,

$$|m(t)| = (\langle S_i^x \rangle^2 + \langle S_i^y \rangle^2)^{1/2}. \quad (2)$$

In the standard NER analysis, the asymptotic behaviors of relaxations are used to analyze the phase transition, and are necessary to be regarded

as those in the thermodynamic limit. In other words, the finite size effect must be avoided in the observed regime of relaxations. Thus, first, we check the size-dependence for the relaxation of $|m(t)|$. Calculations are carried out at around the expected transition temperature $T^* = 2.202$ on 4^3 to $350 - 3$ simple cubic lattices up to the observation time of 200 MCSs. Note that the temperature is measured in the unit of J/k_B hereafter. About 840 samples are taken for statistical averaging. The result is plotted in Fig. 1. It is confirmed that the size dependence disappears for $L \geq 300$ up to 200 MCSs. It is remarked that the relaxation simulated by the event-chain algorithm is much faster than that by the Metropolis one, which is an advantage. Furthermore, the appearance of the size dependence also becomes faster. In the Metropolis case, it does not appear at least in 10^4 MCSs for $L = 200$ lattice, while it does at 100 MCSs in the event-chain case. The latter property is an disadvantage, since we must simulate on larger lattices. Anyway, in the present study, we will use $L = 300$ lattice for the analysis of phase transition.

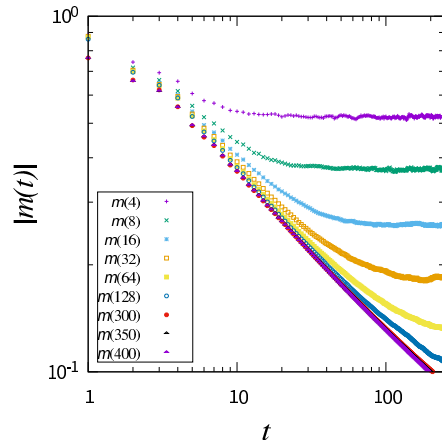


Figure 1: Size dependence for the relaxation of $|m(t)|$ at $T = 2.202$ for the 3D XY model.

The relaxation of the order parameter $|m(t)|$ are calculated for $2.182 \leq T \leq 2.222$ on the 300^3 simple cubic lattice up to an observation time of 200

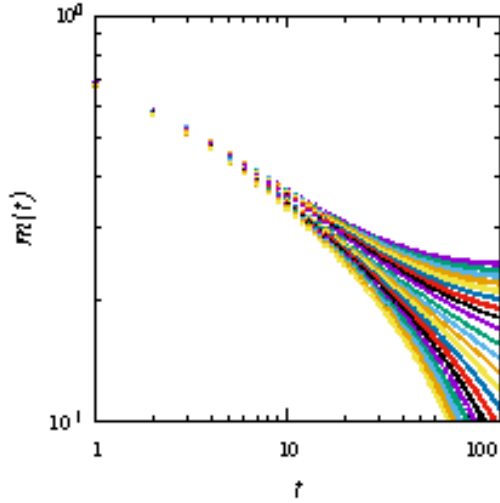


Figure 2: Relaxation of $|m(t)$ for the 3D XY model in $2.182 \leq T \leq 2.222$ with the interval $\Delta T = 0.002$.

MCSs. About 864 samples are taken for statistical averaging. The estimations are plotted in Fig. 2. Using the improved dynamical scaling analysis for the NER data [4], we analyze the dynamical scaling form,

$$|m(t, T)| = \tau^{-\lambda} Y[t/\tau], \quad (3)$$

where $\tau(T)$ is the relaxation time and λ is a dynamical critical exponent. In Fig. 2, the relaxation curves show downward trend in $2.204 \leq T \leq 2.222$, which indicates the paramagnetic phase. Thus, applying the scaling form (3), the data for these temperatures collapse as in Fig. 3 with $T_c = 2.20216$ and $z = 1.461$. Furthermore in Fig. 2, the relaxation curves show upward trend in $2.182 \leq T \leq 2.200$, which indicates the ferromagnetic phase. Thus, applying the scaling form (3), the data for these temperatures collapse as in Fig. 4 with $T_c = 2.20183$ and $z = 1.478$.

The estimated transition temperature $T_c = 2.202$ is consistent with $T_c = 2016$ obtained previously [5]. The estimated dynamical exponent $z \sim 1.47$ is greater than $z \sim 1$ estimated previously for the event-chain algorithm [1], while it keeps still a smaller value than $z \sim 2$ which is expected for the short-range algorithm such as the Metropolis one. Consequently, the event-chain algorithm can be used in the NER analysis with an efficient relaxation performance, and would be applicable to various slowly relaxing problems such as frustrated and/or random systems.

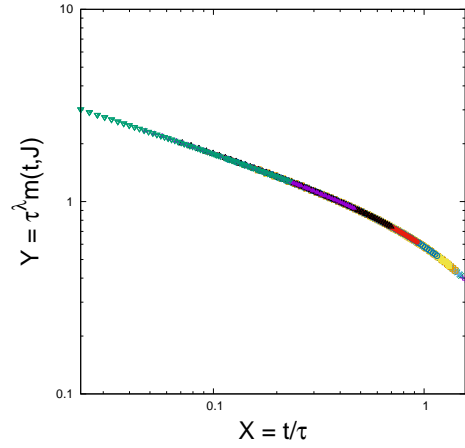


Figure 3: Scaling plot for the data in $2.204 \leq T \leq 2.222$ in Fig. 2

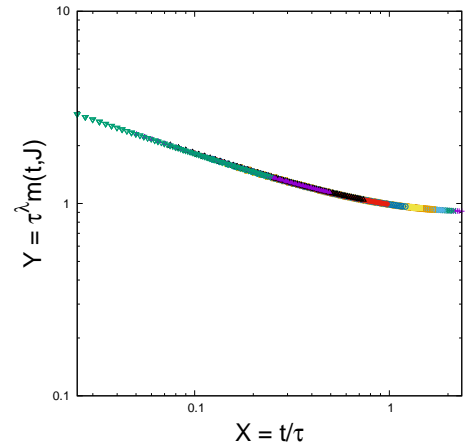


Figure 4: Scaling plot for the data $2.182 \leq T \leq 2.200$ in Fig. 2

References

- [1] Y. Nishikawa *et. al.*, *Phys. Rev.* **E92** 063306 (2015)
- [2] M. Michel *et. al.*, *Europhys. Lett.* **112** 20003 (2015)
- [3] Y. Ozeki and N. Ito, *J. Phys.: Math. Theor.* **40** R149 (2007).
- [4] Y. Echinaka and Y. Ozeki, *Phys. Rev.* **E94** 043312 (2016).
- [5] A. P. Aloysius and M. Harsenbusch, *Physica* **A201** 593 (1993)

Entanglement, Quantum Phase Transition, and Quantum Dynamics in Quantum Many-body Systems

Syngé Todo

Department of Physics, University of Tokyo, Tokyo 113-0033, Japan
Institute for Solid State Physics, University of Tokyo, Kashiwa, 277-8581, Japan

We have developed various novel numerical methods for quantum/classical many-body systems with strong correlations. An efficient quantum Monte Carlo method has been developed to calculate the entanglement entropy of quantum spin systems. The entanglement entropy is an essential index that characterizes quantum correlations and the topological order in quantum many-body systems. Our method works directly at absolutely zero temperature, and thus it is entirely free from systematic errors coming from extrapolation to the zero-temperature limit, unlike the previous methods.

We also have developed a nonlocal-update quantum Monte Carlo method for quantum dimer models on general lattices. By implementing the technique recently suggested for quantum Monte Carlo simulation on quantum dimer model with the help of priority queue, which can help find the next operator for updating efficiently, we can simulate on the finite temperature region of the quantum dimer model. By the finite-size scaling, the phase boundary between low-temperature columnar phase with the maximum number of parallel neighboring dimers, and disordered phase at high temperatures can be decided in a broad region of dimer-dimer interaction potential, and the value of which is both consistent of the classical limit, where a KT phase transition is known, and also tends to a constant slope near the RK-point.

In the meantime, the real-space renormalization group methods based on the tensor networks have been widely used in recent years.

The tensor renormalization group method can efficiently calculate physical quantities of large-scale classical/quantum systems. However, the existing methods, such as the tensor renormalization group (TRG) and the higher-order tensor renormalization group (HOTRG), suffer from the huge computational cost in higher dimensions. To solve this problem, we have developed the anisotropic tensor renormalization group (ATRG) that can dramatically reduce the computational complexity in high-dimensional systems such as three-dimensional quantum systems. In addition, we further improve the accuracy of ATRG by combining with techniques such as the tensor renormalization group method that incorporates bond weights, etc.

Spins coupled with photon degrees of freedom in the cavity exhibit a non-equilibrium phase transition with bistability in the number of photons. We have performed simulation based on the quantum master equations. From the eigenvalues and eigenstates of the time evolution operator, we discussed the correspondence to the first-order phase transition in the equilibrium system. We have calculated the hysteresis loop under the periodic modulation of laser intensity, from the viewpoint of the Floquet operator, and clarified that a dynamical phase transition phenomenon appears with respect to the period of laser intensity.

Superconducting dome in electron doped FeSe intercalates

Harald JESCHKE

*Research Institute for Interdisciplinary Science, Okayama University
3-1-1 Tsushima-naka, Kita-ku, Okayama 700-8530*

The van-der-Waals gap of iron chalcogenide superconductors can be intercalated with a variety of inorganic and organic compounds that modify the electron doping level of the iron layers. In $\text{Li}_x(\text{C}_3\text{N}_2\text{H}_{10})_{0.37}\text{FeSe}$, a dome in the superconducting transition temperature T_c has been reported to occur in the doping range of $x = 0.06$ to $x = 0.68$ [1]. We used massive parallel computer simulations to address magnetic and superconducting properties of $\text{Li}_x(\text{C}_3\text{N}_2\text{H}_{10})_{0.37}\text{FeSe}$ [2]. With a combination of density functional theory and spin fluctuation theory, we capture the evolution of superconducting transition temperatures theoretically. We clearly demonstrate how the changing electronic structure supports an increasing superconducting T_c (Figure 1). The suppression of T_c at high doping levels can, however, only be understood by analyzing the magnetic tendencies. We determine the Heisenberg exchange couplings between the iron moments; superconductivity is realized out of these underlying interactions. We can show that with doping, they evolve from stripe-type at low doping to bicollinear at high doping. With increasing carrier density, magnetic interactions mutate from FeSe-like to FeTe-like, explaining a T_c suppression at high doping.

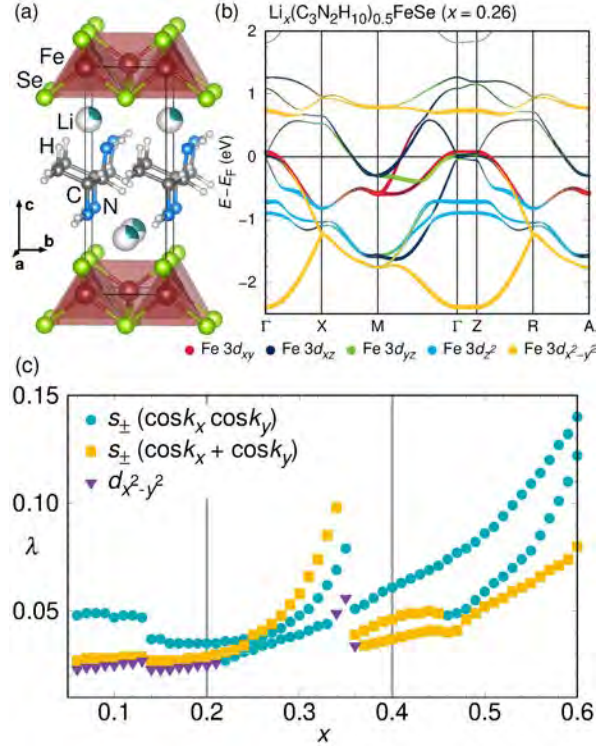


Figure 1: Structure, band structure and leading eigenvalues of the gap equation for $\text{Li}_x(\text{C}_3\text{N}_2\text{H}_{10})_{0.37}\text{FeSe}$.

- [2] M. Shimizu, N. Takemori, D. Guterding and H. O. Jeschke, Importance of Fermi surface and magnetic interactions for the superconducting dome in electron doped FeSe intercalates, under review (2020).

References

- [1] R. J. Sun *et al.*, Phys. Rev. B **98**, 214508 (2018).

Properties of electron doped iron based superconductor LaFe_2As_2

Harald JESCHKE

*Research Institute for Interdisciplinary Science, Okayama University
3-1-1 Tsushima-naka, Kita-ku, Okayama 700-8530*

For more than a decade after the discovery of Fe-based superconducting pnictides it seemed that superconductivity existed in a relatively narrow range of dopings away from the nominal Fe^{2+} valency. One of the few examples of strongly overdoped (up to $\text{Fe}^{2.5+}$ valency) pnictides was provided by the 1111 material LaFeOAs , with up to 50% of O^{2-} replaced by H^- . Recently, another compound with formally $\text{Fe}^{2.5+}$ has been synthesized [1], LaFe_2As_2 . It was found experimentally that the material can exist in two distinctly different crystallographic phases, “collapsed-tetragonal” (CT) and “uncollapsed-tetragonal” (UT). We used massive parallel computer simulations to address structural, magnetic, and electronic properties of LaFe_2As_2 [2]. We show that the UT phase, as opposed to the CT one, bears a strong short-range magnetism of the stripe type driven by the next-nearest-neighbor exchange. The structural changes are triggered by magnetic collapse, as in CaFe_2As_2 . Even though the orbitals relevant for the low-energy physics are not the usual d_{xz} and d_{yz} , the electron pockets do not exclude the usual spin-fluctuation driven mechanism with an overall s symmetry (Figure 1). Importantly, La in this compound assumes a non-integer valence closer to $2.7+$ than to $3+$, corresponding to doping of $\sim 0.35e$, rather than $0.5e$. It is thus overdoped, but not dramatically.

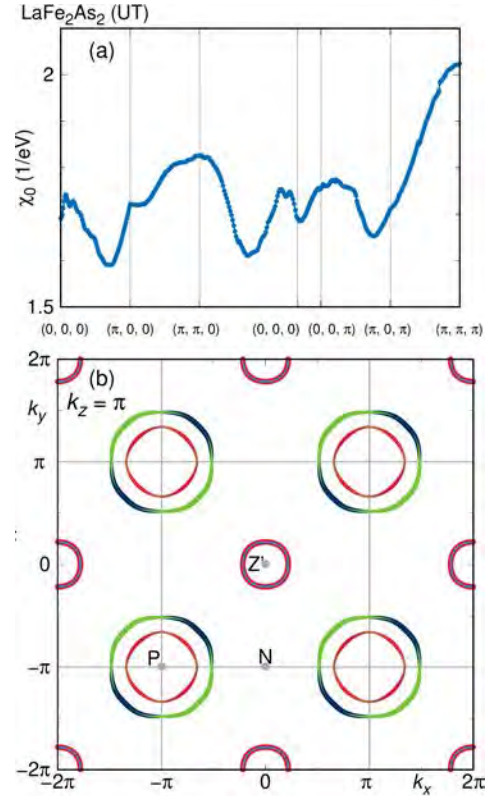


Figure 1: Susceptibility and Fermi surface of LaFe_2As_2 .

References

- [1] A. Iyo *et al.*, J. Phys. Chem. Lett. **10**, 1018 (2019).
- [2] I. I. Mazin, M. Shimizu, N. Takemori, and H. O. Jeschke, Novel Fe-Based Superconductor LaFe_2As_2 in Comparison with Traditional Pnictides, Phys. Rev. Lett. **123**, 267001 (2019).

Novel phases and dynamics in frustrated spin systems

Tsuyoshi OKUBO

Department of Physics, The University of Tokyo
7-3-1 Hongo, Bunkyo-ku, Tokyo 113-0033

Frustrated interactions in spin systems often induce novel phenomena, *e.g.*, non-magnetic ground states including spin liquid and topological orders. Conventionally, geometrically frustrated spin systems, such as the kagomé lattice and the pyrochlore lattice Heisenberg antiferromagnets have been investigated actively. Recently, a different kind of frustrated interaction introduced by the strong spin-orbit coupling has attracted much interest. For example, in Na_2IrO_3 and $\alpha\text{-RuCl}_3$, the dominant magnetic interaction induced by the strong spin-orbit coupling is considered to be the Kitaev interaction: it is an Ising like anisotropic interaction with different spin component depending on the bonds. When we consider the $S = 1/2$ quantum spin model on the honeycomb lattice with only the Kitaev interaction (Kitaev model), its ground state is a spin liquid state without any spontaneous symmetry breakings [1]. This fact indicate real compounds might have a spin liquid ground states. However, real compounds contain other interactions such as the Heisenberg interaction, further neighbor interactions, or the off-diagonal interactions, and they can induce magnetic long range orders at low temperature.

In this year, in order to clarify effects of additional interactions in the Kitaev materials, we numerically investigated the ground state and finite temperature properties of the models with the Kitaev interaction and the Γ interactions (the Kitaev- Γ model) by means of tensor network methods. The Γ term is an off-diagonal interaction and the Hamiltonian

of the model is given by

$$\mathcal{H} = \sum_{\gamma \in x, y, z} \mathcal{H}_\gamma, \quad (1)$$

where for $\gamma = z$,

$$\mathcal{H}_z = \sum_{\langle i, j \rangle_z} [K S_i^z S_j^z + \Gamma (S_i^x S_j^y + S_i^y S_j^x)]. \quad (2)$$

For $\gamma = x, y$, we consider similar interaction with cyclic rotation of x, y, z components. We consider the honeycomb lattice and $\gamma = x, y, z$ corresponds to three directions of the bonds. This model is considered to be an effective model for $\alpha\text{-RuCl}_3$ [2, 3].

Firstly, we investigated the phase diagram of the Kitaev- Γ model by using a two-dimensional infinite tensor network approach. We represented the ground state wave function as products of small tensors, and optimize each tensor element so that the energy expectation value becomes smaller. By assuming several transnational symmetries of the ground state, we can represent infinitely large system by using finite numbers of tensors. As a network of tensors, we used the infinite tensor product states (iTTPS), which is also called as the infinite projected entangled-pair states (iPEPS). As the optimization algorithm, previously, we have used the imaginary time evolution. However, it have become clear that the imaginary time evolution often trapped at local minima and it was very hard to obtain novel spin liquid state from random initial states. Thus, this year, we used a different type of optimization, so called variational optimization [4]. We confirmed that by using the variational optimization

tion, we correctly obtained the Kitaev spin liquid state at the pure Kitaev model ($\Gamma = 0$) even from the random initial states. Then we applied the variational optimization to finite Γ and draw the phase diagram. Although the obtained variational energies were largely improved from those obtained by the imaginary time evolution, the phase diagram was almost unchanged; except for the vicinity of the pure Kitaev model, the ground states were magnetically ordered states. This observation was contrasted with the phase diagrams obtained by the exact diagonalization (ED) [2] or by the infinite density matrix renormalization group (iDMRG) [3]; they concluded much wider spin liquid phases. In order to clarify nature of the phase diagram further, we might need larger scale calculation with iTPS.

Secondly, we investigated finite temperature properties of the model. In order to calculate physical quantities at a finite temperature, we represented the density matrix of the system in tensor network representations. We employed two types of the tensor network representations: the local purification, *e.g.*, Ref. [5], and the direct tensor product operator (TPO) [6]. By applying them to the pure Kitaev model, we found that the former representation failed to reproduce the expected lower temperature specific heat peak [7], while the latter TPO representation reproduced it, at least qualitatively. This observation indicated that the direct TPO representation was more efficient than the local purification. The applications of the developed technique to the model with finite Γ is on going.

References

- [1] A. Kitaev: *Ann. Phys.* **321** (2006) 2.
- [2] A. Catuneanu, Y. Yamaji, G. Wachtel, H.-Y. Kee, and Y. B. Kim: *npj Quantum Materials* **3** (2018) 23.
- [3] M. Gohlke, G. Wachtel, Y. Yamaji, F. Pollmann, and Y. B. Kim: *Phys. Rev. B* **97** (2018) 075126.
- [4] P. Corboz: *Phys. Rev. B* **94** (2016) 035133.
- [5] P. Czarnik, J. Dziamaga, and P. Corboz: *Phys. Rev. B* **99** (2019) 035115.
- [6] A. Kshetrimayum, M. Rizzi, J. Eisert, and R. Orús: *Phys. Rev. Lett.* **122** (2019) 070502.
- [7] J. Nasu, M. Udagawa, and Y. Motome: *Phys. Rev. B* **92** (2015) 115122.

Thermal effects on quantum frustrated magnetisms

Tokuro Shimokawa

*Okinawa Institute of Science and Technology Graduate University,
Tancha, Onna-son, Kunigami-gun, Okinawa 904-0495*

We know well that quantum frustrated magnetisms often exhibit rich many-body physics, but we also know difficulties to investigate the effects of the thermal fluctuations numerically, hence thermally induced novel phases still remain unexplored.

We use a state of art numerical method, quantum typicality method [1-2] for investigating the finite-temperature properties of $S=1/2$ bilayer-breathing-kagome (BBK) Heisenberg model for $\text{Ca}_{10}\text{Cr}_7\text{O}_{28}$ and $S=1/2$ Shastry-Surtherland (SS) Heisenberg model for $\text{SrCu}_2(\text{BO}_3)_2$. The former magnet joined recently the family of quantum spin liquid candidates [3] in spite of the complexity of its Hamiltonian. The latter magnet has been known well, but recent experiments under high pressures [4] could reveal successfully the existence of the intermediate plaquette state, so the theoretical studies at finite temperatures are required.

The BBK model: We computed the several physical quantities such as specific heat, magnetization curve, and equal-time spin structure factor at finite-temperature with the quantum typicality method and found the possible existence of a spiral spin liquid state at

moderate temperatures exhibiting a characteristic ring-like structure in the equal-time spin structure factor. These obtained results are reasonable for explaining qualitatively the nature of the $\text{Ca}_{10}\text{Cr}_7\text{O}_{28}$. [5]

The SS model: Owing to the Ising degrees of freedom in the intermediate plaquette ground state, we found the signature of the finite-temperature phase transition associated with the breaking of the mirror symmetry at moderate temperatures via specific heat and correlation functions calculations. We also investigate the relationship the transition and the existence of the degenerated excited states by the exact diagonalization method. [6]

References

- [1] A. Hams and H. De Raedt, Phys. Rev. E **62**, 4365 (2000).
- [2] S. Sugiura and A. Shimizu, Phys. Rev. Lett. **111**, 010401 (2013).
- [3] C. Balz, et al, Nat. Phys. **12**, 942 (2016).
- [4] M. E. Zayed et al, Nat. Phys. **13**, 962 (2017).
- [5] T. Shimokawa, R. Pohle, N. Shannon, in preparation.
- [6] T. Shimokawa, in preparation.

Numerical studies on magnetization process of the Kitaev spin liquid

Kota IDO

*Institute for Solid State Physics, University of Tokyo
Kashiwa-no-ha, Kashiwa, Chiba 277-8581*

The Kitaev model is one of the prominent examples of quantum many-body systems where quantum spin liquids emerge[1]. In the Kitaev model, the nearest-neighbor spins interact with each other via bond-dependent Ising-type interactions. Although the Kitaev model seems to be an artificial model, it has been proposed that the Kitaev model can be realized in real materials[2]. Inspired by the proposal, it is now one of the hot topics in the condensed matter physics how to synthesize and characterize the Kitaev-like materials.

The Kitaev model under a magnetic field has been intensively studied, because the magnetization processes offer useful information for characterizing the nature of the quantum spin liquid in the Kitaev model. Recently, it was reported that an intermediate gapless state appears in the antiferromagnetic coupling Kitaev honeycomb model under a magnetic field. For example, exact diagonalization (ED) calculations showed that the magnetization curve has two abruptly changes by increasing the field[3, 4]. This feature was observed by other numerical methods such as the density matrix renormalization group (DMRG)[5] and Majorana mean-field (MF) theory[6]. However, ED and DMRG studies were done in small system size and quasi-one-dimensional system on cylindrical boundary condition, respectively. It is desired to perform accurate analysis based on a numerical calculation method applicable to the large two-dimensional system.

In this study[7], by using the variational

Monte Carlo (VMC) method, we investigate whether the intermediate state exists as the ground state of the Kitaev model in two dimensions in a [001] magnetic field. We used a generalized Bardeen-Cooper-Schrieffer trial wavefunction with Jastrow factor, which can exactly represent the ground state of the pure Kitaev model fermionized by the Jordan-Wigner transformation[8, 9]. Our benchmark for a small system show that this trial wavefunction well reproduces the exact magnetization process. In applications to the antiferromagnetic Kitaev model with large system sizes, a double-peaked structure is found in the magnetic susceptibility, which signals the existence of the intermediate phase. In the intermediate strength of the magnetic field, we find that the local Z_2 gauge field takes non-integer values, which is consistent with the spin liquid phase with fluctuating flux for [111] case. Our results also show that the momentum distribution of the complex fermions changes topologically at the first transition point, suggesting that this is a topological phase transition resembling the Lifshitz transition. We cannot find these properties in the ferromagnetic Kitaev model. Our results show that in the antiferromagnetic Kitaev model, the intermediate state is stable against many-body correlations beyond the MF approximation.

Our VMC results also suggest that it is a useful and accurate way to analyze the Kitaev model in a magnetic field by using fermionization of the localized spin different from the

spinon representation. Using other types of the fermionizations, it would be possible to accurately analyze the magnetization process of the Kitaev model with additional interactions such as the Heisenberg term and the Γ term within the framework of VMC. Our study offers a firm basis for such extended treatments.

In addition, we have proposed how to calculate the charge (density) dynamical structure factors for the ground states of correlated electron systems based on the VMC method[10]. It is a future issue to study complex fermion dynamics of quantum spin liquids by using our proposed method.

References

- [1] A. Kitaev: *Ann. Phys.* **321** (2006) 2.
- [2] G. Jackeli and G. Khaliullin: *Phys. Rev. Lett.* **102** (2009) 017205.
- [3] Z. Zhu, I. Kimchi, D. N. Sheng, and L. Fu: *Phys. Rev. B* **97** (2018) 241110(R).
- [4] C. Hickey and S. Trebst: *Nat. Commun.* **10** (2019) 530.
- [5] M. Gohlke, R. Moessner, and F. Pollmann: *Phys. Rev. B* **98** (2018) 014418.
- [6] J. Nasu, Y. Kato, Y. Kamiya, and Y. Motome: *Phys. Rev. B* **98** (2018) 060416(R).
- [7] K. Ido, and T. Misawa: *Phys. Rev. B* **101** (2020) 045121.
- [8] H.-D. Chen and Z. Nussinov: *J. Phys. A* **41** (2008) 075001.
- [9] X.-Y. Feng, G.-M. Zhang, and T. Xiang: *Phys. Rev. Lett.* **98** (2007) 087204.
- [10] K. Ido, M. Imada, and T. Misawa: *Phys. Rev. B* **101** (2020) 075124.

A new block-spin transformation in Potts models

Yusuke TOMITA

*College of Engineering, Shibaura Institute of Technology
Saitama, Saitama 337-8570*

In usual block-spin transformation, the majority rule is mainly used as a renormalization scheme. Many studies using the block-spin transformation have shown that spin configurations are well renormalized well by the majority rule. But the legitimacy of the majority rule has not been understood. In this study, I propose a block-spin transformation rule, which utilizes the fractality of the Kasteleyn-Fortuin cluster on the critical point. The new block-spin transformation is constructed to conform Kasteleyn-Fortuin clusters to the usual finite-size scaling form, $L^{-\beta/\nu}$.

Magnetic susceptibilities for 2D Potts models through the new block-spin transformation are shown in Fig. 1. The original system size is 8192. Slopes of lines in Fig. 1 are drawn by using exact critical exponents, γ/ν 's. The result indicates the new transformation rule works well for each q -state Potts model. While the newly proposed transformation utilizes the fractal property of Kasteleyn-Fortuin cluster on critical points, I also examined the renormalization properties at off-critical points. Figure 2 shows numbers of clusters for the 2D Ising model for $T = 0.95 \times T_c, T_c$, and $1.05 \times T_c$. At the critical point, the number of clusters is well fitted by a power function with exponent $4/(2 - \beta/\nu)$. On the other hand, the numbers of clusters at off-critical points suddenly drop at some block-spin transformation steps. A renormalized cluster expands almost whole the system at a some finite renormalized step when the temperature is lower than the critical temperature, while all of the clusters disappear at a some finite renormalized step

when the temperature is higher than the critical temperature. Therefore, we can estimate critical points by the linearity of the number of clusters.

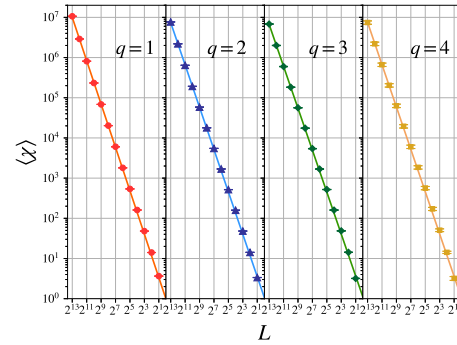


Figure 1: Plot of the susceptibilities for the 2D Potts models. Slopes of lines are drawn by using exact critical exponents, γ/ν

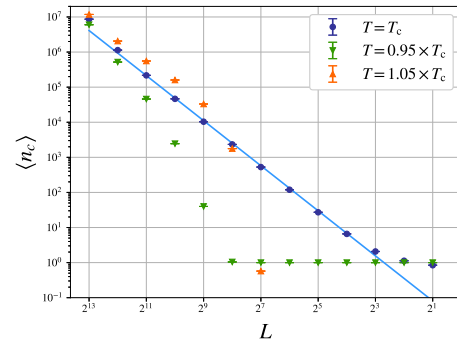


Figure 2: Plot of the numbers of clusters for the 2D Ising ($q = 2$) models. A slope of line is drawn by using exact critical exponents, $4/(2 - \beta/\nu)$

Screening for Thermal Functional Materials using Materials Informatics

Junichiro SHIOMI

7-3-1, Hongo, Bunkyo-kun, The University of Tokyo, Tokyo 113-8656

Controlling the thermal boundary conductance (TBC) between copper and carbon crystals is important since it can bottleneck the thermal conductivity when reinforcing copper with carbon-crystals fillers, namely diamond or graphite, to develop heat sinks and spreaders needed for the thermal management. In the work of this year [1], we demonstrate the spectral control of TBC between copper and carbon crystal by self-assembled monolayers (SAMs) using the non-equilibrium molecular dynamics simulation.

The resultant values of TBC for copper/diamond and copper/graphite interfaces are 9.06 ± 0.16 MW/m²K and 81.76 ± 14.85 MW/m²K, respectively. The result indicates the TBC at copper/graphite interfaces is almost an order of magnitude greater than that at copper/diamond interface. In order to interpret the behavior, the vibrational density of states (VDOS) of copper/diamond and copper/graphite interfaces are calculated, as shown in Fig. 1. The result indicates the out-of-plane VDOS of graphite surface provides the overlap in phonon vibrational modes with that of copper surface. In view of elastic energy transport, which is usually the main contribution to interfacial heat

conduction, the overlap results in the higher value in TBC compared with the copper/diamond interface.

To improve the TBC at the copper/diamond interface, the covalently bonded SAMs with different chain lengths are installed at the interface. The resultant values of TBC with SAMs of various chain lengths are plotted in Fig. 2. The data at $n=0$ refers to the TBC at copper/diamond and copper/graphite interfaces without SAMs. For the chain length studied in this work, the value of TBC increases monotonically with the chain length for chain length shorter than C15 and reaches a plateau afterward. The highest value of TBC approaches to that of bare copper/graphite interface.

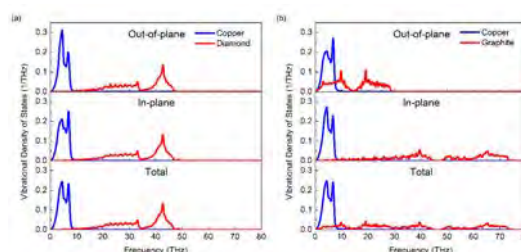


Fig. 1: Vibrational density of states of various components of (a) copper/diamond and (b) copper/graphite interfaces.

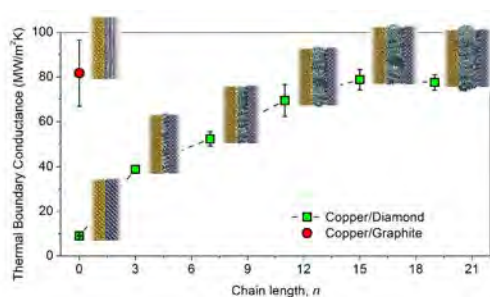


Fig. 2: Thermal boundary conductance as a function of chain length of SAMs. $n=0$ refer to the interfaces without SAMs.

Both the spectral and structural analysis are implemented to further understand the underlying mechanism. The analysis identifies that this is because the SAMs becomes softer with increasing chain length due to disordering of the collective SAMs structure, enhancing the spectral overlap with copper at low frequency vibrational modes. In the future, the materials informatics techniques can be conducted to find out the optimum design of SAMs to enhance the interfacial heat transfer. The obtained results are

useful to improve the thermal conductivity of metal/carbon-crystal composite materials in the industry applications.

In summary, we have demonstrated (1) the poor TBC at copper/diamond interface is mainly due to the mismatch of VDOS between copper and diamond (2) the installation of SAMs at copper/diamond interface can improve the TBC significantly. The TBC shows a strong dependence on chain length that the TBC increases with the increasing chain length for chain length shorter than C15 and reaches a plateau afterward. The materials informatics technique will be helpful for the design of SAMs to enhance the thermal conductivity of metal/carbon-crystal composite materials.

References

- [1] S.-W. Hung, S. Hu, and J. Shiomi, *ACS Appl. Electron. Mater.* **1** (2019) 2594.

Wave function analyses in disordered electron systems

TOMI OHTSUKI¹
 TOHRU KAWARABAYASHI²
 KEITH SLEVIN³
 KOJI KOBAYASHI⁴
 TOMOHIRO MANO¹

- 1) Dept. Phys., Sophia University, Chiyoda-ku, Tokyo 102-8554, Japan
 2) Dept. Phys., Toho University, Miyama 2-2-1, Funabashi 274-8510, Japan
 3) Dept. Phys., Osaka University, Toyonaka, Osaka 560-0043, Japan
 4) IMR, Tohoku University, Sendai 980-8577, Japan

Recent discoveries of Weyl semimetal (WSM) have inspired extensive research of these novel topological materials, especially from the point of the new universality classes, which has discrete symmetries such as particle-hole symmetry. Here we have studied the Anderson transition in chiral orthogonal class as well as class BDI, the latter showing the nodal line Weyl semimetal phase[1]. We have also studied the various quantum phase transitions by analyzing the wave functions via convolutional neural network (CNN) [2]. The typical wave functions in disordered quantum systems are shown in Fig. 1. The method is especially powerful when analyzing the quantum percolation, where the transfer matrix method breaks down due to the irregular lattice structure. We have trained CNN to capture the features of wave functions in topological as well as nontopological phases, and let CNN draw the phase diagram (Fig.2) [3]. In addition, we have calculated the distribution of Kondo temperature at the Anderson transition from the local density of states obtained by kernel polynomial method[4].

References

1. X. Luo, B. Xu, T. Ohtsuki, R. Shindou: Physical Review B **101**, 020202(R), (2020).
2. T. Ohtsuki, T. Mano: Journal of the Physical Society of Japan **89**, 022001 (2020).
3. T. Mano, T. Ohtsuki: Journal of the Physical Society of Japan **88**, 123704 (2019).

4. K. Slevin, S. Kettemann, T. Ohtsuki: The European Physical Journal B **92**, 281 (2019).

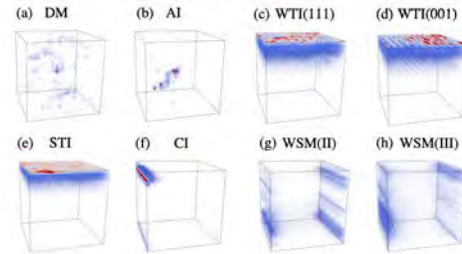


Figure 1: Typical 3D wave functions in real space in various phases. Taken from [2].

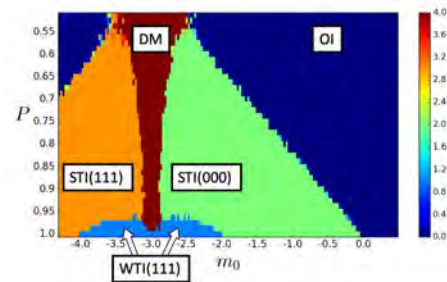


Figure 2: Phase diagram of quantum percolation in 3D topological insulator. OI (ordinary insulator), WTI (weak topological insulator), STI (strong topological insulator), and DM (diffusive metal). (ijk) indicates the weak indices.

Numerical study on low-energy states of quantum spin systems

Hiroki NAKANO

*Graduate School of Material Science, University of Hyogo
3-2-1 Kouto, Kamigori-cho, Ako-gun, Hyogo 678-1297, Japan*

It is difficult to precisely estimate physical quantities for many-body problems. Particularly, we often have to tackle such many-body problems in condensed matter physics. Quantum spin systems are typical many-body problems. Under circumstances, numerical approaches have widely and effectively been employed to examine the systems. Many computational investigations have been carried out and provided us with useful information and deeper understanding of the target systems.

It is well known that within the field of quantum spin systems, three methods are effectively used; the numerical diagonalizations, the quantum Monte Carlo (QMC) simulations, and the density matrix renormalization group (DMRG) calculations. Each of them has advantages and disadvantages at the same time. In the QMC simulations, large systems can be treated irrespective of their spatial dimensions although it is difficult to obtain precise evaluations due to the negative sign problem when the systems include frustrations. On the other hand, the DMRG method is very useful when spatial dimension of a target system is one irrespective of whether frustrations is present or absent in the system. However, this method is still under development for the cases when the spatial dimension is larger than one. The numerical diagonalization method can be applied irrespective of the spatial dimension and the presence of frustrations. Unfortunately, this method has a serious weak point that it can treat only very small system sizes. As one way to overcome this disadvantage, we successfully developed a hybrid-type parallelized code of Lanczos diagonalization[1]. If we use this Lanczos-diagonalization code, it

is possible to treat various large systems that have not been previously treated yet within this method. Therefore, we investigate various quantum spin systems by this method as a primary approach.

In the project in 2019, we tackled two systems. The first one is the $S = 1/2$ Heisenberg antiferromagnet on the kagome lattice with a specific distortion[2, 3]. We investigated a family of materials with Ti^{3+} $S = 1/2$ ions forming distorted kagome lattices. Employing all electron density functional theory technique, the Heisenberg Hamiltonian was established for each material; finite-size clusters for the Hamiltonians were numerically diagonalized. Our calculations successfully provided us with the magnetization processes, which enable us to analyze experimental measurements. The comparisons were quite good; our theoretical calculations succeeded in predicting the behavior in fields higher than the maximum field which the present experiments can reach presently.

The second one is the large- S Heisenberg antiferromagnet in one dimension[4]. Particularly, we focused our attention on the cases of $S = 5$ and $S = 6$. The case of $S = 5$ had been studied before in Ref. [1] where systems up to 10 sites were treated. We successfully carried out our huge-scale parallel calculation in the K computer using approximately 97% of the total computational nodes without any troubles and obtained novel results up to 14 sites of the target system. Note also that the Hilbert space dimension of 14-site cluster for the $S = 5$ chain is larger than the case of 20-site cluster for the $S = 2$ chain[5]. From the new results, our analysis gave a more precise estimation of

the $S = 5$ Haldane gap. In this study, we also attempted to estimate the Haldane gap for the case of $S = 6$, which had not been examined before. From our new estimates of the Haldane gaps for large S , the asymptotic formula of the Haldane gap was examined; we successfully determined the coefficient in the formula more precisely.

Our studies contribute to our deeper understandings of the various antiferromagnets and the nontrivial effect of quantum nature and frustration in magnetic materials.

References

- [1] H. Nakano and A. Terai: J. Phys. Soc. Jpn. **78** (2009) 014003.
- [2] H. O. Jeschke, H. Nakano, and T. Sakai: Phys. Rev. B **99** (2019) 140410(R)(1-6)
- [3] R. Shirakami, H. Ueda, H. O. Jeschke, H. Nakano, S. Kobayashi, A. Matsuo, T. Sakai, N. Katayama, H. Sawa, K. Kindo, C. Michioka, and K. Yoshimura: Phys. Rev. B **100** (2019) 174401(1-7)
- [4] H. Nakano, N. Todoroki, and T. Sakai: J. Phys. Soc. Jpn. **88** (2019) 114702(1-4)
- [5] H. Nakano and T. Sakai: J. Phys. Soc. Jpn. **87** (2018) 105002(1-2)

Efficient Sampling Simulation of the Soft Modes Significantly Contribute to Protein Properties

Kazuhiro TAKEMURA, Duy TRAN, Hiroaki HATA, Kenichiro TAKABA,
Mohamed Marzouk SOBEH, and Akio KITAO

School of Life Science and Technology, Tokyo Institute of Technology

Ookayama, Meguro, Tokyo 152-8550

We have developed a method to evaluate binding free energy differences of complex models generated by docking prediction using the all-atom molecular dynamics simulation and solution theory in the energy representation (ER), termed evERdock (evaluation with ER method of docking generated decoys)[1]. By evaluating binding free energy difference with the method, we previously showed that “near-native” models similar to crystal structure are successfully selected as the lowest energy structures in several complex systems. The method requires relatively short MD simulations (2 ns) and can calculate binding free energy difference among several hundreds of complex models. We also reported that refinements of docking generated decoys by relatively long MD simulation and averaging the binding free energies obtained from multiple snapshots further improved the evaluation of evERdock[2]. However, such treatments required additional computational costs. To address this problem, we propose a method

for efficiently selecting near-native decoys using Best Arm Identification (BAI), called evERDock BAI[3].

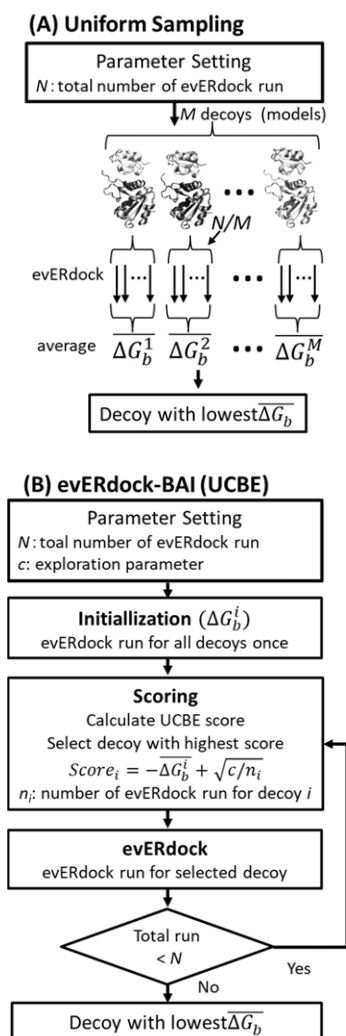


Fig. 1 Flows of (A) uniform sampling and (B) BAI (UCBE) based evaluation.

Let the number of evERdock runs decoys are N be M , respectively. If we conduct evERdock runs for all decoys equally (uniform sampling, US), all decoys are evaluated M/N times (Fig.1A). Fig. 1B shows the flow chart of evERdock-BAI using UCBE as a BAI algorithm. After all decoys are evaluated once, the algorithm repeatedly calculates UCBE scores, selects the decoy with the highest score, and conducts evERdock run for the selected decoy. Promising decoys for exploitation are evaluated by the first term of the score (binding free energy, $-\overline{\Delta G_b^i}$). The second term of the score contains the number of evERdock runs for the decoy i (n_i) in its denominator. Thus, the score decreases as the number of evERdock runs for a decoy i increases. As a result, unpromising decoys are sometimes selected, and exploration is realized. Such a balance between exploitation and exploration is essential to achieve an efficient and accurate prediction of the correct decoy.

We applied evERdock-BAI to three protein-protein complex systems (Fig. 2). Decoys are generated by rigid-body dockings. The number of decoys (N_{decoys}), the number of near-native decoys ($N_{\text{near-native}}$), and the number of total evERdock runs to achieve a prediction accuracy 95 % ($N_{95\%}$) using US and UCBE are shown in Table 1. For all three cases, $N_{95\%}$ using UCBE were smaller than those using US. The UCBE algorithm

successfully reduced computational cost by a factor of 2.20, 1.22, and 4.05 (values in parentheses in Table 1) for 1AY7, 1PPE, and 3SIC, respectively.

As shown above, we successfully improved the computational efficiency of the evERdock evaluation of protein-protein complex models by combining with BAI algorithm.

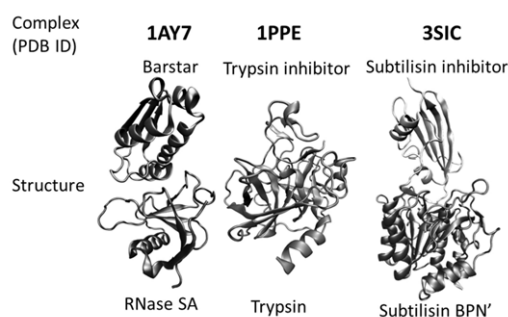


Fig. 2 Structures of target complexes

Table 1 Summary of results

Complex	1AY7	1PPE	3SIC
N_{decoys}	11	11	21
$N_{\text{near-native}}$	2	4	1
$N_{95\%}$ (US)	33	33	336
$N_{95\%}$ (UCBE)	15 (2.20)	27 (1.22)	83 (4.05)

References

- [1] K. Takemura, N. Matubayasi, and A. Kitao, J. Chem. Phys. 148, 105101 (2018).
- [2] A. Shinobu, K. Takemura, N. Matubayasi, and A. Kitao, J. Chem. Phys. 149, 195101 (2018).
- [3] K. Terayama, A. Shinobu, K. Tsuda, K. Takemura, and A. Kitao. J. Chem. Phys. 151, 215104 (2019).

Pseudo-fermion functional renormalization group approach for frustrated quantum spin systems

Kiyu FUKUI, Yukitoshi MOTOME, and Yusuke KATO

Department of Physics, The University of Tokyo, Bunkyo, Tokyo 113-0033

Department of Applied Physics, The University of Tokyo, Bunkyo, Tokyo 113-8656

Department of Basic Science, The University of Tokyo, Meguro, Tokyo 153-8902

Frustrated quantum spin systems have been studied intensively for very long time [1, 2]. It is impossible to solve them exactly mathematically in general. Therefore, numerical approaches to investigate frustrated quantum spin systems are indispensable. Numerical approaches used widely to study them are, for example, exact diagonalization (ED), quantum Monte Carlo (QMC), density matrix renormalization group (DMRG). Each method has pros and cons, of course. Since 2010s, a new method called pseudo-fermion functional renormalization group (PFFRG or pf-FRG) has been used gradually [3]. Although PFFRG overestimates ordering tendencies to magnetic orders [4], it can treat large-size systems and strongly-frustrated systems and detect quantum paramagnetism due to strong frustration.

In order to study quantum paramagnetism, particularly quantum spin liquid, we made up a PFFRG numerical code and tested it by reproducing previous studies. At first, we made PFFRG codes for SU(2) symmetrical systems (i.e. systems with Heisenberg-type interactions) [3] and benchmarked it. Then we extended our codes to systems with XXZ-type [4] and Kitaev-type [5] interactions.

Computational complexity of PFFRG calculation is scaled by $\mathcal{O}(N_L^2 \cdot N_\omega^4 \cdot N_\Lambda \cdot N_\sigma)$. N_L , N_ω , N_Λ , and N_σ are symmetry-reduced system size, the number of frequency mesh points, the number of energy cut-off grid points, and relative complexity due to symmetry of Hamilto-

nian (1 = Heisenberg Hamiltonian with time-reversal symmetry), respectively. Typically, $N_L = 10-20$, $N_\omega = 50-100$, and $N_\Lambda = 200-500$. Therefore, it is necessary to exploit parallelization. We submitted jobs parallelized by openMP+MPI to F144cpu queue using 64-144 nodes and $\mathcal{O}(1000)$ MPI processes. One PFFRG calculation with spin susceptibility calculation with vertices obtained by PFFRG takes one to several days. In addition, we tried to use GPU nodes by openACC directives in order to accelerate our PFFRG calculation.

References

- [1] C. Lacroix, P. Mendels, and F. Mila, *Introduction to Frustrated Magnetism* (Springer, New York, 2011).
- [2] H. T. Diep, *Frustrated Spin Systems* (World Scientific, Singapore, 2013) 2nd ed.
- [3] J. Reuther and P. Wölfle, Phys. Rev. B **81**, 144410 (2010).
- [4] S. Göttel, S. Andergassen, C. Honerkamp, D. Schuricht, and S. Wessel, Phys. Rev. B **85**, 214406 (2012).
- [5] J. Reuther, R. Thomale, and S. Trebst, Phys. Rev. B **84**, 100406(R) (2011).

Precise measurement of crystal nucleation rate in a hard-sphere colloidal system

Michio Tateno and Hajime Tanaka

*Department of Fundamental Engineering, Institute of Industrial Science, University of Tokyo
4-6-1 Komaba, Meguro-ku, Tokyo 153-8505*

Hard-sphere colloids have been intensively studied as one of the most fundamental systems that show a liquid-crystal transition [1]. In 2001, Auer and Frenkel pointed out [2] a huge mismatch in the crystal nucleation rate between results of light scattering experiments and numerical prediction based on Monte Carlo simulations using the Umbrella Sampling method. Revealing the physical origin behind this huge discrepancy is one of the central issues in this field [1]. Hydrodynamic interactions (HI) among colloids are viewed as one of the possible factors to cause the discrepancy since simulation results used for the comparison completely neglect HI. So far, two simulation studies based on different models incorporating HI have been performed to address this problem. However, these studies reported conflicting results: one concluded that HI might speed up crystal nucleation [3], whereas the other claimed that HI slows down it [4].

In this project, we study the crystallization kinetics of hard-sphere colloids by two simulation methods with HI (Fluid Particle Dynamics method: FPD [5]) and without (Brownian Dynamics method: BD). By comparing two results, we can investigate the impact of HI on the crystal nucleation process. By combining the FPD method with fluctuating hydrodynamics, we have shown that FPD simulations can almost perfectly reproduce the motion of colloids under thermal noise at low volume fractions while retaining statistical mechanical consistency between colloids and a

solvent. Furthermore, we have confirmed that this simulation approach can precisely reproduce the phase separation process of colloidal suspensions observed by confocal microscopy measurements without any adjustable parameters [6]. However, crystal nucleation is a rare event, and thus, the resulting computational cost is quite high. We have overcome this problem by speeding up our code, utilizing ISSP's GPGPU implementation services [7].

According to Ref. [2], the theoretical values of I change mainly by a small change in the volume fraction ϕ : for example, I at $\phi = 52.8\%$ differs from that at 53.4% by at least 4 orders of magnitude. Thus, in order to study the nucleation rate accurately, we need to estimate the volume fraction ϕ precisely. To realize this, we first check the volume fraction dependence of the virial pressure. In Fig. 1a, we show the results obtained by BD and FPD together with theoretical predictions (the Carnahan-Starling equation of a state in the liquid phase and the Speedy equation of a state in the solid phase). Here we can see almost perfect agreement between them, supporting the validity of our numerical simulation methods from the thermodynamic point of view.

Now we turn our attention to a dynamic aspect. Here we examine the volume-fraction dependence of the long-time self-diffusion constant, D_L as one of the most fundamental quantities to characterize colloidal dynamics. Figure 1b shows the results for FPD and BD, where we can see that D_L deviates from the diffusion coefficient for a free isolated particle

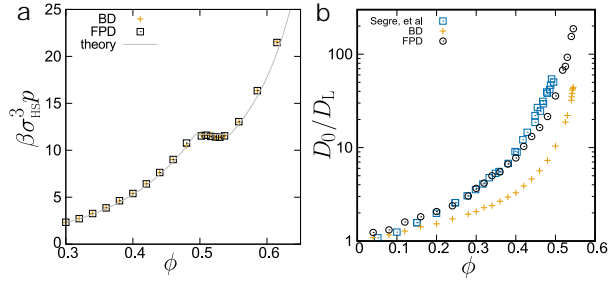


Figure 1: (a) Virial pressure in equilibrium states. Cross and square symbols represent the results obtained by BD and FPD simulations, respectively. Gary curve is the theoretical prediction for a hard-sphere system. (b) Volume fraction dependence of the long-time diffusion constant D_L scaled by that in the dilute limit D_0 . Cross and circle symbols represent the results obtained by BD and FPD simulation, respectively. The light blue square symbols are experimental data obtained by dynamic light scattering measurements for hard-sphere-like colloids with 5 % polydispersity [8].

D_0 for large ϕ , but the deviation is more significant for FPD than for BD, which depends on the presence or absence of hydrodynamic interactions. For example, we can see that D_L in BD is approximately four times larger than that in FPD at $\phi = 0.54$. In the figure, we also compare the simulation results with experimental data obtained by dynamic light scattering measurements for hard-sphere-like colloids with 5 % polydispersity [8]. Here we can see that there is a mismatch between FPD and BD, but there is a good agreement between FPD and the experimental results at least at intermediate volume fractions. To determine the nucleation rate I , we used an approach to monitor the temporal change of a cluster with the largest size. We compare I at $0.54 \leq \phi \leq 0.545$ between BD and FPD, by using D_L and the diameter of colloids as spatiotemporal units, and find that all nucleation rates collapse onto a single curve.

In summary, to examine the influence of HI on crystallization kinetics of hard-sphere colloids, we precisely compare simulation results with and without HI. We show that the long-

time diffusive dynamics of the colloids is more rapidly slowed down by HI with increasing volume fraction. We find that this long-time diffusion controls the nucleation rate and that it is possible to account for most of the effects of HI by rescaling with this time scale. The research results are summarized in Ref. [9].

References

- [1] T. Palberg: J. Phys. Cond. Matt. **33** (2014) 333101
- [2] S. Auer and D. Frenkel: Nature **409** (2001) 1020
- [3] M. Radu and T. Schilling: EPL **105** (2014) 26001
- [4] D. Roehm, S. Kesselheim and A. Arnold: Soft matter **10** (2014) 30
- [5] H. Tanaka and T. Araki: Phys. Rev. Lett. **85**, (1999) 1338; A. Furukawa and H. Tanaka: Phys. Rev. Lett. **104**, (2010) 245702; A. Furukawa, M. Tateno and H. Tanaka: Soft Matter **14** (2018) 3738
- [6] M. Tateno and H. Tanaka: npj Comput. Mater. **5** (2019) 40
- [7] M. Tateno, K. Takae and H. Tanaka, “GPGPU implementation of Fluid Particle Dynamics method”, Activity Report in 2017
- [8] P. N. Segre and S. P. Meeker, P.N. Pusey and W. C. K. Poon: Phys. Rev. Lett. **75** (1995) 958
- [9] M. Tateno, T. Yanagishima, J. Russo, and H. Tanaka: Phys. Rev. Lett. **123**, (2019) 258002

Impact of hydrodynamic interactions on colloidal dynamics near a critical point

Michio Tateno and Hajime Tanaka

*Department of Fundamental Engineering, Institute of Industrial Science, University of Tokyo
4-6-1 Komaba, Meguro-ku, Tokyo 153-8505*

The behaviors of simple liquids near a critical point are well-understood both from a theoretical and experimental point of view. The density fluctuation decays exponentially with single relaxation time. Contrary to this knowledge, several studies on colloidal suspensions using light scattering experiments report that time correlation function of concentration fluctuations in the vicinity of the critical point show nonexponential decay [1].

The central aim of this project is to reveal the physical mechanism underlying the non-exponential decay. As a possible candidate to bring about this unconventional dynamical behavior in colloidal suspensions, we focus on hydrodynamic interactions (HI), which is an essential difference between simple liquids and colloidal suspensions. We use two different simulation methods; the Brownian dynamics (BD) method neglecting HI and Fluid particle dynamics (FPD) method incorporating HI [2]. We compare the results from two simulation methods and aim to examine the effect of HI on dynamical critical phenomena.

In order to capture dynamical critical phenomena numerically, a long time simulation is required, since the relaxation time for density fluctuation grows dramatically as approaching to a critical point. However, FPD method is numerically costly because it is based on the direct computation of Navier-Stokes equations. To overcome this, we implemented GPU on our FPD codes utilizing a service provided by ISSP. To further suppress numerical cost, we

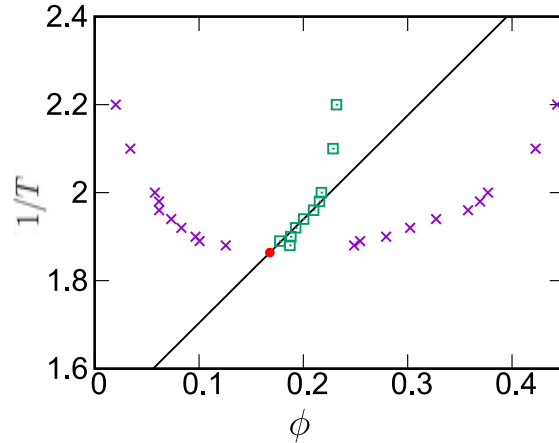


Figure 1: Temperature-volume fraction phase diagram. The cross symbols show the gas and liquid phases. The black line represents the tieline, which is obtained from asymptotic behavior of median between two phases (square) towards the vertex of binodal line. We fit a parabolic function to the cross symbols with volume fraction and tieline as two axis, and determine the critical point (circle).

adopt a rather short-range interaction. More specifically, we use the modified Lennard-Jones potential with cutoff length $r_c = 1.7\sigma$: $U(r) = 4\epsilon((\sigma/r)^{24} - (\sigma/r)^{12} + c_2(r/\sigma)^2 + c_0)$ for $r < r_c$ and $U(r) = 0$ for otherwise. Here c_2 and c_0 are constants to satisfy $U(r_c) = 0$ and $U'(r_c) = 0$. This short-range nature of intercolloid potential suppresses the correlation length of density fluctuations and allows us to perform simulations with a rather small system size ($L = 17.3\sigma$).

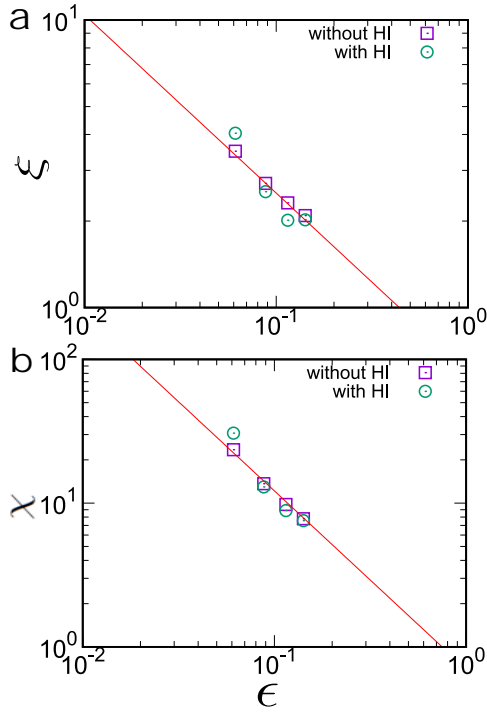


Figure 2: The correlation length ξ (a) and susceptibility χ (b) as a function of critical parameter $\epsilon := T_c/(T - T_c)$. The red line represents a power-law function with critical exponent (approximately 0.62 and 1.24 for ξ and χ , respectively)

We study the static behavior of colloidal suspensions near a critical point. We perform simulations for states on tieline (see the black line in Fig. 1) approaching to a critical point (red circle point). Figure 2 shows the correlation length ξ and susceptibility χ , which is determined by fitting the static structure factor with the Ornstein-Zernike form. Here we can see that the two results obtained from BD and FPD show an excellent agreement with each other, and both follow to power-law function with the critical exponent. These trends are consistent with a well-known fact that HI does not influence the thermodynamic behaviors of colloidal suspensions. Next, we compute the auto-correlation function of density fluctuation and evaluate the dependence of lifetime on the critical parameter ϵ . We find that the auto-

correlation function decays exponentially with a single time τ_ξ scale, and τ_ξ is proportional to the cube of ξ , which coincides with the case of dynamical critical phenomena for simple liquids.

In summary, we performed numerical simulations for colloidal suspensions with and without HI and examined the effect of HI on the dynamical critical phenomena. We obtained the results that HI does not influence both static and dynamical behaviors. However, due to the constraint by numerical cost, the critical parameter that we accessed is limited ($0.05 < \epsilon$), and the anomaly in the time correlation function of concentration fluctuations is reported in a smaller ϵ . To make a definitive conclusion for this phenomenon, we realize a much larger simulation.

References

- [1] J. Rouch, et al.: Phys. Rev. Lett. **71**, (1993) 1947; B. M. Fine, et al.: Phys. Rev. Lett. **74**, (1995) 198; B. M. Fine, et al.: J. Chem. Phys., **104**, (1996) 326
- [2] H. Tanaka and T. Araki: Phys. Rev. Lett. **85**, (1999) 1338

Coarsening mechanism of network-forming phase separation in colloidal suspensions

Michio Tateno and Hajime Tanaka

*Department of Fundamental Engineering, Institute of Industrial Science, University of Tokyo
4-6-1 Komaba, Meguro-ku, Tokyo 153-8505*

Phase separation is one of the most fundamental physical phenomena in nature to form a spatially inhomogeneous structure, whose basic coarsening laws were well-established in the 20th century. However, the conventional mechanisms are valid only near the critical point, and the coarsening behavior under deep quench remains elusive. We noticed that for network-forming deeply-quenched phase separation, unusual coarsening behavior of network structures had been reported in experiments for various soft matter such as colloidal suspensions [1], protein solutions [2] and lyotropic liquid crystal [3]: their characteristic network size ℓ commonly grows as $\ell \sim t^{1/2}$ while retaining their connectivity. The goal of this project is to reveal the physical principle behind the growth exponent 1/2.

To address this problem, we used a hydrodynamic simulation model for colloidal suspensions, Fluid Particle Dynamics (FPD) method [5], which is based on the direct computation of the Navier-Stokes equation, and studied network-forming process during gas-liquid phase demixing. To capture the coarsening of network structure without suffering from a finite-size effect, we developed GPU-MPI hybrid codes utilizing a service provided by ISSP and realized a large scale simulation. Since our interest is in phase separation dynamics under a deep quench, we neglect thermal noise.

We show in Fig. 1 the time evolution of phase-separation structures in the colloidal suspension. Here we can clearly see that a

space-spanning network structure is spontaneously formed in the early stage, and its characteristic length scale grows afterward. By computing the temporal change of the first moment of the structure factor, we confirmed that the characteristic length of network structure ℓ follows a power-law growth with exponent 1/2 while retaining self-similarity.

In the absence of thermal noise at zero temperature, the coarsening cannot be due to thermal activation but should be of purely mechanical nature. Then, we focus on the slow elastic dynamics of dense colloidal aggregates and analyze the strain field ϵ by coarse-graining the displacements of colloidal particles. Here in particular, we consider the time evolution of the distribution function, $P(\epsilon)$, from a reference time t_0 to an arbitrary time $t_0 + t'$. We find that the distribution functions are collapsed onto a master curve after scaling the argument ϵ by t'/t_0 (see Fig. 2), indicating that the elastic relaxation of network structure controls the speed to the coarsening process.

Here we note that the exponent 1/2 is observed only in the presence of solvent component: for example, the Brownian dynamics method completely neglecting the motion of a solvent does not reproduce the exponent 1/2 (see, e.g., Ref. [4]). This fact implies that dynamic coupling between densely-packed colloid and a solvent saturated in the colloid-rich domain plays a crucial role. Biot's poroelastic theory is known as a model to describe the motion of fluid saturated elastic materials. By

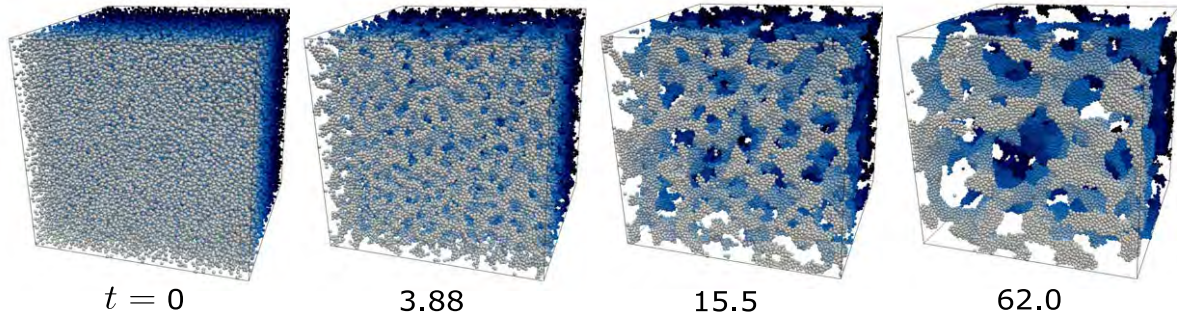


Figure 1: Coarsening behavior of network-forming phase separation of colloidal suspensions. Particles are colored to distinguish front particles from back ones.

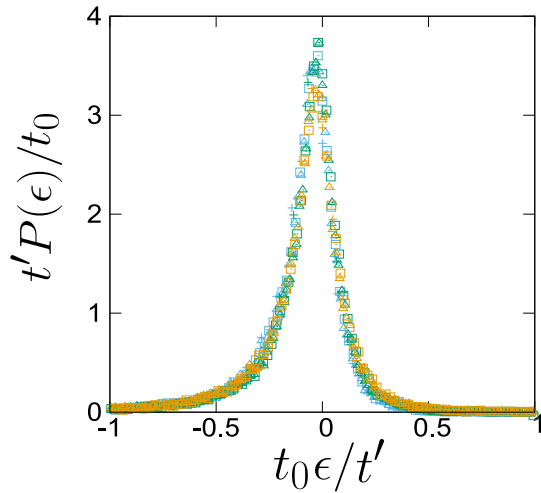


Figure 2: $P(\epsilon)$ after scaling ϵ by t'/t_0 . The data are sampled from the data whose reference time is $t_0 = 31.0$ (blue), 46.5 (green), 62.0 (brown). Then, cross, triangle and square symbols represent the data at $t'/t_0 = 0.001, 0.01, 0.02$, respectively.

performing a scaling analysis on this theory, we obtain a coarsening law, $\ell \sim (D_p t)^{1/2}$, where D_p is a poroelastic diffusibility. See Ref. [6] for further discussion on the validity of the coarsening law.

In summary, we performed a large-scale hydrodynamic simulation for colloidal suspensions and studied the dynamic process of network-forming phase demixing. We found that the coarsening process has self-similarity,

and the domain grows with the growth exponent of $1/2$. We revealed that the exponent is a consequence of slow elastic relaxation of the network-forming dense phase, whose limiting process is permeation flow of the solvent.

References

- [1] H. Tanaka, et al., J. Phys.: Condens. Matter, **17**, (2005) L143; A. Bailey, et al.: Phys. Rev. Lett. **99**, (2007) 205701; M. Tateno and H. Tanaka, npj Comput. Mater., **5**, (2019) 40
- [2] H. Tanaka and Y. Nishikawa: Phys. Rev. Lett., **95**, (2005) 078103
- [3] Y. Iwashita and H. Tanaka: Nat. Phys., **5**, (2006) 147
- [4] A. Furukawa and H. Tanaka: Phys. Rev. Lett. **104**, (2010) 245702.
- [5] H. Tanaka and T. Araki: Phys. Rev. Lett. **85**, (1999) 1338
- [6] M. Tateno and H. Tanaka: Nat. Commun., under review.

Structural origin of glassy slow dynamics

Hua Tong and Hajime Tanaka

*Department of Fundamental Engineering, Institute of Industrial Science, University of Tokyo
4-6-1 Komaba, Meguro-ku, Tokyo 153-8505*

Despite the use of glasses for thousands of years, the nature of glass and the glass transition remains probably “the deepest and most interesting unsolved problem” in condensed matter physics and materials science. In contrast to crystallization where the solidity emerges as a result of the formation of long-range periodic order, the drastic dynamical slowing down toward the glass transition is accompanied by little change in the geometric structure, as measured by two-point correlators accessible through diffraction and scattering experiments [1, 2]. Therefore, glasses are widely thought as the epitome of completely disordered state of materials and the glass transition is described as a purely dynamical phenomenon in kinetically constrained models. The physical scenarios which posit a growing static order and hence a thermodynamic origin behind the slowing down of glassy dynamics have regained popularity since the discovery of the so-called dynamic heterogeneity in 1990s. The spatially correlated domains which move significantly faster or slower than the average are proposed to be the long sought-after cooperatively relaxing regions (CRRs), which is the core concept of Adam-Gibbs theory of glass transition and its modern version, i.e., the random first-order transition (RFOT) theory. Meanwhile, a growing correlation length characterizing the extent of heterogeneous dynamics is also suggestive of a similarity between glass transition and the critical phenomena [3–5]. However, since the dynamic heterogeneity is only accessible through dynamic variables [6, 7], the crucial physical mechanism is still not established, namely a quantitative characterization of the glassy structural order and its link to dynamics, which precludes a decisive

underpinning to the (thermodynamic) nature of the glass transition.

To look for key structural features responsible for glassy dynamics, one typical approach is to consider specific physical aspects of the local atomic environment, e.g., free volume, potential energy, and symmetry. The free volume approach [8, 9] and the inherent potential energy based on the potential energy landscape (PEL) formalism enjoyed early success showing a clear macroscopic correlation (that is, for globally averaged quantities) with dynamics, but not microscopically at a particle level [10–12]. Therefore, more efforts have been devoted to the identification of locally favored structures (LFSs) based on symmetry considerations. For instance, icosahedral [13, 14], crystal-like orders [3, 4, 15], or more complicated topological clusters [16] are identified and suggested as the origin of slow dynamics in different glass-forming liquids. However, the general relevance of LFSs in glassy slow dynamics remains controversial due to its strong and sensitive system dependence. This may arise from the system-dependent nature of locally low free-energy configurations [4]. Another approach developed by Cubuk *et al.* recently is to define some structural quantity, “softness”, based on machine-learning methods [17, 18]. The strong correlation observed between softness and structure relaxation suggests that important structural features are captured. However, softness is defined in a high-dimensional space with more than 100 structure functions, prohibiting a clear identification of glassy structural order. It is desirable to unveil the structural characteristics of glass-forming liquids from a physically inspired perspective.

Recently in ref. [12], we constructed a set of structural order parameters, namely Θ in 2D and Ω in 3D, to capture sterically favored structures with high local packing capability in hard-sphere-like glass formers. In the absence of obvious density fluctuations beyond the particle scale, such sterically favored structures provide more room for particle motions through better arrangement, and hence higher correlational (or, vibrational) entropy and lower free energy [4]. This is analogous to the crystallization process of hard spheres. We showed at a picture level that the mobility develops systematically following the structural order parameter field and confirmed a common structural origin for both fast β and slow α dynamics.

In this study, we move a crucial step forward to study *quantitatively* the formation of

structural order and its relation to slow glassy dynamics. We find that the degree of glassy structural order follows a linear scaling law with temperature, which initiates around the onset temperature T_{on} of the super-Arrhenius dynamics and is ceased by the dynamical glass transition T_g . This provides us with a direct quantitative relation between structural order and structure relaxation time τ_α , and therefore represents a key thermodynamic characteristic of the glass transition. More interestingly, based on a nonlocal excitation scenario, we confirm that such an intimate structure-dynamics correlation is valid even microscopically at a particle level. Therefore, our results may provide an essential piece in the microscopic theoretical description of the long-standing glass transition problem from a structural perspective.

-
- [1] J. C. Dyre, Rev. Mod. Phys. **78**, 953 (2006).
 [2] K. Binder and W. Kob, *Glassy materials and disordered solids: An introduction to their statistical mechanics* (World Scientific, 2011).
 [3] H. Tanaka, T. Kawasaki, H. Shintani, and K. Watanabe, Nature Mater. **9**, 324 (2010).
 [4] H. Tanaka, Eur. Phys. J. E **35**, 113 (2012).
 [5] J. S. Langer, Phys. Rev. E **88**, 012122 (2013).
 [6] M. D. Ediger, Annu. Rev. Phys. Chem. **51**, 99 (2000).
 [7] L. Berthier and G. Biroli, Rev. Mod. Phys. **83**, 587 (2011).
 [8] M. H. Cohen and G. S. Grest, Phys. Rev. B **20**, 1077 (1979).
 [9] F. W. Starr, S. Sastry, J. F. Douglas, and S. C. Glotzer, Phys. Rev. Lett. **89**, 125501 (2002).
 [10] A. Widmer-Cooper and P. Harrowell, Phys. Rev. Lett. **96**, 185701 (2006).
 [11] A. Widmer-Cooper and P. Harrowell, J. Non-Cryst. Solids **352**, 5098 (2006).
 [12] H. Tong and H. Tanaka, Phys. Rev. X **8**, 011041 (2018).
 [13] F. C. Frank, Proc. R. Soc. Lond. A **215**, 43 (1952).
 [14] P. J. Steinhardt, D. R. Nelson, and M. Ronchetti, Phys. Rev. B **28**, 784 (1983).
 [15] M. Leocmach, J. Russo, and H. Tanaka, J. Chem. Phys. **138**, 12A536 (2013).
 [16] C. P. Royall and S. R. Williams, Phys. Rep. **560**, 1 (2015).
 [17] E. D. Cubuk, S. S. Schoenholz, J. M. Rieser, B. D. Malone, J. Rottler, D. J. Durian, E. Kaxiras, and A. J. Liu, Phys. Rev. Lett. **114**, 108001 (2015).
 [18] S. S. Schoenholz, E. D. Cubuk, D. M. Sussman, E. Kaxiras, and A. J. Liu, Nature Phys. **12**, 469 (2016).

Universality of bulk-edge correspondence by numerical methods

Y. Hatsugai

*Department of Physics, University of Tsukuba
1-1-1 Tennodai, Tsukuba 305-8571, Ibaraki, Japan*

One of the key concepts of the topological phases is the bulk-edge correspondence, that relates non-trivial topology of the bulk to the low energy physics near boundaries or impurities[1]. Non-trivial bulk topology is hidden for low energy physics of the bulk and most of the characteristic and experimental features appear as generalized edge states living near the boundaries. Although its historical example is a quantum phenomenon (quantum Hall effect), its validity is much more universal and the concept is applicable even for non-quantum phenomena such as photonic crystals of classical electromagnetic field and even classical mechanics of periodic systems. Using a formal analogy among the various systems, one can define a Berry connection for the bulk (even for the classical systems). Although there is no physical, at least, direct meaning for the topological quantities based on the Berry connection, the edges states predicted by the bulk-edge correspondence are physical observables. Such a hidden Berry connection of the bulk and topological numbers support the edge states of various physical phenomena. This is the universality of the bulk-edge correspondence, which we numerically try to establish in the project.

The corner states of the higher order topological phases are such generalized edge states which characterize the specific bulk topology reversely. We have shown such examples supported by the quantized Z_N ($n \in \mathbb{Z}$) Berry phases as a bulk topological invariants for a quantum three dimensional model [2] and classical mechanics on a Kagome lattice[3]. We have further proposed a higher order topological Mott insulator that hosts spin-charge separated corner states and demonstrated its validity numerically[4].

We also performed a topological characterization of the $J_1 - J_2$ spin ladder for higher integer spins using a quantized Berry phases[5]. It justifies a generalized valence bond solid state as the adiabatic limit of the ground state obtained numerically. Then sequential topological phase transitions associated with the valence bond reconstruction are clearly demonstrated.

We further discussed several other topics related such as non hermitian topological phenomena[6, 7, 8, 9] and obtained new insight for the adiabatic heuristic argument[10] that is a conceptual/historical background of topological characterization.

References

- [1] Yasuhiro Hatsugai, Phys. Rev. Lett. **71**, 3697 (1993).
- [2] Hiromu Araki, Tomonari Mizoguchi and Yasuhiro Hatsugai: Phys. Rev. Research **2**, 012009(R) (2020).
- [3] Hiromasa Wakao, Tsuneya Yoshida, Hiromu Araki, Tomonari Mizoguchi, and Yasuhiro Hatsugai: Phys. Rev. **101**, 094107 (2020).
- [4] Koji Kudo, Tsuneya Yoshida, and Yasuhiro Hatsugai : Phys. Rev. Lett. **123**, 196402 (2019).

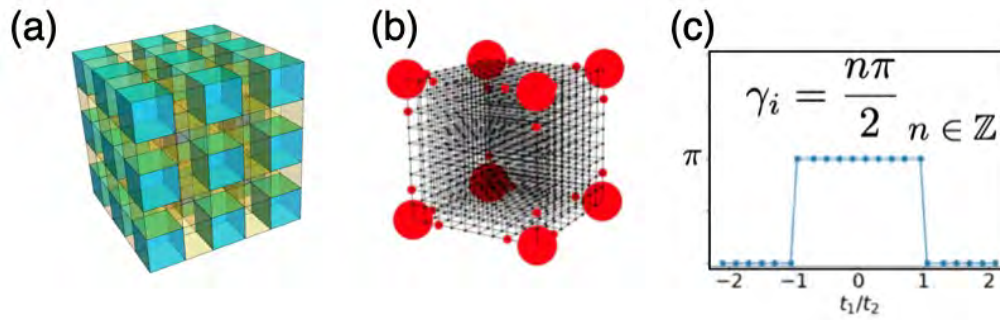


Figure 1: (a) Schematic lattice structure of the three dimensional BBH model, (b) corner states and (c) Z_4 Berry phases (See. Ref.[2])

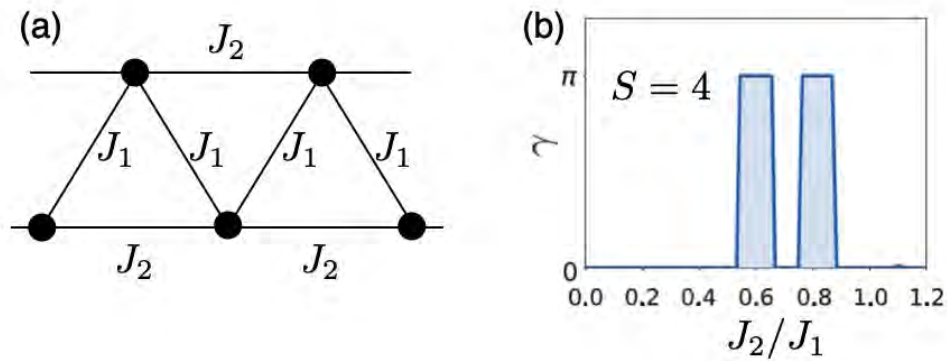


Figure 2: (a) $J_1 - J_2$ Heisenberg spin chain of integer $S(\geq 1)$ and (b) Z_2 Berry phase of $S = 4$ (8 site system with periodic boundary condition) (See Ref. [5])

- [5] Shota Fubasami, Tomonari Mizoguchi and Yasuhiro Hatsugai: Phys. Rev. B **100**, 014438 (2019).
- [6] Tsuneya Yoshida, Koji Kudo, and Yasuhiro Hatsugai: Scientific Reports **9**, 16895 (2019).
- [7] Tsuneya Yoshida and Yasuhiro Hatsugai: Phys. Rev. B **100**, 054109 (2019).
- [8] Tsuneya Yoshida, Robert Peters, Norio Kawakami, Yasuhiro Hatsugai: arXiv:2002.11265
- [9] Tsuneya Yoshida, Tomonari Mizoguchi, and Yasuhiro Hatsugai: arXiv:1912.12022
- [10] Koji Kudo and Yasuhiro Hatsugai : arXiv:2004.00859.

Kinetics of phase transition and polyamorphism

Kazuhiro Fuchizaki, Kei Watanabe, and Hiroki Naruta

Department of Physics, Ehime University, Matsuyama 790-8577

In FY2019, we have undertaken two subjects, as reported briefly below. The first task has been almost completed, and its full report will soon be submitted elsewhere. The second one is still at a preliminary stage and will be ongoing in FY2020.

Growth of density fluctuations at the beginning of a phase separation

The concept of spinodal has been examined for an Ising system [1]. However, no explicit discussion has been found for a fluid system, which is believed to belong to the same unitary class. Ushcats has suggested [3], extending the equation of state beyond the thermodynamically stable region, that the spinodal line of the modified Lennard-Jones (mLJ) system [2] approaches the liquid-gas coexistence (binodal) line. Our prediction based on the coarse-graining limit for the coarse-grained free energy, estimated by applying the block-spin coarsening technique, supports Ushcats' conjecture [4]. It is then highly anticipated that the "dynamics" of a system also depends on a coarsening level.

We conducted isothermal–isobaric molecular dynamics (MD) simulations for an mLJ system consisting of 4×10^6 particles to examine the dynamical process of liquid–gas phase separation. Length, time, and temperature are expressed in units of σ , $\sqrt{m\sigma^2/\epsilon}$, and ϵ/k_B [5], respectively, where σ and ϵ are the fundamental length and energy scales of the mLJ potential function and k_B denotes Boltzmann's constant. The critical temperature, pressure, and density of the mLJ system are $T_c = 1.0762(2)$, $p_c = 0.09394(17)$, and $\rho_c = 0.331(3)$, respectively. We treated two systems with differ-

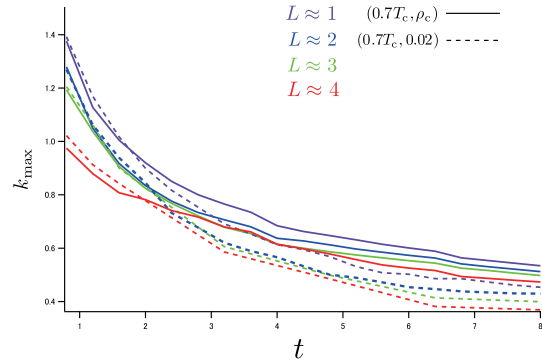


Figure 1: The peak position of S_L is plotted against time with the same color for every coarsening scale of L . Those at ρ_c (0.02) are delineated by solid (dotted) lines.

ent density; 0.02 and ρ_c . The fluid system well-equilibrated at $20T_c$ was instantaneously brought to $0.7T_c$ to undergo phase separation. The lower- and critical-density systems were expected to be quenched in the metastable and unstable regions, respectively, judging from the shape of the coarse-grained free energy.

The term, "local density," has been quite often used in mesoscopic descriptions. However, it has been far unclear what is meant by "local." In this case, we can define the local density unambiguously using the length L , the coarse-graining scale based on which the coarse-grained free energy was defined [4].

Based on this well-defined "local" density and its fluctuations around the average density, we defined the structure factor S_L . Figure 1 shows the time evolution of S_L after quenching. On the short-time side ($t < 2$), L predominantly determines the peak position of S_L , whereas it approaches the value determined by the average density on the long-time side ($t > 2$).

To examine in detail the L -dependence of the wavelength at which structural destabilization occurs, S_L was scaled by its peak position and height. The dynamical process in another state, obtained by quenching the critical-density system to $0.97T_c$, was also examined. We could identify in the short-time region the new universal process (Figure 2), in which phase separation proceeds in a statistically self-similar fashion irrespective of the average density, quenching temperature as well as the coarsening length. We name this stage a “super-early” stage.

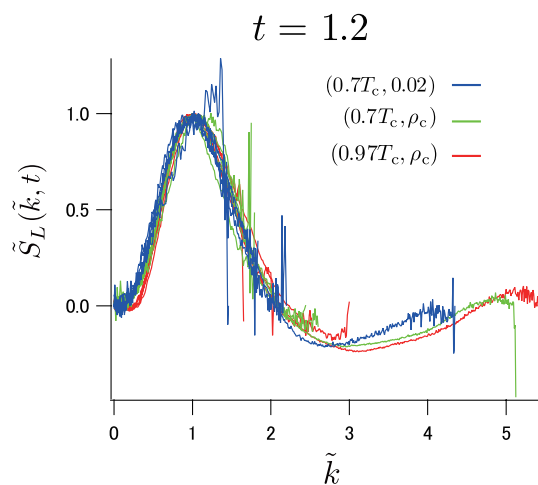


Figure 2: The scaled structure factors at three different states fall into a single curve when plotted against scaled wavelength, implying the existence of universality in a phase separation process right after a quench.

Estimating entropy of a fluid

A method proposed by Goddard *et al.* [6] has been widely used for evaluating entropy of a disordered system even with such a kind of network structure. The entropy is generally estimated from the density of states (DOS), which is obtainable through Fourier inversion of the velocity autocorrelation. Goddard *et al.* have claimed that a DOS of a fluid state can be constructed from those of solid and gas states [6]. This claim does not have any physical basis. Although an LJ fluid was used to testify their claim [6], we employ as another simple liquid an mLJ system to thoroughly examine their

assertion.

An isochoric–isothermal MD simulation generated an equilibrated mLJ fluid consisting of 2048 particles. We employed such a small number of particles because Goddard *et al.* used for a similar size for an LJ fluid [6]. Similar finite-size effects would then be involved in the results. We chose for this purpose three states with density 5.00×10^{-2} , ρ_c , and 0.600 along the isotherm $1.001T_c$, where T_c is the aforementioned critical temperature of the mLJ system [6]. The density is again expressed in terms of the mLJ units.

The entropy of the three states was also calculated using the λ -integration [7], which is too costly but can give the numerically exact result. The entropies based on the method of Goddard *et al.* could not well reproduce the λ -integration based ones. We should undertake a critical review of their basic idea.

References

- [1] K. Kaski, K. Binder, and J. D. Gunton, *Phys. Rev. B* **29**, 3996 (1984).
- [2] Y. Asano and K. Fuchizaki, *J. Chem. Phys.* **137**, 174502 (2012).
- [3] M. V. Ushcats, *J. Chem. Phys.* **141**, 101103 (2014).
- [4] K. Fuchizaki and K. Watanabe, *J. Phys. Soc. Jpn.* **87**, 114006 (2018).
- [5] K. Okamoto and K. Fuchizaki, *J. Phys. Soc. Jpn.* **86**, 034003 (2017).
- [6] S. Lin, M. Blanco, and W. A. Goddard, *J. Chem. Phys.* **119**, 11792 (2003).
- [7] J. Q. Broughton and G. H. Gilmer, *J. Chem. Phys.* **79**, 5095 (1983).

Ground-State Phase Diagram of the $S=1/2$ Kitaev- Γ model on a Honeycomb Lattice

Takafumi SUZUKI

Graduate School of Engineering,

University of Hyogo, Shosha, Himeji, Hyogo 670-2280

We have studied the ground-state phase diagram of the $S=1/2$ Kitaev- Γ model on a honeycomb lattice [1] and quantized $\Delta S=2$ excitation spectra by confinement in an $S=1$ spin chain [2].

First, we have investigated the ground-state phase diagram of the $S=1/2$ Kitaev- Γ model on a honeycomb lattice with the numerical exact diagonalization method, DMRG and cluster-series expansion method [3]. By changing the magnitude of interactions on each bond, the model connects with three characteristic points, where the model is described by spin chains, isolated dimers, or an isotropic honeycomb-lattice model. The obtained results have clarified that in the spin chain limit, two Tomonaga-Luttinger (TL) liquid phases and three non-TL liquid phases appear when the ratio of the Kitaev interaction and the Γ interaction changes. In the dimer limit, the dimerized state with the lowest energy is $|t_x\rangle = (|\uparrow\uparrow\rangle - i|\downarrow\downarrow\rangle) / \sqrt{2}$, when the positive Γ interaction and the negative Kitaev interaction are considered. We have found that this $|t_x\rangle$ state can survive up to the isotropic point.

Next, we have studied low-energy excitations of an $S=1$ Ising spin chain with the negative single-ion anisotropy in magnetic fields. We have calculated the dynamical structure factor with the infinite time-evolving block decimation (iTEBD) method [4]. We have found that when the transverse magnetic field is absent, both a $\Delta S=2$ excitation continuum and one-magnon isolated mode appear in the low-lying excitation. This $\Delta S=2$ excitation continuum is quantized by the weak longitudinal magnetic field. The quantized $\Delta S=2$ excitation spectra originate from the confinement of two domain walls and the excitation energies of the quantized $\Delta S=2$ spectra are well explained the negative zeros in the Airy function.

References

- [1] Y. Yamada, et al., in preparation.
- [2] T. Suzuki and S. Suga, *J. Phys. Soc. Jpn.* **88** (2019) 053702.
- [3] J. Oitmaa, et al., *Series Expansion Methods for Strongly Interacting Lattice Models*, Cambridge University Press, 2006.
- [4] H. N. Phien, et al., *Phys. Rev. B* **86** (2012) 245107.

Macroscopic properties characterized by an extended thermodynamic functions to nonequilibrium

Naoko NAKAGAWA

*Department of Physics, Ibaraki University
2-1-1 Bunkyo, Mito, Ibaraki 310-8512*

Thermodynamic functions such as entropy and free energy play an essential role in equilibrium systems. In order to extend these powerful functions to various non-equilibrium systems, such as thermal conduction systems and external force-driven systems, we have performed numerical experiments on the systems shown in Figs. 1 and 2.

Figure 1 shows a one-dimensional system of particles under thermal conduction that interact with each other at the Leonard-Jones potential, and each particle is subjected to a constant external force (gravity). Various local thermodynamic quantities such as temperature, density, pressure, and chemical potential were determined by molecular dynamics simulations, and from these quantities the free energy and entropy of the whole system were estimated. The thermodynamic relation is found to give the free energy change of the whole system when the temperature equivalent to the total kinetic energy of the system and the spatial average pressure are adopted as temperature and pressure for the system, respectively. The equation of state has an additional effect from the second order of the external force, implying a limit to the global view of the thermodynamic system under the external force.

Figure 2 shows a two-component fluid under thermal conduction separated by a semi-permeable membrane. The osmotic pressure is determined from the balance of the chemical potentials in the isothermal state, but the

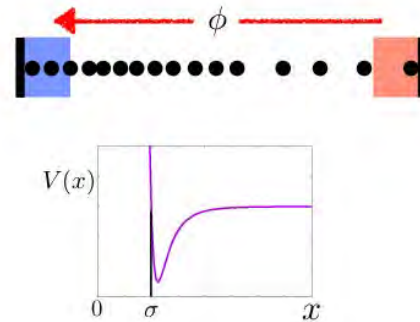


Figure 1: Heat conduction system under an external force.

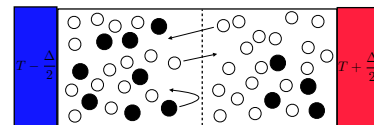


Figure 2: Two component fluid separated by a semi-permeable membrane.

chemical potentials are not spatially uniform in the thermal conduction state. In order to explore the principle of determining the osmotic pressure under thermal conduction, molecular dynamics simulations are performed and the dependence of the osmotic pressure on various parameters is investigated. We used the LAMMPS in order to achieve efficient results.

References

- [1] N. Nakagawa and S.-i. Sasa: J. Stat. Phys. **177** (2019) 825.

Development of data-driven science to materials science

Koji HUKUSHIMA

*Department of Basic Science, University of Tokyo
3-8-1 Komaba, Meguro-ku, Tokyo 153-8902*

In recent years, data-driven science methods have been attracting attention and have been applied to condensed matter physics and materials sciences. There are two main purposes to analyze the data obtained as a result of experiments and numerical experiments. One would be to extract the mathematical structure behind the data, and the other would be to make predictions to get the next data.

In this project, we carried out the tasks corresponding to the above-mentioned two purposes as actual problems. As the former problem, the model Hamiltonian was estimated from experimental data with a magnetic compound. As an example of the latter problem, we have conducted research on data-driven scientific methodologies in crystal structure search.

First, we proposed a data-driven methods to extract the spin Hamiltonian with uncertainty from multiple experiments. Using our method, an effective model of $\text{KCu}_4\text{P}_3\text{O}_{12}$ is determined from the experimentally observed magnetic susceptibility and magnetization curves with various temperatures under high magnetic fields. An effective model is the quantum Heisenberg model on a zigzag chain with eight spins in which four independent parameters are contained. Based on Bayesian statistics, these four parameters were estimated using MCMC sampling from the posterior distribution with experimental data as input. Our method yields that $J_1 = 8.54 \pm 0.51$ meV, $J_2 = -2.67 \pm 1.13$ meV, $J_3 = -3.90 \pm 0.15$ meV, and $J_4 = 6.24 \pm 0.95$ meV, describes these measured results well. Evaluation of these error bars is possible only by evaluating noise. The relations among the estimated magnetic

interactions or physical quantities are also discussed. These are the advantages of sampling from the posterior distribution. The obtained effective model is useful to predict hard-to-measure properties such as spin gap, spin configuration at the ground state, magnetic specific heat, and magnetic entropy.

Next, we studied the efficiency of Bayesian optimization as a method of selecting the next candidate when searching for a crystal structure. Bayesian optimization is a global optimization machine learning technique for a black-box function that requires a large amount of computation to be evaluated. A crystal structure is represented by a numerical vector called a descriptor that is used to quantify how similar structures are. This descriptor is an input of the crystal structure search with Bayesian optimization. The efficiency of the optimization significantly depends on the choice of the descriptor. We evaluated its efficiency with a varying parameter value in the descriptor[1]. Applying the crystal structure search to crystalline silicon shows that the efficiency of the search depends heavily on the parameter value. We find that the efficiency is linked to the distribution of the descriptor. Therefore, we introduce an information measure of the distribution to estimate an appropriate parameter value for performing the crystal structure search efficiently. The measure can also be used to predetermine an appropriate parameter value. The validity of the measure is confirmed with its applications to silicon oxide and yttrium cobalt alloy.

[1] N. Sato, *et al.* Phys. Rev. Materials **4**, (2020) 033801.

Unified understanding of early-time nonequilibrium relaxation in Monte Carlo simulations

Yoshihiko NONOMURA

MANA, National Institute for Materials Science

Namiki 1-1, Tsukuba, Ibaraki 305-0044

Recently we numerically revealed that the critical nonequilibrium relaxation (NER) behaviors in cluster algorithms are described by the stretched-exponential simulation-time dependence of physical quantities in various spin systems [1], and we derived such a relaxation formula phenomenologically [2].

Quite recently, we found a general derivation of a scaling for off-critical relaxation in local- and cluster-update algorithms. As an example, we consider the magnetic susceptibility in cluster-update algorithms. From the initial-time critical relaxation $\chi(t; T_c) \sim \exp(ct^\sigma)$ and the temperature dependence in equilibrium $\chi(t = \infty, T) \sim (T - T_c)^{-\gamma}$, we have $\chi(t, T)(T - T_c)^\gamma \sim \exp[ct^\sigma + \ln(T - T_c)^\gamma]$, or

$$\chi(t, T) \sim (T - T_c)^{-\gamma} f_{sc}[ct^\sigma + \ln(T - T_c)^\gamma], \quad (1)$$

which means that all the off-critical relaxation data near T_c are scaled on a single curve.

Here we assume that the relaxation process along the Kibble-Zurek mechanism [3], namely the controlled annealing process in accordance with critical relaxation, is expressed by the above scaling curve, and try to reconstruct the annealing process from the NER data in the two-dimensional (2D) Ising model. Although various attempts within the standard power-law annealing are not successful, the following stretched-exponential modified KZ process,

$$T(t) = T_0 + T_d \exp[-C(t/\tau)^\sigma], \quad (2)$$

$$T_0 = \frac{T_f - aT_i}{1 - a}, \quad T_d = \frac{T_i - T_f}{1 - a}; \quad a = e^{-C}, \quad (3)$$

gives consistent results for $L = 4096$ with the

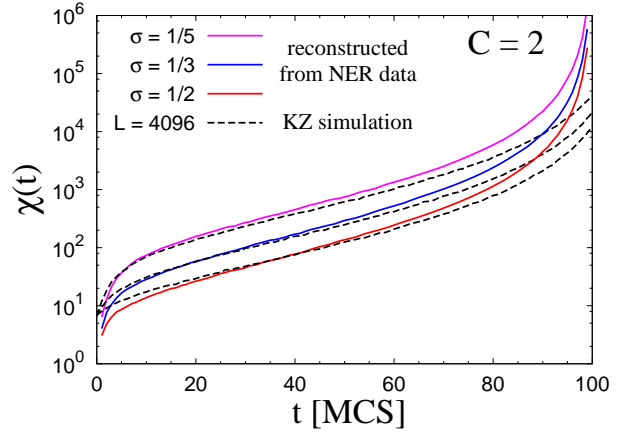


Figure 1: Simulation-time dependence of the magnetic susceptibility in the 2D Ising model in the SW algorithm for the modified KZ process explained in the main text. The dashed and solid lines are the simulated and reconstructed data based on Eq. (1), respectively.

relaxation process in the Swendsen-Wang algorithm with a set of parameters for a rather slow relaxation: $T_i = 1.5T_c$, $T_f = T_c$, $\tau = 100$, $C = 2$, and $\sigma = 1/5, 1/3, 1/2$ with the exact critical temperature T_c as shown in Fig. 1.

References

- [1] Y. Nonomura, *JPSJ* **83**, 113001 (2014); YN & Y. Tomita, *PRE* **92**, 062121 (2015), **93**, 012101 (2016), **101**, 032105 (2020).
- [2] YT & YN, *PRE* **98**, 052110 (2018).
- [3] C.-W. Liu et al., *PRB* **89**, 054307 (2014); Refs. therein (including originals by KZ).

Generalization of temperature scaling in early-time nonequilibrium relaxation

Yoshihiko NONOMURA

MANA, National Institute for Materials Science

Namiki 1-1, Tsukuba, Ibaraki 305-0044

Recently we numerically revealed that the critical nonequilibrium relaxation (NER) behaviors in cluster algorithms are described by the stretched-exponential simulation-time dependence of physical quantities in various classical spin systems [1, 2, 3] and in a quantum phase transition [4], and derived such a relaxation formula phenomenologically [5]. There we utilized the nonequilibrium-to-equilibrium scaling (NE-ES) which connects initial-time and equilibrium relaxation behaviors.

Here we generalize this derivation to off-critical behaviors. As an example, we consider the magnetic susceptibility. From the initial-time critical relaxation $\chi(t; T_c) \sim \exp(ct^\sigma)$ and the temperature dependence in equilibrium $\chi(t = \infty, T) \sim (T - T_c)^{-\gamma}$, we have $\chi(t, T)(T - T_c)^\gamma \sim \exp[ct^\sigma + \ln(T - T_c)^\gamma]$, or

$$\chi(t, T) \sim (T - T_c)^{-\gamma} f_{sc}[ct^\sigma + \ln(T - T_c)^\gamma]. \quad (1)$$

We confirm this temperature scaling by analyzing the NER process of the three-dimensional Heisenberg model in the Swendsen-Wang algorithm from the perfectly-disordered states [3].

Here we take the $L \times L \times L$ system with the periodic boundary condition for $L = 560$, the largest size used in Ref. [3]. The data up to 225 Monte Carlo steps are scaled with Eq. (1) in Fig. 1. Minimizing the mutual residuals using our previous estimates with the NE-ES, $T_c = 1.442987(2)J/k_B$ and $\sigma = 0.47(1)$ [3], we have

$$\gamma = 1.3945 \pm 0.0019, \quad c = 1.2593 \pm 0.0043, \quad (2)$$

which is consistent with the previous estimate from detailed simulations, $\gamma = 1.3960(9)$ [6].

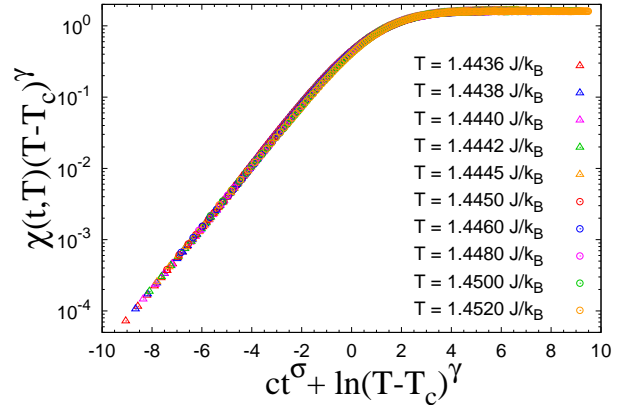


Figure 1: Temperature scaling plot of the magnetic susceptibility in the 3D Heisenberg model for various temperatures in a semi-log scale using the estimates of T_c and σ in Ref. [3].

References

- [1] Y. Nonomura, J. Phys. Soc. Jpn. **83**, 113001 (2014).
- [2] Y. Nonomura and Y. Tomita, Phys. Rev. E **92**, 062121 (2015).
- [3] Y. Nonomura and Y. Tomita, Phys. Rev. E **93**, 012101 (2016).
- [4] Y. Nonomura and Y. Tomita, Phys. Rev. E **101**, 032105 (2020).
- [5] Y. Tomita and Y. Nonomura, Phys. Rev. E **98**, 052110 (2018).
- [6] M. Campostrini, M. Hasenbusch, A. Pelissetto, P. Rossi, and E. Vicari, Phys. Rev. B **65**, 144520 (2002).

Finite-temperature properties of the Kitaev-Heisenberg models on kagome and triangular lattices

Takami TOHYAMA

Department of Applied Physics, Tokyo University of Science, Tokyo 125-8585

Frustrated quantum spin systems such as the Heisenberg and Kitaev models on various lattices have been known to exhibit various exotic properties not only at zero temperature but also for finite temperatures. Inspired by the remarkable development of the quantum frustrated spin systems in recent years, we decided to investigate the finite-temperature properties of the $S = 1/2$ Kitaev-Heisenberg models on kagome and triangular lattices.

For calculating accurate low-temperature properties, we developed two types of improved version for finite-temperature Lanczos method (FTLM) [1]: replaced FTLM and orthogonalized FTLM. In standard FTLM [2], a very large number of samplings of initial vector is required to obtain good accuracy at low temperatures. The low-temperature FTLM [2] is known as one of the solutions to this problem. However, this method has a difficulty for large-scale calculations because it requires huge random access memory to keep all vectors in the Krylov subspace. In RFTLM, low-lying eigenstates obtained by the ground-state Lanczos method are used in the partition function and other thermodynamic quantities. In OFTLM, initial random vectors are prepared to be orthogonal to the low-lying eigenstates. We also developed a Lanczos code that equips a technique to save the memory for the Hamiltonian by dividing H into two subsystems. These techniques lead us to calculate finite-temperature properties up to 36 lattice sites with good accuracy even at low temperatures.

The newly developed RFTLM was also used in the calculation of specific heat and magnetic susceptibility for $S = 1/2$ frustrated J_1 - J_2 Heisenberg model on kagome, triangular, and square lattice up to 36 sites [3].

In both kagome and triangular lattices for the Kitaev-Heisenberg model, multiple peaks are confirmed in the specific heat. To find the origin of the multiple peaks, we calculate the static spin structure factor. The origin of the high-temperature peak of the specific heat is attributed to a crossover from the paramagnetic state to a short-range ordered state whose static spin structure factor has zigzag or linear intensity distributions in momentum space. In the triangular Kitaev model, the order by disorder due to quantum fluctuation occurs. On the other hand, in the kagome Kitaev model it does not occur even with both quantum and thermal fluctuations [1].

References

- [1] K. Morita and T. Tohyama: Phys. Rev. Research **2** (2020) 013205.
- [2] P. Prelovsek and J. Bonca: Ground state and finite-temperature Lanczos methods, in *Strongly Correlated Systems, Numerical Methods*, Vol. 176 of Springer Series in Solid-State Sciences (Springer, 2013).
- [3] P. Prelovsek, K. Morita, T. Tohyama, and J. Herbrych: Phys. Rev. Research **2** (2020) 023024.

Constructing the electronic structure database for the molecular design of pigments utilizing near infrared light

Yu KOMATSU

National Institutes of Natural Sciences Astrobiology Center

National Astronomical Observatory of Japan

2-21-1 Osawa, Mitaka, Tokyo 181-8588

Novel dye molecules absorbing NIR radiation are being anticipated for dye-sensitized solar cells and imaging. Moreover, cyanobacteria, oxygenic photosynthetic bacteria, turn to utilize chlorophyll *f*, which is the reddest chlorophyll, for photochemistry after growing under the far-red light [1]. Thus, the red limit of photosynthesis has been updated. In this study, in order to explore redder molecules with possibly working as photosynthetic pigments, the database has been constructed using ab initio calculations for ring molecules like porphyrins with certain properties, combined with high-throughput methods.

The physical-chemical quantities of molecules, were estimated at DFT level as follows: *[total energies in ground and excited states, orbital energies, ionization potentials (IPs), electronic affinities (EAs), binding energies for central metals, electronic structures for each orbital, ...]*. Dye molecules are calculated with different central metals (Mg, Ca, Ni, Zn, Sr, Pd, Cd, Ba, Pt, Hg, Pb and H₂) in vacuum and water, methanol and benzene with PCM. In Fig.1, IPs and EAs for three pigments

are shown with 12 kinds of metals in four solvents. The data will be combined with an existing dataset like QM9 for further analysis to search for functional molecules effectively.

The computation in related work has been done using supercomputers of Tokyo Institute of Technology and National Astronomical Observatory of Japan, as well.

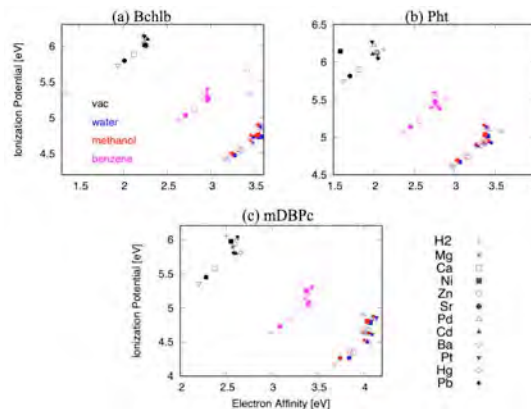


Fig. 1: Estimated ionization potentials and electronic affinities for (a) bacteriochlorophylls *b*, (b) phthalocyanines and (c) meso-dibenzoporphycenes with different central metals in 4 kinds of solvent conditions (CAM-B3LYP/Def2tzvp//B3LYP-D3/Def2tzvp).

References

[1] D. J. Nürnberg *et al.*: Science 360 (2018) 1210.

Application of numerical renormalization group method in condensed- matter physics

Kenji HARADA

Graduate School of Informatics, Kyoto University, Kyoto 606-8501, Japan

We have applied the tensor renormalization group (TRG) methods [1-4] to various condensed matter systems. We tried to use them for the non-equilibrium systems.

The directed percolation (DP) show a continuous phase transition in the phase diagram in the long-time limit. We have studied the phase diagram through the Renyi entropy by using a TEBD method on the matrix product states representation of a state-probability distribution [5]. In the case of one-dimensional DP, we have found a critical relaxation at the critical point and a new phase transition point in the active phase of the one-dim. DP.

The state-probability distribution of the d -dim. DP can be written as a $(d+1)$ -dim. tensor network. In the case of one-dim. DP, the TRG shows better accuracy than the TEBD method.

To check the existence of the new transition point in the activity phase of higher dim. DP, we tried to apply the TRG method on the two-dim. DP by a massively parallel computer on the ISSP.

In the case of the $(2+1)$ -dim. tensor network, the performance of the TRG method is not stable. The average density of active objects is not consistent with the Monte Carlo results, not near a critical point. The accuracy of the oblique projection in the TRG method is bad. However, due to the higher complexity of the TRG method, we could not increase the bond-dimension of tensors even using the system B. The reduction of the complexity of the TRG method is a future work to improve the accuracy of the TRG method.

Reference

- [1] M. Levin and C. P. Nave, Phys. Rev. Lett. **99**, 120601 (2007).
- [2] Z. Y. Xie, J. Chen, M. P. Qin, J. W. Zhu, L. P. Yang, and T. Xiang, Phys. Rev. B **86**, 045139 (2012).
- [3] G. Evenbly and G. Vidal, Phys. Rev. Lett. **115**, 180405 (2015).
- [4] S. Yang, Z.-C. Gu, and X.-G. Wen, Phys. Rev. Lett. **118**, 110504 (2017).
- [5] K. Harada and N. Kawashima, Phys. Rev. Lett., **123**, 090601, (2019).

Clarification of thermal transport spectra in hierarchical structured organic bulk materials

Takuma Shiga

Department of Mechanical Engineering,

The University of Tokyo, Hongo, Bunkyo, Tokyo 113-8656

Material design of cellulose nanostructure has been recently paid much attention because cellulose structure was identified by X-ray and neutron scattering spectroscopies. Cellulose nanomaterial is expected as candidates such as transparent conductive film and thermal insulator since it has high degree of self-organization and high mechanical property. Turning to thermal insulation, thermal conductivity of cellulose thermal insulators such as aerogel and foam is around $15\text{--}18\text{ mWm}^{-1}\text{K}^{-1}$, and it is lower than widely-used glass wool and urethane foam. However investigation of microscopic heat conduction mechanism of cellulose nanomaterial is very limited. In order to further improve thermal insulation performance, it is necessary to get insight into the knowledge on cellulose nanocrystal and fibrils.

We have evaluated heat conduction and its size effect of I- β type cellulose nanocrystal and single chain by performing non-equilibrium molecular dynamics (NEMD) simulation. In the NEMD calculation, we employed the GLYCAM06 [1] force field which reproduces thermal expansion coefficient of cellulose well.

This force field is composed of bond stretching, bond angle, dihedral angle, van der Waals, and Coulombic interaction. For non-bonding, we used the combination of particle-particle particle mesh and cutoff methods [2]. In the calculation, we applied periodic boundary conditions along all directions. After equilibration with $T=300\text{ K}$, hot and cold thermostats with $T=330\text{ K}$ and $T=270\text{ K}$ were attached to the simulation cell as illustrated in Fig. 1. Heat flux and temperature gradient were evaluated after the system reaches non-equilibrium steady-state, and then thermal conductivity was evaluated through the Fourier's law. All calculations were done by LAMMPS package.

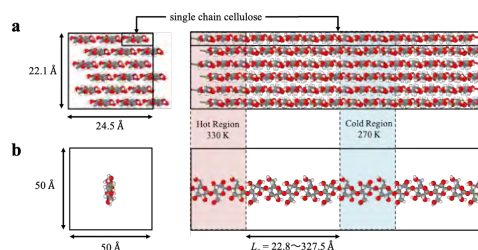


Fig. 1 Schematics for (a) cellulose nanocrystal (CNC) and (b) single chain cellulose.

Size effect of thermal conductivity of cellulose nanocrystal is shown in Fig. 2. As thermal conductivity increases with long-axis length increasing, we found that phonon

transport inside cellulose nanocrystal is quasi-ballistic. This feature is attributed to strong covalent bond of intra-interaction. From the obtained results and linear-relationship between an inverse of thermal conductivity and an inverse of long-axis length (L_c), we estimated the thermal conductivity of bulk cellulose nanocrystal as $4.50 \pm 0.60 \text{ Wm}^{-1}\text{K}^{-1}$, which is similar with reported literatures.

As for single cellulose chain, it was expected that thermal conductivity of single chain is larger than that of nanocrystal however these two thermal conductivities are actually quite similar with each other, which is different with the reported works on polyethylene [3]. Similar to the results of poly-dimethylpolysiloxane [4], this result can be understood because non-linear vibration of side structure arising from thermal fluctuation impedes phonon transport along long-axis direction. The non-linear vibration of side structure is strongly dependent on dihedral angle interaction and then we calculated thermal conductivity by strengthening or softening spring constant of dihedral angle, which are shown in Fig. 3 denoted as stiff and soft chains. While strength of dihedral interaction increases thermal conductivity, heat conduction along long-axis direction is found to be insensitive to the softening of dihedral interaction.

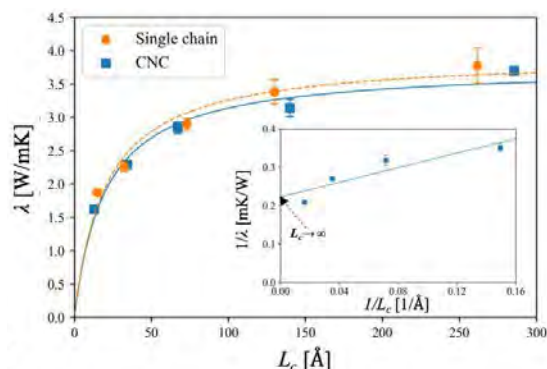


Fig. 2 Thermal conductivity of CNC (solid line) and cellulose single chain (dashed line) as a function of the conduction region length. The inset shows extrapolation of inverse of thermal conductivity in infinite conduction region length.

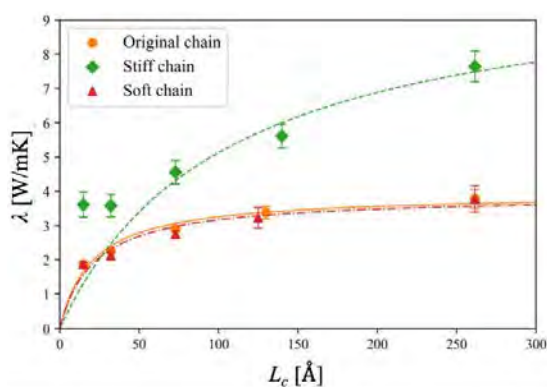


Fig. 3 Thermal conductivity of original single cellulose chain (solid line), stiff chain (dashed line) and soft chain (dash-dotted).

References

- [1] S. Hashmi, et al., Int. J. Clin. Exp. Pathol., **8** (2015), 8786.
- [2] R.W.Hockney, et al., "Computer simulation using particles", Adam Hilger, NY,(1989).
- [3] A. Henry, et al., Phys. Rev. Lett., **101**-23(2008), 235502.
- [4] T. Luo, et al., J. Appl. Phys., **109**-7(2011), 074321.

Heat conduction analysis for phononic crystal

Takuma Shiga

Department of Mechanical Engineering,

The University of Tokyo, Hongo, Bunkyo, Tokyo 113-8656

It has been known that phononic crystal (PnC) such as superlattice and thin-film with air-holes leads to significant modulation of phonon dispersion relation, which finally results in large reduction of thermal conductivity while crystallinity remains. In order to qualitatively evaluate a thermal conductivity reduction, we need to directly calculate thermal conductivity of PnC by means of microscopic simulation.

Before considering actual PnCs, we have considered heat conduction of silicon thin films with a thickness of an order of nanometer by performing anharmonic lattice dynamics (ALD) simulation. For interatomic force constants which are needed in ALD calculation, we employed the optimized Stillinger-Weber potential [1]. Surface orientation of silicon film is set to (001) and 20×20 sampling mech for two-dimensional Brillouin zone is chosen for the calculation of scattering rate [2].

Figure 1(a) shows phonon dispersion relation of silicon thin-film with the thickness of 10 nm. Because of the presence of surface, there are surface phonon modes labeled by S_1 - S_5 . From the analysis of eigenvectors, we identified S_1 and S_2 are Love and Rayleigh waves, respectively.

Figure 1(b) shows thickness-dependent in-plane thermal conductivity of silicon thin-films at $T=300$ K. We found that the thickness dependence is largely different with the convectional theory considering size effect.

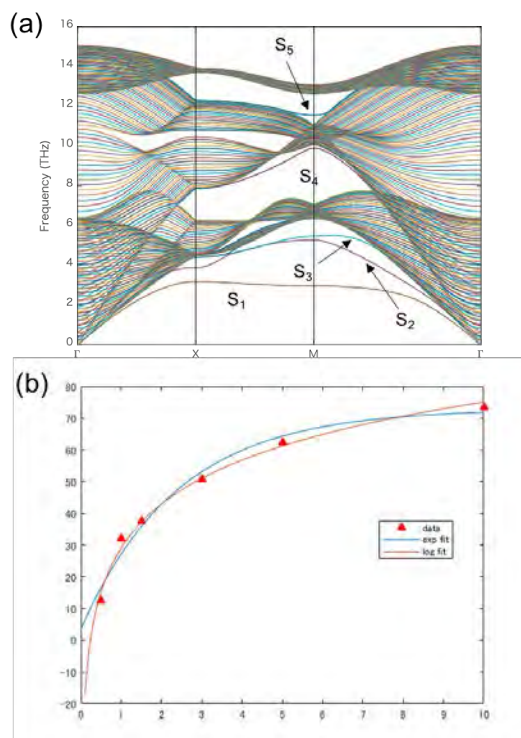


Fig. 1 (a) phonon dispersion relation of silicon thin film with 10 nm thickness. (b) thickness-dependent thermal conductivity at $T=300$ K.

References

- [1] Y. Lee, et al., Phys. Rev. B **85**, 125204 (2012).
- [2] T. Tadano, et al., J. Phys. Condens. Mater **26**, 225402 (2014).

Comprehensive study on transition between heat conduction and radiative heat transfer

Takuma Shiga

Department of Mechanical Engineering,

The University of Tokyo, Hongo, Bunkyo, Tokyo 113-8656

It has been so far revealed that thermal transport across two substrates with nanogap is known to be attributed by phonon-polariton resonance and tunneling of acoustic phonons and therefore such a near-field heat transfer can exceed black-body limit. In order to explore thermally-functionalized devices utilizing near-field heat transfer such as thermal switch, thermal rectifier, and so on, microscopic mechanism of transport regime changing from near-field heat transfer to heat conduction is needed to be investigated.

In order to realize such investigation, we chose a combination of spectral heat current and non-equilibrium molecular dynamics (NEMD) simulations. Figure 1 shows frequency-dependent spectral thermal boundary conductance at the interface across solid argon and heavy-mass argon crystals for different temperatures. As temperature increases, inelastic terms of interfacial scattering contribute to overall heat conduction. In addition, we calculated dielectric function of β -cristobalite SiO_2 on the basis of fluctuation-dissipation theorem. These two results are in good agreement with previous works [1,2], and

we realized the framework for investigating transition between heat conduction and near-field radiation.

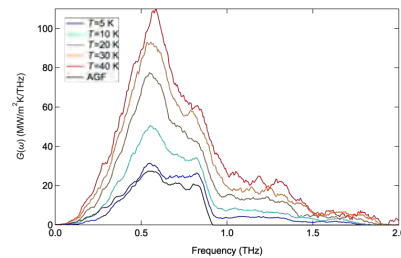


Fig. 1 Spectral thermal boundary conductance across the interface between Ar and heavy-Ar solids at different temperatures.

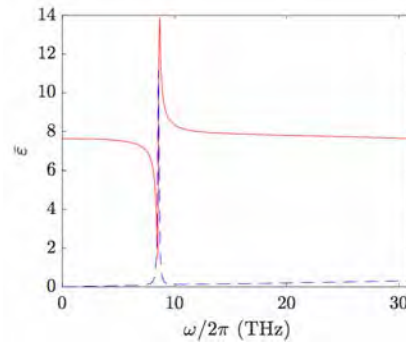


Fig. 2 Frequency-dependent dielectric function of β -cristobalite SiO_2 at $T=300$ K.

References

- [1] K. Sääskilähti, et al., Phys. Rev. B **90**, 134312 (2014).
- [2] Y. Chalopin, et al., Appl. Phys. Lett. **104**, 011905 (2014).

Ground-State Phase Diagram of an Anisotropic $S=1/2$ Two-Leg Ladder

Takashi Tonegawa

Professor Emeritus, Kobe Univ. and Visiting Professor, Osaka Prefecture Univ.

The purpose of this report is to explore the ground-state phase diagram of an anisotropic $S=1/2$ two-leg ladder by using mainly numerical methods. We express the Hamiltonian which describes this system as

$$\mathcal{H} = \sum_{j=1}^L \sum_{\ell=1,2} [\vec{S}_{j,\ell}, \vec{S}_{j+1,\ell}]_{\Delta} + J_r \sum_{j=1}^L [\vec{S}_{j,1}, \vec{S}_{j,2}]_{\Delta} \quad (1)$$

with

$$[\vec{S}_{j,\ell}, \vec{S}_{j',\ell'}]_{\Delta} \equiv S_{j,\ell}^x S_{j',\ell'}^x + S_{j,\ell}^y S_{j',\ell'}^y + \Delta S_{j,\ell}^z S_{j',\ell'}^z. \quad (2)$$

Here, $\vec{S}_{j,\ell} = (S_{j,\ell}^x, S_{j,\ell}^y, S_{j,\ell}^z)$ is the $S=1/2$ operator acting at the (j, ℓ) site assigned by rung j and leg $\ell (=1 \text{ or } 2)$; J_r denotes the magnitude of the rung interactions; Δ is the parameter which controls the the XXZ -type anisotropy of both the leg and rung interactions; L is the total number of rungs, which is assumed to be even. It is noted that the magnitude of the leg interactions is set to be unity as the unit of energy.

The phase diagrams on the Δ versus J_r plane have already been discussed by Li *et al.* [1] who have used the tensor network representation of quantum many-body states, and also and by Roy *et al.* [2] who have analyzed the variation of bipartite and multipartite entanglements. Unfortunately, however, their phase diagrams contain some unphysical results. Firstly, the XY phase region extends to the $\Delta > 0$ region, but this is physically unreasonable. Secondly, in Roy *et al.*'s phase diagram, the ferromagnetic phase does not exist, but this is also unreasonable since the ground state is the ferromagnetic state at least when $\Delta \ll -1$ and $J_r \gg 1$. Finally, the term ' $XY2$ ' in Li *et al.*'s phase diagram is misleading, because the $XY2$ state proposed originally by Schulz [3] is characterized not only by the formation of two-magnon bound state or, almost equivalently, the exponential-decay behavior of the transverse two-spin correlation function $\langle S_{j,\ell}^+ S_{j+j',\ell}^- \rangle$, but also by the fact that the nematic four-spin correlation function (with power-decay behavior) $\langle S_{j,1}^+ S_{j,2}^+ S_{j+j',1}^- S_{j+j',2}^- \rangle$ is more dominant

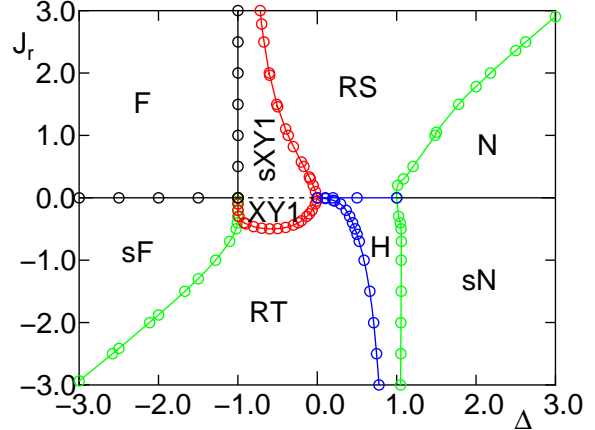


Figure 1: Ground-state phase diagram on the Δ versus J_r plane obtained in the present work.

than the longitudinal two-spin correlation function (with power-decay behavior) $\langle S_{j,\ell}^z S_{j+j',\ell}^z \rangle$. This is not the case for the $XY2$ state in Li *et al.*'s paper, and in our opinion the term ' $staggered XY1$ ' should be used (for details, see the last sentence of the next paragraph).

In this report we numerically determine the ground-state phase diagram as accurately as possible. Estimating the phase boundary lines, we make a variety of analyses such as the level spectroscopy (LS) analysis, the phenomenological renormalization-group (PRG) analysis, and so on, of the numerical data obtained by the exact diagonalization (ED) method. The resultant phase diagram is shown in Fig. 1. Here, the solid and dotted black lines are the first-order and second-order phase transition lines, respectively. In spite of the present simple system, this phase diagram is rather rich and consists of nine kinds of phases; these are the ferromagnetic (F), stripe ferromagnetic (sF), staggered $XY1$ (s $XY1$), $XY1$ ($XY1$), rung triplet (RT), rung singlet (RS), Haldane (H), Néel (N), and stripe Néel (sN) phases. The schematic picture of the sF, N, and sN states are given in Fig. 3 of Hiji *et al.*'s paper [4], which treats the case of isotropic rung interactions. (Also in this paper, the term ' $XY2$ ' is misleadingly used.) It

is noted that the sF state is essentially the N state. We note also that both the XY1 and sXY1 states are the usual Tomonaga-Luttinger liquid states, but in the former state the relation $(-1)^{j'} \langle S_{j,\ell}^+ S_{j+j',\ell'}^- \rangle > 0$ holds, while in the latter state $(-1)^{j'} (-1)^{\ell+\ell'} \langle S_{j,\ell}^+ S_{j+j',\ell'}^- \rangle > 0$ holds [4].

Let us now discuss how to numerically determine the phase boundary lines shown in Fig. 1. We denote, respectively, by $E_0^P(L, M)$ and $E_1^P(L, M)$, the lowest and second-lowest energy eigenvalues of the Hamiltonian \mathcal{H} under the periodic boundary condition within the subspace of L and M , where M is the total magnetization ($M=0, \pm 1, \dots, \pm L$). We also denote by $E_0^T(L, M, P)$ the lowest energy eigenvalue of \mathcal{H} under the twisted boundary condition within the subspace of L, M , and P , where $P(=\pm 1)$ is the eigenvalue of the space inversion operator with respect to the twisted bond. We have numerically calculated these energies for finite-size systems with up to $L=12$ spins by means of the ED method. The ground-state energy of the finite- L system is given by $E_0^P(L, L)$ in the F region and by $E_0^P(L, 0)$ in the other regions.

In the following way, we estimate the finite-size critical values of J_r (or Δ) for various values of Δ (or J_r), for each phase transition. Then, the phase boundary line for the transition is obtained by connecting the results for the $L \rightarrow \infty$ extrapolation of the finite-size critical values.

The phase transition between the H and RS phases as well as that between the H and RT phases is the Gaussian transition. In this case, the Kitazawa's LS method [5] is very powerful to determine the phase boundary lines. That is to say, we numerically solve the equation

$$E_0^T(L, 0, +1) = E_0^T(L, 0, -1) \quad (3)$$

to calculate the finite-size critical values. The results of our calculations show that, for the transition between the H and RS phases, the finite-critical value of J_r for a given value of Δ ($0.0 < \Delta < 1.0$) is equal to 0.0, independently of L .

Since the phase transition between the RS and sXY1 phases and that between the RT and XY1 phases are of the Berezinskii-Kosterlitz-Thouless type [6], the phase transition line can be very accurately estimated by using the LS method developed by Nomura and Kitazawa [7]. Then, the finite-size critical values are calculated from

$$E_0^P(L, 2) = E_0^T(L, 0, +1). \quad (4)$$

The three phase transitions between the RS and N phases, between the H and sN phases, and between the RT and sF phases are the 2D Ising-type transitions. Then, it is well known that the phase transition lines are determined by the PRG

method [8]. Then, to estimate the finite-size critical values, we solve the PRG equation,

$$L \Delta E^P(L, 0) = (L+2) \Delta E^P(L+2, 0), \quad (5)$$

where

$$\Delta E^P(L, 0) = E_1^P(L, 0) - E_0^P(L, 0). \quad (6)$$

It is apparent that the finite-size critical values for the phase transitions between the F and sXY1 phases and between the F and sF phases are calculated from

$$E_0^P(L, L) = E_0^P(L, 0). \quad (7)$$

The results show that, for the transition between the F and sXY1 phases, the finite-critical value of Δ for a given value of J_r ($0.0 < J_r$) is equal to -1.0 , independently of L . Furthermore, for the transition between the F and sF phases, the finite-size critical value of J_r for a given value of Δ ($\Delta < -1.0$) is equal to 0.0, independently of L .

Lastly, we note that the phase transition between the sN and N phases is of the first-order, while that between the XY1 and sXY1 phase is of the second-order. These have been discussed in detail in Hijii *et al.*'s paper [4].

Invaluable discussions with K. Okamoto, K. Nomura, and T. Sakai are gratefully acknowledged.

[1] S.-H. Li, Q.-Q. Shi, M. T. Batchelor, and H.-Q. Zhou: *New J. Phys.* **19** (2017) 113027.

[2] S. S. Roy, H. S. Dhar, D. Rakshit, A. Sen(De), and U. Sen: *J. Magn. Mater.* **444** (2017) 227.

[3] H. J. Schulz: *Phys. Rev. B* **34** (1986) 6372.

[4] K. Hijii, A. Kitazawa, and K. Nomura: *Phys. Rev. B* **72** (2005) 014449.

[5] A. Kitazawa: *J. Phys. A* **30** (1997) L285.

[6] Z. L. Berezinskii: *Sov. Phys.-JETP* **34** (1971) 610; J. M. Kosterlitz and D. J. Thouless: *J. Phys. C: Solid State Phys.* **6** (1973) 1181.

[7] K. Nomura and A. Kitazawa: *J. Phys. A: Math. Gen.* **31** (1998) 7341.

[8] M. P. Nightingale: *Physica A* **83** (1976) 561.

Spin multipole dynamics and spin transport in frustrated magnets

Hiroaki ONISHI

*Advanced Science Research Center, Japan Atomic Energy Agency
Tokai, Ibaraki 319-1195*

In a spin-1/2 J_1 - J_2 Heisenberg chain with ferromagnetic J_1 and antiferromagnetic J_2 in a magnetic field, there appear a series of spin multipole liquid ground states, i.e., quadrupole, octupole, hexadecapole, etc. To clarify magnetic and transport properties in the quadrupole state, we have studied spin and quadrupole excitation spectra [1] and spin Drude weight [2] by numerical methods. We have argued that low-energy excitations are governed by bound two-magnon pairs, so that magnon pairs would carry spin current.

Here, we extend our focus to the octupole regime. By using a dynamical DMRG method, we examine the dynamical octupole structure factor at zero temperature, given by

$$O^{---}(q, \omega) = -\text{Im} \frac{1}{\pi} \langle 0 | O_q^{---\dagger} \frac{1}{\omega + E_0 - H + i\eta} O_q^{---} | 0 \rangle,$$

where O_q^{---} is the Fourier transform of $O_i^{---} = S_i^- S_{i+1}^- S_{i+2}^-$. Note that we perform one DMRG run to obtain the spectral weight for a set of q and ω , so that we need to do many runs to scan a wide range of the q - ω space. The computations are accelerated by parallel simulations using the system B of the ISSP supercomputer.

We present intensity plots of $O^{---}(q, \omega)$ in Fig. 1. We find a finite gap in the quadrupole regime [Fig. 1(a)], while we observe a gapless mode at $q = \pi$ in the octupole regime in accordance with quasi-long-range antiferro-octupole correlations [Fig. 1(b)]. Since a bound three-magnon cluster is excited with zero energy in

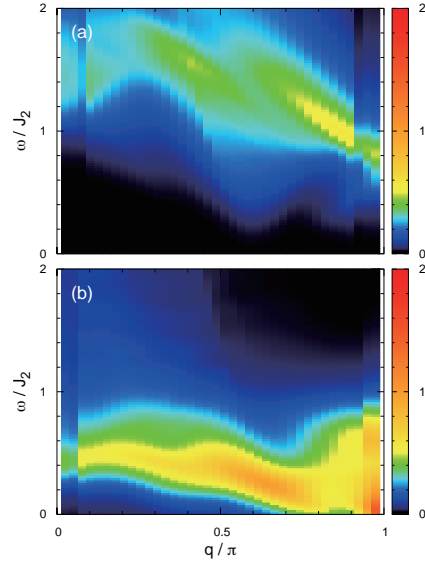


Figure 1: $O^{---}(q, \omega)$ at (a) $J_1/J_2 = -2$ and $M = 0.35$ and (b) $J_1/J_2 = -3$ and $M = 0.35$, where M is the magnetization. DMRG results with 40 sites.

the octupole state, we envisage that magnon clusters would contribute to the spin transport. The analyses of current correlation functions and wavepacket dynamics are also on going to clarify the relationship between magnetic and transport properties.

References

- [1] H. Onishi, J. Phys. Soc. Jpn. **84**, 083702 (2015); J. Phys.: Conf. Ser. **592**, 012109 (2015); Physica B **536**, 346 (2018).
- [2] H. Onishi, J. Magn. Magn. Mater. **479**, 88 (2019).

Molecular Dynamics Simulation of Ferroelectrics Using a Shell Model V

T. Hashimoto

*Research Center for Computational Design of Advanced Functional Materials (CD-FMat),
National Institute of Advanced Industrial Science and Technology (AIST),
Tsukuba Central 2, 1-1-1 Umezono, Tsukuba, Ibaraki 305-8568, Japan*

Amorphous BaTiO₃ can be formed by sputtering. Its structure is assumed to be a random network of TiO_{*n*} local bonding units (LBUs). By X-ray absorption fine-structure (XAFS) spectroscopy, *n* was found to be 6[1]. But, due to the experimental difficulty, the LBU linkage for amorphous BaTiO₃ is not clear. We have developed a classical molecular dynamics (MD) simulation code that can handle shell models that reproduce physical properties of BaTiO₃[2], and applied it to the study of amorphous BaTiO₃.

In the shell model, each atom is composed of a core and a shell. The intra-atomic core-shell interaction is expressed by $V(r) = c_2 r^2/2 + c_4 r^4/24$, where r is the core-shell distance and c_2 and c_4 are parameters. The inter-atomic interaction is through the Coulomb interaction and the Buckingham type shell-shell interaction $V(r) = A \exp(-r/\rho) - C/r^6$, where r is the inter-atomic shell-shell distance and A , ρ , and C are parameters. The computations were carried out in constant temperature and constant pressure (NPT) ensembles. The pressure and the temperature were controlled by the Parrinello-Rahman method and the massive Nose-Hoover chain method, respectively. The externally applied pressure was set to 0 Pa. Because we cooled the system slow enough, the densities were very close to each other, and the susceptibilities were also very close to each other, both in agreement with experiments[3].

As shown in Fig. 1, the probability of TiO₆

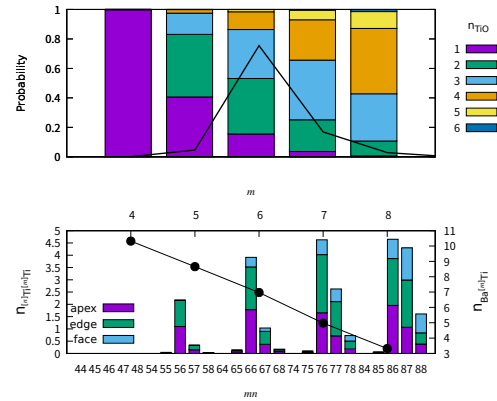


Figure 1: The probability of $[m]$ Ti and the number of Ti around O (n_{TiO}) (upper panel), and $n_{[m]\text{Ti}[m]\text{Ti}}$ and $n_{\text{Ba}^{[m]\text{Ti}}}$ (lower panel).

was the largest, and the probability of NBOs (purple) was larger for smaller m . The number of Ti (Ba) around $[m]$ Ti was larger (smaller) for larger m . $[7]$ Ti and $[8]$ Ti were in an O rich, Ti rich, and Ba poor environment with fewer NBOs and many edge or face-sharings, while $[5]$ Ti was in an O poor, Ti poor, and Ba rich environment with many NBOs.

- [1] A. I. Frenkel *et al.*: Phys. Rev. B **71** (2005) 024116.
- [2] S. Tinte *et al.*: J. Phys.: Condens. Matter **16** (2004) 3495.
- [3] T. Hashimoto and H. Moriwake: Physica B: Condens. Matter **579** (2020) 411799.

Transport properties of the antiferromagnetic classical XXZ model in two dimensions

Kazushi AOYAMA

*Department of Earth and Space Science, Graduate School of Science, Osaka University
Machikaneyama-cho, Toyonaka-shi, Osaka 560-0043*

Transport phenomena in magnetic systems reflect dynamical properties of interacting spins, such as magnetic excitations and fluctuations. In this work, we theoretically investigate transport properties of two-dimensional antiferromagnetic insulators, putting emphasis on how the occurrence of a phase transition is reflected in spin and thermal transports. In the classical nearest-neighbor (NN) antiferromagnetic XXZ model on the square lattice,

$$\mathcal{H} = -J \sum_{\langle i,j \rangle} (S_i^x S_j^x + S_i^y S_j^y + \Delta S_i^z S_j^z), \quad (1)$$

the anisotropy Δ plays a role to control the universality class of the transition, i.e., either a second-order transition at T_N into a magnetically ordered state or the Kosterlitz-Thouless (KT) transition at T_{KT} , which respectively occur for the Ising-type ($\Delta > 1$) and XY -type ($\Delta < 1$) anisotropies, while for the isotropic Heisenberg case of $\Delta = 1$, a phase transition does not occur at any finite temperature. The dynamics of the spins \mathbf{S}_i is determined by the following semiclassical equation of motion:

$$\begin{aligned} \frac{d\mathbf{S}_i}{dt} &= \mathbf{S}_i \times \mathbf{H}_i^{\text{eff}}, \\ \mathbf{H}_i^{\text{eff}} &= J \sum_{j \in N(i)} (S_j^x, S_j^y, \Delta S_j^z), \end{aligned} \quad (2)$$

where $N(i)$ denotes all the NN sites of i .

The spin current and the associated spin conductivity $\sigma_{\mu\nu}^s$ are respectively given by

$$\begin{aligned} \mathbf{J}_s^z(t) &= J \sum_{\langle i,j \rangle} \mathbf{r}_{ij} (\mathbf{S}_i \times \mathbf{S}_j)^z, \\ \sigma_{\mu\nu}^s &= \frac{1}{T L^2} \int_0^\infty dt \langle J_{s,\nu}^z(0) J_{s,\mu}^z(t) \rangle, \end{aligned} \quad (3)$$

where \mathbf{r}_{ij} and L denote a vector connecting two sites i and j and the linear system size, respectively. We numerically integrate Eq. (2) with initial equilibrium spin configurations generated by Monte Carlo simulations and calculate the time correlations $\langle J_{s,\nu}^z(0) J_{s,\mu}^z(t) \rangle$ at each time step. By using the second order symplectic method, we perform long-time integrations typically up to $t = 100|J|^{-1} - 800|J|^{-1}$ with the time step $\delta t = 0.01|J|^{-1}$ until the time correlations $\langle J_{s,\nu}^z(0) J_{s,\mu}^z(t) \rangle$ is completely lost. The thermal conductivity $\kappa_{\mu\nu}$ can also be calculated in a similar way.

It is found that the spin current probes the difference in the ordering properties, while the thermal current does not. Figure 1 shows the temperature dependence of the longitudinal spin conductivity σ_{xx}^s for the Ising-type ($\Delta = 1.05$), XY -type ($\Delta = 0.95$), and Heisenberg-type ($\Delta = 1$) spin systems. For the XY -type anisotropy, σ_{xx}^s exhibits a divergence at T_{KT} of the exponential form, $\sigma_{xx}^s \propto \exp[B/\sqrt{T/T_{KT} - 1}]$ with $B = \mathcal{O}(1)$, while for the Ising-type anisotropy, the temperature dependence of σ_{xx}^s is almost monotonic without showing a clear anomaly at T_N and such a monotonic behavior is also the case in the Heisenberg-type spin system [see the dashed curve in Fig. 1 (c)] [1]. Noting that in the XY -type spin system, the inter-free-vortex distance ξ_s diverges toward T_{KT} in the form of $\xi_s \sim \exp[(\pi/2)/\sqrt{T/T_{KT} - 1}]$, the significant enhancement of σ_{xx}^s at T_{KT} can be understood as a manifestation of the topological nature of

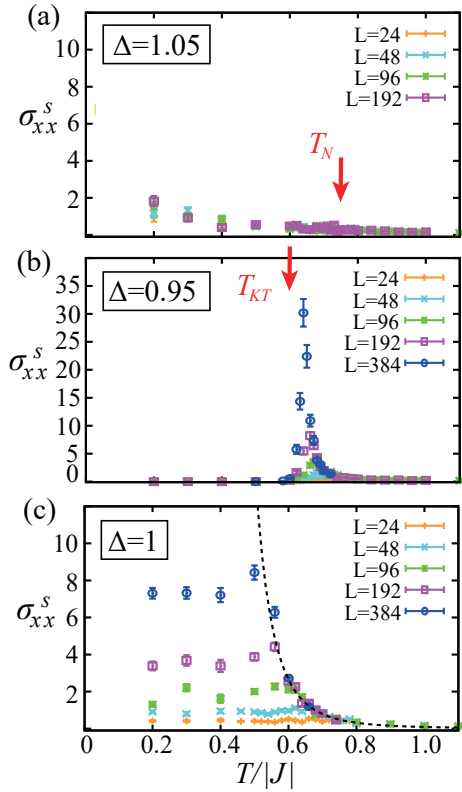


Figure 1: The temperature dependence of the longitudinal spin-current conductivity $\sigma_{\mu\mu}^s$ in the (a) Ising-type ($\Delta = 1.05$), (b) XY -type ($\Delta = 0.95$), and (c) Heisenberg-type ($\Delta = 1$) spin systems. In (a) and (b), red arrows indicate the magnetic and KT transition temperatures, $T_N/|J| \simeq 0.75$ and $T_{KT}/|J| \simeq 0.6$, respectively. In (c), a dashed curve represents the $\sigma_{xx}^s(T)$ curve extrapolated to the thermodynamic limit of $L \rightarrow \infty$.

a vortex whose lifetime τ_v gets longer toward T_{KT} due to the diffusive vortex motion characterized by the relation $\tau_v \propto \xi_s^2$.

Such an anomalous spin transport is also found in the NN antiferromagnetic Heisenberg model on the triangular lattice. In contrast to the XXZ antiferromagnets on the square lattice, the triangular-lattice antiferromagnet is a frustrated system. In the latter frustrated system, a KT-type binding-unbinding topological transition of \mathbb{Z}_2 vortices is predicted to occur at T_v , although spins do not order except at $T = 0$ with the spin correlation length ξ_s be-

ing finite at any finite temperature. It is found that the longitudinal spin-current conductivity exhibits a divergence at the \mathbb{Z}_2 -vortex transition temperature T_v , while the thermal conductivity only shows a monotonic temperature dependence with no clear anomaly at T_v [2].

Our results suggest the strong association between the spin transport and the binding-unbinding topological transition of vortex excitations.

References

- [1] K. Aoyama and H. Kawamura, Phys. Rev. B **100**, 144416 (2019).
- [2] K. Aoyama and H. Kawamura, Phys. Rev. Lett. **124**, 047202 (2020).

Study on Dynamic Mechanical Properties of Slide-Ring Gels using Coarse-Grained MD Simulations

Koichi Mayumi

Material Innovation Research Center (MIRC) and Department of Advanced Materials Science, Graduate School of Frontier Sciences, The University of Tokyo, 5-1-5 Kashiwanoha, Kashiwa, Chiba 277-8561, Japan

Polyrotaxane (PR) is a supramolecular polymer composed of many ring molecules, α -cyclodextrins (CDs) and one linear polymer, poly (ethylene glycol) (PEG), threading on these rings. By cross-linking rings belonging to PRs, Okumura and Ito succeeded in fabricating supramolecular polymer gels called slide-ring gels (SR gels)[1]. SR gels do not have direct cross-links between polymer chains, but topological interlock by figure-of-eight shaped cross-links composed of two ring molecules. Because SR gels have slidable cross-links, they show unique mechanical properties. For example, SR gels show lower Young's moduli than conventional fixed cross-linking polymer gels. So far, no molecular models have succeeded in representing the quantitative relationship between the sliding motion of the cross-linking points and the low Young's moduli of SR gels. In this study, we investigate the relationship between the sliding of figure-of-eight cross-links and Young's moduli by means of coarse-grained molecular dynamics simulations.

For the modeling of SR gels, we fabricated

a coarse-grained model of PR with 7-membered rings which can slide freely along the axial chain[2]. By cross-linking rings of the PRs, we prepared SR gels. We conducted uniaxial elongation simulations of the SR gels, and obtained Young's moduli E_{SR} , which were lower than theoretical values by the classical affine network model. Then, we analyzed the partial chain length distribution in SR gels under uniaxial deformation. While the distribution was described by a single exponential function in un-deformed state, while it became bimodal by stretching: longer and shorter chains appeared.

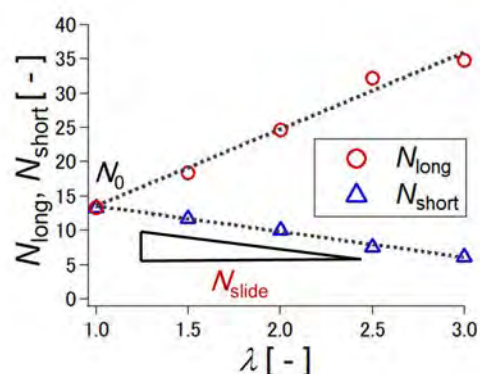


Fig. 1. λ dependence of the average length of long and short chain.

The average length of short and long chains

change linearly with λ (Fig.1). We defined this decay rate of the segment number of the shorter partial chain length as N_{slide} . By considering the chain movement through the slidable cross-links, we have succeeded in establishing a molecular model for SR gels based on the classical three chain model [3] (Fig. 2.), and obtained the simple equation :

$$E_{SR} = E_{Affine} \left(1 - \frac{N_{slide}}{N_0}\right)^2$$

Where E_{Affine} is the theoretical prediction by classical three-chain model, N_0 is the average partial chain length in undeformed state.

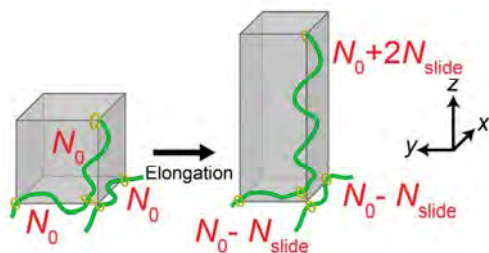


Fig. 2. Schematic illustration of the proposed

In order to verify this equation, we compare the Young's moduli obtained from the simulation results and theoretical estimation. We found that this estimation is realistic enough to reproduce the simulation results. Thus we succeeded in quantitatively evaluating the effect of the sliding on the elasticity of the slide-ring gels.

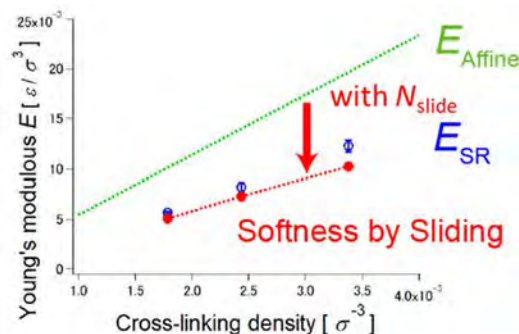


Fig. 3. The Young's moduli of SR gels plotted against the cross-linking density.

References

1. Okumura Y.; Ito K. *Adv. Mater.*, **2001**, *13*, 485
2. Y. Yasuda et al., *Macromolecules*, **2019**, *52*, 3787.
3. James, H. M.; Guth, E. *J. Chem. Phys.* **1943**, *11*, 455.
4. Y. Yasuda et al., *ACS Macro Letters*, under review.

Study on Microscopic Dynamics of Polyrotaxanes using Full-Atomistic MD Simulations

Koichi Mayumi

Material Innovation Research Center (MIRC) and Department of Advanced Materials Science, Graduate School of Frontier Sciences, The University of Tokyo, 5-1-5 Kashiwanoha, Kashiwa, Chiba 277-8561, Japan

Polyrotaxane (PR) is a supramolecular polymer which consists of an axial linear polymer and multiple ring-shaped molecules threaded on the chain. A unique feature of PR is that the rings can slide and rotate along the axial polymer, and this feature has been utilized for fabricating biomaterials[1] and topological gels[2]. However, the internal dynamics such as the sliding and rotation have not been disclosed yet. In this study, we investigated the internal molecular dynamics of PR composed of α -cyclodextrins (CDs) and poly (ethylene glycol) (PEG) chain in solution by means of full-atomistic molecular dynamics (MD) simulations [3].

We measured the mean squared displacement and estimated the diffusion coefficient of free PEG, free CD, and CD in PR. The simulation results agree well with the diffusion coefficients measured by the quasi-elastic neutron scattering experiment (Table 1). From this result, we consider that our model is realistic enough. Then we tried the analysis of intramolecular motion: the sliding dynamics.

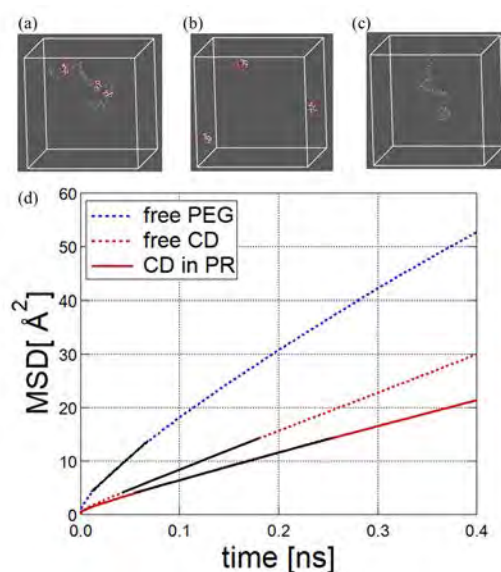


Figure 1. Simulation snapshot of the full-atomistic model for (a) PRs, (b) free CD, (c) free PEG, and (d) MSD for translational diffusion of CD in PR (red solid line), free CD (red dotted line), and free PEG (blue dotted line)

Table 1. Diffusion coefficients of CD in PR, free CD, and free PEG from the quasi-elastic neutron scattering (QENS) experiment and MD simulation.

Sample	Free PEG	Free CD	CD in PR
$D_{\text{QENS}} [10^{-7} \text{ cm}^2/\text{s}]$	40	13	11
$D_{\text{MD}} [10^{-7} \text{ cm}^2/\text{s}]$	27	12	8.6

In order to evaluate the sliding dynamics in PR, we tracked the one-dimensional trajectory of CD along PEG. The mean squared displacement corresponding to the sliding motion ($\text{MSD}_{\text{slide}}$) increased linearly with time, which suggests that the sliding motion is diffusive (Fig. 2.). From the time dependence of $\text{MSD}_{\text{slide}}$, we calculated from the diffusion coefficient for the sliding motion D_{slide} at 300 K as $1.42 \text{ \AA}^2/\text{ns}$, which is quite smaller value than that of the translational diffusion of CD in PR.

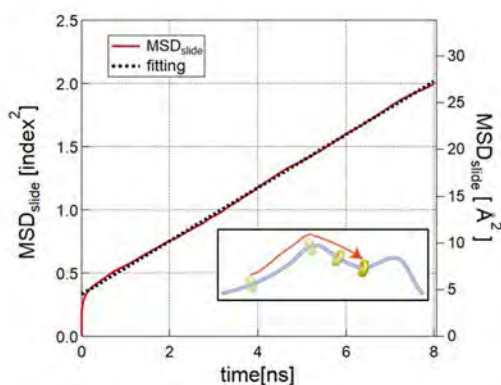


Fig. 2. $\text{MSD}_{\text{slide}}$ of CD along the PEG chain.

In order to clarify the molecular origin of this slow sliding dynamics, we analyzed the temperature dependence of D_{slide} (Fig. 3). We found that the diffusion coefficients of the sliding dynamics was dominated by the energy barrier between CD and PEG. This energy barrier was 8.92 kJ/mol , which corresponds to the energy potential barrier for CD on PEG, $2 \text{ kcal/mol} = 8.37 \text{ kJ/mol}$ [4].

In conclusion, we succeeded in representing the diffusion coefficient for the sliding motion of PR by the combination of the jump diffusion term with the Einstein-Stokes equation:

$$D_{\text{slide}} \propto \frac{k_B T}{\eta} \exp\left(-\frac{E_a}{k_B T}\right)$$

This relationship is valuable for controlling the sliding speed in polyrotaxanes.

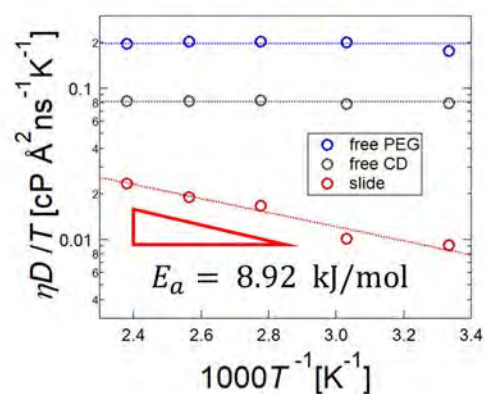


Fig. 3 Temperature dependence of the diffusion coefficient of free CD, free PEG and sliding motion.

References

- (1). Yui, N. et al., *Chem. Eur. J.* **2006**, *12*, 6730
- (2). Okumura, Y. et al., *Adv. Mater.* **2001**, *13*, 485
- (3). Yasuda, Y. et al., *J. Am. Chem. Soc.* **2019**, *141* (24), 9655.
- (4). Liu, P. et al., *J. Phys. Chem. C* **2012**, *116*, 17913.

Comparison of X-ray pinhole topographs experimentally obtained and computer-simulated based on the Ewald-Laue and Takagi dynamical theories

Kouhei OKITSU

Institute of Engineering Innovation, School of Engineering,

The University of Tokyo, 2-11-16 Yayoi Bunkyo-ku Tokyo 113-8656

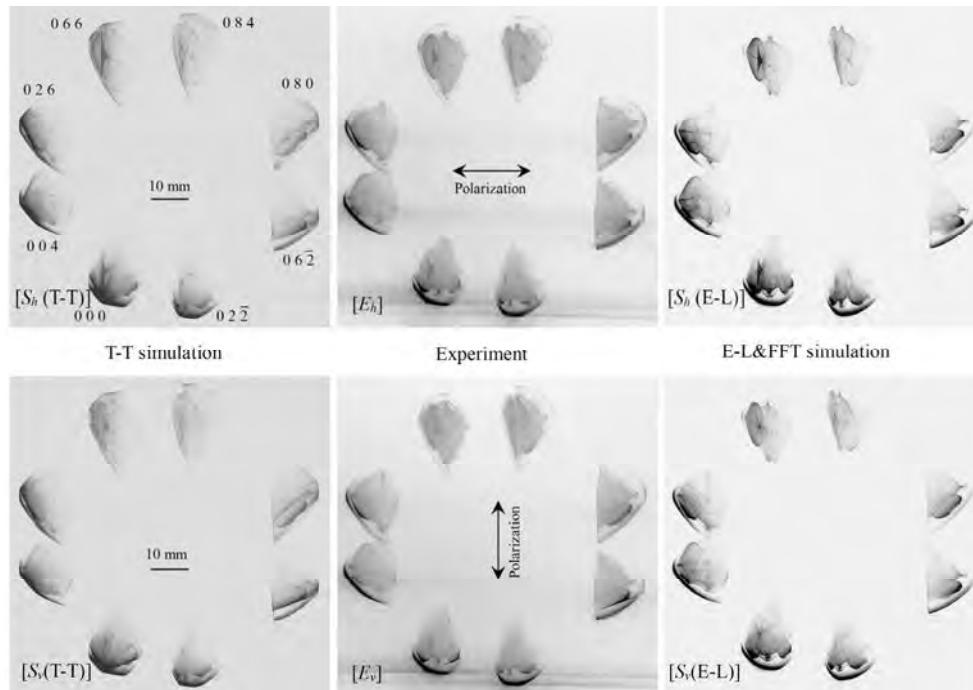


Fig.1 $[S_x(\text{T-T})]$, $[E_x]$ and $[S_x(\text{E-L})]$ ($x \in \{h, v\}$) show T-T simulated, experimentally obtained and E-L&FFT simulated eight-beam pinhole topographs for horizontally ($x = h$) and vertically ($x = v$) polarized incident X-rays [2].

The present author verified the simple relation between the n -beam Ewald-Laue (E-L) and Takagi (T-T) X-ray dynamical theories explicitly [1-4] for the first time. It can be described with Fourier transformation. Then, the behavior of diffracted X-rays in a perfect crystal can be described by both the E-L and T-T dynamical theories.

Figs. 1 $[S_x(\text{T-T})]$, $[E_x]$ and $[S_x(\text{E-L})]$ ($x \in \{h, v\}$) show T-T simulated, experimentally obtained and E-L&FFT simulated eight-beam pinhole topographs for horizontally ($x = h$) and vertically

($x = v$) polarized incident X-rays whose photon energy was adjusted or assumed to be 18.245 keV. The experiment was performed with the polarization state of the monochromated synchrotron radiation by using the four-quadrant phase retarder system [1, 2, 4] at the BL09XU of SPring-8. A $[1 \ -1 \ 1]$ -oriented floating zone silicon crystal with a thickness of 9.6 mm was used as the sample. The indices of reflections are as described in Fig. 1 $[S_h(\text{T-T})]$. The T-T simulated topographs were computed by integrating the T-T equation

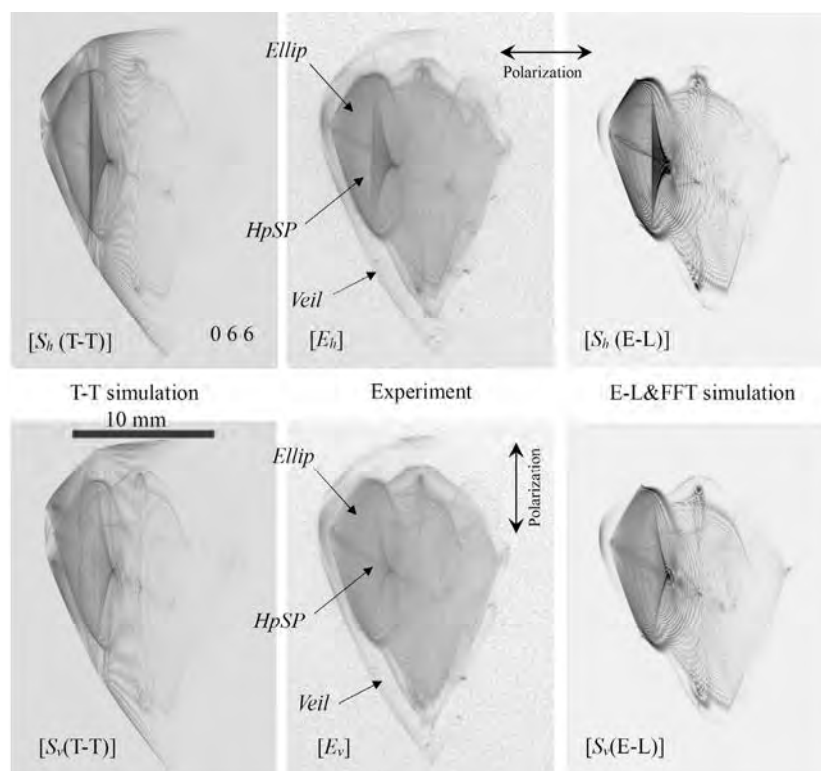


Fig. 2 Enlargement of the 0 6 6 transmitted-reflected images in Fig. 1 [2].

with the finite-difference method. However, the E-L&FFT topographs were obtained by fast Fourier transforming the solution of the E-L dynamical theory.

Figs. 2 $[S_x(T-T)]$, $[E_x]$ and $[S_x(E-L)]$ are enlargements of the 0 6 6 transmitted-reflected images in Figs. 1 $[S_x(T-T)]$, $[E_x]$ and $[S_x(E-L)]$. Good agreements among Figs. 2 $[S_x(T-T)]$, $[E_x]$ and $[S_x(E-L)]$ are found both for $x=h$ and for $x=v$, respectively. However, evident discrepancies are also found between the cases of $x=h$ and $x=v$.

The present author has a hypothesis that too large R factors for protein crystals is caused by interferences of multiple-reflected wave fields and bankruptcy of the two-beam approximation that has been used for over 100 years. The present author has prepared to verify this hypothesis

concerning the too large R factors in protein crystallography by estimating them with n -beam approximation in place of the conventional two-beam approximation.

References

- [1] K. Okitsu, Y. Imai, and Y. Yoda: *Recent Advances in Crystallography*, (2012) pp. 67-86. InTech Open. <http://dx.doi.org/10.5772/47846>.
- [2] K. Okitsu, Y. Imai, Y. Yoda and Y. Ueji: *Acta Cryst.* **A75** (2019) 474-482; <https://doi.org/10.1107/S2053273319001499>.
- [3] K. Okitsu, Y. Imai, and Y. Yoda: *Acta Cryst.* **A75** (2019) 483-488; <https://doi.org/10.1107/S2053273319002936>.
- [4] K. Okitsu: *J. Jpn. Soc. Synchrotron Rad. Res.* **33** (2020) 61-80 [Invited].

Numerical verification of the higher-order ETH in quantum XXZ spin ladder

Eiki IYODA

*Department of Physics, Tokai University
Kitakaname, Hiratsuka-shi, Kanagawa 259-1292*

Recently, isolated quantum many-body systems, which are realized in artificial systems such as cold-atoms or superconducting qubits, have attracted much attention, because they are useful to study fundamental problems in statistical mechanics. Especially, it has been shown that even an isolated quantum many-body system exhibits thermalization. The eigenstate thermalization hypothesis (ETH) [1] is a promising mechanism of thermalization, which is closely related to quantum chaos. Many numerical studies have shown that ETH holds in non-integrable systems.

We propose a higher-order generalization of the ETH, to which we refer as the k -ETH ($k = 1, 2, \dots$) [3]. The lowest order ETH ($k = 1$) is the conventional ETH. The k -ETH gives many conditions which are obtained by comparing Hamiltonian dynamics with the Haar-random unitary of the k -fold channel. As a non-trivial contribution of the higher-order ETH, we show that the Page correction of the k th Renyi entanglement entropy of individual energy eigenstates originates from the k -ETH.

In this study, we numerically investigated 2-ETH for the one-dimensional spin-1/2 Heisenberg XXZ ladder model, which is composed by two chains whose lengths are p and $p + 1$ respectively. In order to numerically investigate 2-ETH, we should discuss finite size scaling of indicators of 2-ETH by changing the system size. The 2-ETH gives many conditions. For example, 2-ETH states that diagonal and off-diagonal matrix elements such as

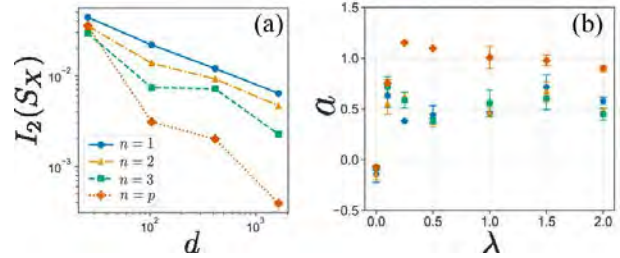


Figure 1: (a) d -dependence of $I_2(S_X)$. (b) λ -dependence of a .

$\langle E_i E_j | O | E_i E_j \rangle$ equal some value. There are totally d^2 equalities, where d is the dimension of the energy shell. We adopt $I_2(O)$ as an indicator of 2-ETH, which is defined as the maximum value of the deviation of the d^2 equalities. $I_2(O)$ is a straightforward extension of the indicator of strong 1-ETH [2]. By numerically exact diagonalization, we calculate $I_2(O)$ by changing parameters about energy shell and the Hamiltonian.

We numerically calculated $I_2(S_X)$, where S_X is the partial swap operator which swaps the region X between the original system and a replicated system. Figure 1(a) shows the d -dependence of $I_2(S_X)$ with $\lambda = 1$, where λ is the coupling constant in the rungs and tunes the integrability of the model. In non-integrable systems, the indicator $I_2(S_X)$ decays polynomially with d , which implies the 2-ETH for S_X holds in non-integrable systems.

We fit the numerical data of $\log I_2$ against a fitting function $f(d) := -a \log d + b$. Figure 1(b) shows the λ -dependence of the exponent

a . In the non-integrable cases ($\lambda \neq 0$), the exponent a takes a sufficiently large value. Especially, when the size of the region X equals p , the exponent $a \sim 1$, which is consistent with the typicality prediction.

In this report, we have numerically shown that the higher-order ETH holds by using the indicator $I_2(O)$. Numerical studies about finite size scaling with other indicators and the weaker version of higher-order ETH are left as future issues.

References

- [1] M. Rigol, V. Dunjko, and M. Olshanii, Nature **452**, 854 (2008).
- [2] H. Kim, T. N. Ikeda, and D. A. Huse, Phys. Rev. E **90**, 052105 (2014).
- [3] K. Kazuya, E. Iyoda, T. Sagawa, arXiv:1911.10755.

Analysis on Structuring and Dynamics of Ionic Liquid Forming Electric Double Layer as a Local Interfacial Field

Ken-ichi FUKUI

Department of Materials Engineering Science, Graduate School of Engineering Science,
Osaka University, Machikaneyama, Toyonaka, Osaka 560-8531

The interfacial ionic-liquid (IL) behavior causing bias stress in the electric double layer organic field effect transistor (EDL-OFET) (Fig. 1) has been investigated in the molecular scale using MD simulations combined with experimental techniques [1].

The MD simulations were performed with GROMACS-5.0.7. The rubrene substrate was of linear dimensions $7.2165 \times 7.1930 \times 2.7760$ nm. EMIM-FSI ion pairs were sandwiched between the rubrene substrate (2.7760 nm) and vacuum layer (~9.5 nm). Simulations were performed for the uncharged rubrene surface ($\sigma = 0$) and for the positively charged surfaces ($\sigma = 0.6, 1.2,$ and $1.8 \mu\text{C cm}^{-2}$). Single point charges were placed on each carbon atom consisting of a tetracene backbone of a rubrene molecule corresponding to the HOMO of rubrene, and its magnitude was determined by the overall surface charge density σ . The systems were equilibrated at a constant volume for 100 ps, followed by a constant volume simulation for 20 ns.

Fig. 2 shows the plane-averaged charge density profiles with respect to the amount of injected charge into rubrene electrode and number density profiles of atoms in EMIM cation and FSI anion, respectively, at the charge density of $1.8 \mu\text{C cm}^{-2}$. At this potential, EMIM cations and FSI anions form a checkerboard structure with their major molecular axis perpendicular to the surface. Thus, negative atoms of $-\text{SO}_2\text{F}$ of FSI anions are pointing the rubrene surface ($\text{O} \times 2$ and F). This configuration probably causes the bias stress by efficiently trap the hole carrier at the interface with structured interfacial IL as observed by force curve measurements with EC-FM-AFM [1].

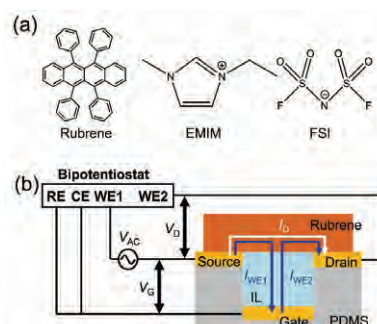


Fig. 1: (a) Molecular structures of rubrene and EMIM-FSI. (b) Schematic of EDL-OFET using rubrene semiconductor and IL gate dielectrics.

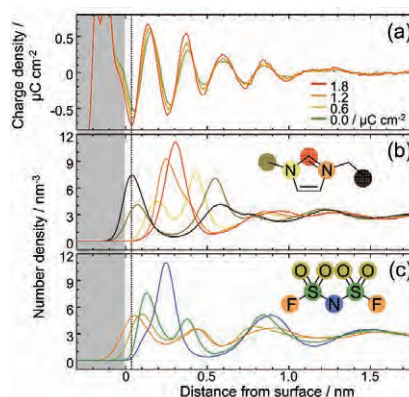


Fig. 2: (a) Plane-averaged charge density profiles with respect to the amount of injected charge into rubrene electrode. (b),(c) Number density profiles of atoms in the EMIM cation and the FSI anion, respectively, at the charge density of $1.8 \mu\text{C cm}^{-2}$. Each line corresponds to the shaded atom with the same color. Gray-shaded area is the rubrene-electrode region. Dotted line at $z = 0.04$ nm suggests the position of negative charge density next to the rubrene electrode surface.

Reference

- [1] D. Okaue, I. Tanabe, S. Ono, K. Sakamoto, T. Sato, A. Imanishi, Y. Morikawa, J. Takeya, K. Fukui, *J. Phys. Chem. C* **124** (2020) 2543.

Calculation of ordered structures and their optical properties of soft materials

Jun-ichi FUKUDA

Department of Physics, Kyushu University, Motoooka 744, Nishi-ku, Fukuoka 819-0395

This year we have studied how a topological defect in a thin cell of a nematic liquid crystal look under optical microscope. Such defects are commonly observed in experimental labs studying liquid crystals. However, usual identifications of topological defects in a nematic liquid crystal relies on the observation of the orientation profile *around* the topological defects. How the image should be *at the center* of topological defects has given little attention so far. It is because the length characterizing the defect core is $\sim 10\text{nm}$, much smaller than the resolution of optical imaging.

We have made use of the technique developed previously [1] which reproduced excellently the microscope images of a thin cell of a chiral liquid crystal. We solve the full Maxwell equations for the electromagnetic wave to investigate the response of the liquid crystal to monochromatic incident light with given wavevector. By doing calculations for different incident wavevectors, one can construct a microscope image, whose details are presented in Ref. [1].

Calculations have been done to investigate

the effect of the variation of the numerical aperture. We have found that the core of a topological defect appears as a dark spot, and also that the spot becomes sharper as the numerical aperture increases. More details will be presented in a manuscript in preparation.

Another subject is the lattice orientation of a cubic lattice of cholesteric blue phase liquid crystal in contact with unidirectionally orienting surfaces. Previous experiments found that the cubic lattice exhibits specific orientation with respect to the direction of the surface orientation. We have simulated the structures of cholesteric blue phases in such a setup using the Landau-de Gennes theory describing the orientational order of the liquid crystal by a second-rank tensor. This study is now under way.

References

- [1] A. Nych, J. Fukuda, U. Ognysta, S. Žumer and I Muševič, *Nature Phys.* **13**, 1215 (2017).
- [2] M. Takahashi *et al.* *J. Phys. D: Appl. Phys.* **51**, 104003 (2018)

Ultrafast relaxation of inhomogeneous electron distribution around the Dirac cone in graphene

Shota ONO

*Department of Electrical, Electronic and Computer Engineering, Gifu University
Gifu 501-1193*

It has been known that the inhomogeneous electron distribution can be created around the Dirac cone of monolayer graphene after photon absorption [1]. Motivated by recent experiment using ultrafast laser pulse [2], we simulate the ultrafast dynamics of the photoexcited Dirac electrons coupled with the optical phonons by solving the Boltzmann equation: $\partial f_{\mathbf{k}s}^{(\nu)}/\partial t = (\partial f/\partial t)_{\text{e-e}} + (\partial f/\partial t)_{\text{e-ph}}$ and $\partial n_{\mathbf{q}}^{(\beta)}/\partial t = (\partial n/\partial t)_{\text{ph-e}}$, where $f_{\mathbf{k}s}^{(\nu)}$ is the electron distribution function with the wavevector $\mathbf{k} = (k_x, k_y)$, the valleys $\nu = \text{K}$ and K' , and the band index $s = \pm 1$. $n_{\mathbf{q}}^{(\beta)}$ is the phonon distribution function, where β and \mathbf{q} denote the phonon mode and wavevector, respectively. The collision terms include the electron-electron (e-e) and the electron-phonon (e-ph) scattering contributions. The e-e interaction matrix element is calculated by using the expression given in Ref. [3]. The expression for the e-ph interaction matrix elements given in Ref. [4] were used to compute the scattering rates, while different e-ph coupling strengths [5] were used for the coupling with the Γ and K phonons, respectively. The initial condition for the electron distribution is imposed to show the inhomogeneous population around the Dirac cones [6].

Figure 1 (upper) shows the time-evolution of $f_{\mathbf{k},+1}^{(\nu)}$: The excited electrons inhomogeneously populated around the Dirac cone initially go to the K point due to the e-e scattering mainly, followed by electron thermalization due to both the e-e and e-ph scattering. The electron relaxation is slowed down from ~ 50 fs to more longer when the e-e scattering is neglected (lower). Using the electron distribution, the time-evolution of absorption

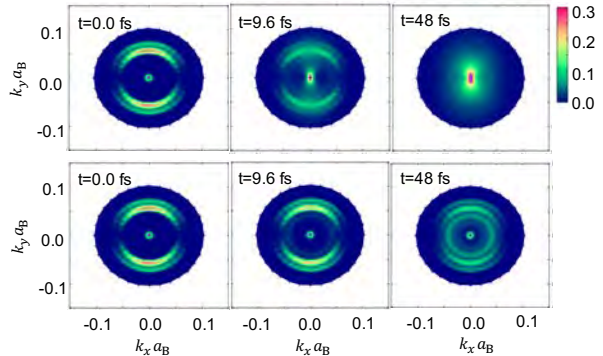


Figure 1: The time-evolution of the electron distribution around the Dirac cone: In upper figure, both the e-e and e-ph scattering are considered, while in lower figure the e-ph scattering is considered only.

spectra can also be calculated. We expect that the present study will stimulate further experimental work on this system.

The author thank I. Katayama (Yokohama National University) for useful discussions.

References

- [1] A. Grüneis *et al.*: Phys. Rev. B **67** (2003) 165402.
- [2] S. Nara *et al.*: JPS 2018 Autumn, 11aPS-20.
- [3] T. Ando: J. Phys. Soc. Jpn. **75** (2006) 074716.
- [4] S. Piscanec *et al.*: Phys. Rev. Lett. **93** (2004) 185503.
- [5] M. Lazzeri *et al.*: Phys. Rev. B **78** (2008) 081406(R).
- [6] M. Trushin *et al.*: Phys. Rev. B **92** (2015) 165429.

Boltzmann equation solver for nonequilibrium electrons and phonons in solids

Shota ONO

*Department of Electrical, Electronic and Computer Engineering, Gifu University
Gifu 501-1193*

It is of importance to establish a theoretical scheme for studying the ultrafast electron dynamics of laser-excited solids, where the nonequilibrium electron distribution approaches thermal distribution within a picosecond time scale through the electron-electron (e-e) and electron-phonon (e-ph) scattering. Recently the author has developed the Boltzmann equation solver to calculate the time-evolution of the electron and phonon distribution [1], where the free-electron, the Debye phonon, and the deformation potential models are used to describe the electron density-of-states (DOS), the phonon DOS, and the Eliashberg function (the e-ph coupling function), respectively. In the present study, based on *ab initio* approach to calculate these three functions, we develop the Boltzmann Equation solver for Nonequilibrium Electrons and Phonons, BENEP, which enables us to study the ultrafast electron and phonon dynamics of realistic materials absorbing a femtosecond laser pulse. It would be useful to analyze the pump-probe experimental data beyond the well-known two-temperature model [2].

By taking the wavevector average of the distribution functions, we calculate the time-evolution of the electron distribution $f(\varepsilon)$ and the phonon distribution $n(\omega)$, where ε and ω are the electron energy and the phonon frequency, respectively. The time-evolution of $f(\varepsilon)$ and $n(\omega)$ is regulated by the Boltzmann equation $\partial f(\varepsilon)/\partial t = (\partial f/\partial t)_{e-e} + (\partial f/\partial t)_{e-ph} + (\partial f/\partial t)_{laser}$ and $\partial n(\omega)/\partial t = (\partial n/\partial t)_{ph-e}$, where the laser excitation as well as the e-e and e-ph collision terms are considered.

We apply our BENEP code to the calculation of the femtosecond infrared photolumi-

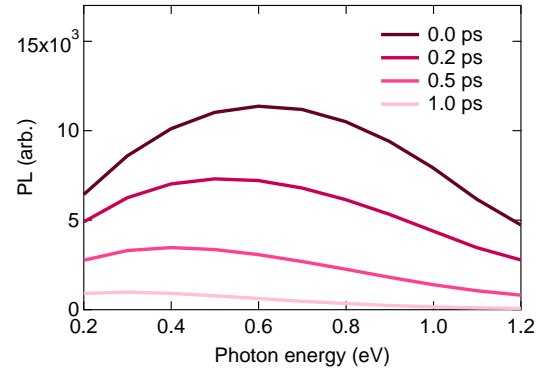


Figure 1: The time-evolution of PL in silver: The excitation density, the effective Coulomb interaction strength, and the electron diffusion time are assumed to be 460 J/cm^3 , 0.37 eV , and 0.5 ps , respectively.

nescence (PL) of metals. Figure 1 shows the time-evolution of PL spectra in silver: The PL spectra changes with time because the electron distribution thermalizes through the e-e scattering and because the electron energy is transferred to phonons. We find that the agreement between the numerical simulation and the experimental data is good, which will be demonstrated in our future paper [3].

The author thank T. Suemoto (Toyota Physical and Chemical Research Institute) for useful discussions.

References

- [1] S. Ono: Phys. Rev. B **97** (2018) 054310.
- [2] P. B. Allen: Phys. Rev. Lett. **59** (1987) 1460.
- [3] S. Ono and T. Suemoto, arXiv:2004.09000.

Entanglement in Remote Electron-phonon Systems Created by Photoirradiation

Kunio ISHIDA

School of Engineering and Center for Optics Research and Education

Utsunomiya University, Yoto, Utsunomiya, Tochigi 321-8585

Recent experiments on quantum entanglement between remote systems has revealed that the irradiated photons mediates quantum correlation between noninteracting material systems[1,2]. Since, however, its mechanism and/or dynamical behavior has not been understood theoretically, we study the dynamics of entanglement generation between remote systems by irradiation of a quantized light pulse. We employed a model of coupled electron-phonon-photon systems described by[3]

$$\mathcal{H} = \sum_{i=1}^3 \Omega_i c_i^\dagger c_i + \sum_{j=1}^2 \left[\omega a_j^\dagger a_j + \{ \mu (a_j^\dagger + a_j) + \varepsilon \} \frac{\sigma_z^{j+1}}{2} + \{ \sum_{i=1}^3 v_i (c_i^\dagger + c_i) + \lambda \} \sigma_x^j \right].$$

Solving the time-dependent Schrödinger equation by numerical calculation on the System B at ISSP, we found that the quantum mutual information for phonons reveals the dynamics of phonon entanglement generation.

Detection methods of entanglement generation dynamics are also studied and we showed that the scattered light, e.g., Stokes light, carries information on the phonon entanglement.

We derived relevant composite modes obtained by the Heisenberg equation of motion for c_i , and found that the heterodyne detection of it will help us distill the information on phonon correlation which slowly increases after a certain number of phonons is created. As shown in the previous study on phonon entanglement between remote diamond crystals[1], the entanglement is generated as a result of measurement on the scattered light, i.e., measurement corresponds to a disentanglement process between photons and phonons. Under the projection hypothesis, this means that the quantum correlation before measurement is also important to find appropriate methods for entanglement control. These results will help us design a method of coherent control of entanglement generation.

References

- [1] K. C. Lee, et al., *Science* **334**, 1253(2011).
- [2] F. Borjans, et al., *Nature* **577**, 195 (2020).
- [3] K. Ishida, *Eur. Phys. J.* **D73**, 117 (2019).

Molecular simulation of patchy particles

Takamichi TERAO

*Department of Electrical, Electronic, and Computer Engineering,
Gifu University, Yanagido 1-1, Gifu, 501-1193*

In colloidal systems, many studies have been performed to clarify the properties of spherical particles with isotropic interactions. Recently, there has been much interest in the studies of patchy particles with anisotropic interactions. It is of interest to create novel functional materials using these particles. In this study, the structural formation of patchy particles was studied by molecular simulations using cluster Monte Carlo method. To describe the effective interaction between patchy particles, the Kern-Frenkel model has been employed [1].

First, computer simulations are performed for 2-patch particles. Each particle has degrees of freedom of rotation in three-dimensional space, and its motion was constrained in a plane. In order to clarify the phase diagram, we analyzed the structure of the system using the generalized local bond order parameter that we have developed in previous studies [2]. As a result, a fluid phase, a hexagonal phase, a Kagome phase, and their coexistence phase have been observed.

Next, we studied tetrahedral patchy particles in a three-dimensional system (Figure 1), and the stability with diamond structure was numerically investigated. The photonic band

structures of colloidal crystals have been analyzed for various crystal structures. It has been revealed that a wide photonic bandgap exists in a colloidal crystal with diamond structure. Melting transition of such crystals have been studied by Monte Carlo simulations, and it was confirmed that the crystals with diamond structure becomes thermodynamically stable if the attractive interaction energy between patchy particles is about $10k_B T$.

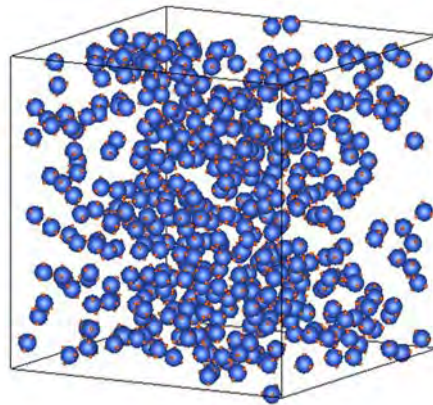


Fig. 1: Snapshot of tetrahedral patchy particles.

References

- [1] F. Romano, E. Sanz, P. Tartaglia, and F. Sciortino: *J. Phys.: Condens. Matter* **24** (2012) 064113.
- [2] R. Mizuno, K. Okumura, J. Oguri, and T. Terao: *Mol. Simul.* **45** (2019) 743.

Effects of Dzyaloshinskii-Moriya interactions and exchange randomness on low-temperature specific heats of spherical-kagome spin-systems

Yoshiyuki Fukumoto

*Department of Physics, Faculty of Science and Technology, Tokyo University of Science
2641 Yamazaki, Noda, Chiba 278-8510*

For cluster magnets described by Heisenberg models, in general, stepwise structures are expected in zero-temperature magnetization curves. However, for a spherical-kagome system $\{W_{72}V_{30}\}$ [1], which contains 30 vanadium ions with $S = 1/2$, it was reported that there is no such structure up to 50 T in a magnetization measurement at 0.5 K [2]. So far, the effects of (i) a distribution in the strength of the exchange interaction [2] and (ii) the Dzyaloshinskii-Moriya (DM) interaction [3] have been investigated. If in (i) the distribution width is about 30% of the average exchange interaction, or if in (ii) the DM interaction strength is about 10% of the exchange interaction, it has been shown that the low temperature magnetization process of $\{W_{72}V_{30}\}$ can be explained.

In this study, we focus on the effects of (i) and (ii) on the specific heat. To be specific, we first notice the fact that the recently reported experimental results for the low-temperature specific heat of $\{W_{72}V_{30}\}$ in several magnetic fields do not match the calculated results in the Heisenberg model; (a) the peak at about 2K in the calculated result is not seen in the experimental result, and (b) the observed magnetic-field dependence is very smaller than the calculation [4]. In order to resolve these two discrepancies, (a) and (b), we use the method of thermal quantum pure state [5] to calculate the specific heat, taking (i) and (ii) into account. As a result, regarding (a), we conclude that

the distribution of low-energy singlet states is affected by the distribution of exchange interactions to wipe out the low-temperature peak. The important finding is that the lowest singlet excitation-energy in the Heisenberg model is a fraction of the lowest triplet excitation-energy, which leads to the distribution width of exchange interaction being about 10% of the average exchange interaction (a fraction of the previous study [2]). Regarding (b), we found that the DM interaction can have the effect of suppressing the magnetic-field dependence of the energy eigenvalues, whose mechanism can also be illustrated by the two-spin model.

In conclusion, the specific heat of the 30-site system has been quantitatively evaluated up to sufficiently low temperatures, and we have qualitatively discussed the differences and similarities between the effects of two types of perturbations (i) and (ii) on the specific heat in magnetic fields and the magnetization process.

References

- [1] N. Kunisada *et al.*, PTEP 2014, 41I01 (2014).
- [2] J. Schnack *et al.*, arXiv:cond-mat/1304.2603v1.
- [3] Y. Fukumoto *et al.*, J. Phys. Soc. Jpn. 87, 124710, 2018.
- [4] T. Kihara *et al.*, PRB 99, 064430 (2019).
- [5] S. Sugiura and A. Shimizu, Phys. Rev. Lett. 108, 240401(2012).

Data-driven determination of a spin Hamiltonian of $\text{KCu}_4\text{P}_3\text{O}_{12}$

Ryo TAMURA

*International Center for Materials Nanoarchitectonics,
National Institute for Materials Science,
1-1 Namiki, Tsukuba, Ibaraki, 305-0044*

The origin of physical properties in materials is often understood through an effective model in materials science. Many methods have been developed in order to construct the effective model for a target material and they are mainly divided into two groups. One is ab initio calculations which determine the model parameters in an assumed effective model only by giving basic information of the target material. The other is a data-driven approach in which model parameters are determined so as to fit the experimentally measured data in the target material. In the latter case, from a view point of effective model estimations, data-driven techniques are considered to be efficient for the acceleration of automatic search for appropriate model parameters[1] and the extraction of relevant model parameters[2, 3, 4].

Here, by a data-driven approach, a spin Hamiltonian as an effective model of $\text{KCu}_4\text{P}_3\text{O}_{12}$ is determined. The crystal structure of $\text{KCu}_4\text{P}_3\text{O}_{12}$ is defined by $a = 7.433 \text{ \AA}$, $b = 7.839 \text{ \AA}$, $c = 9.464 \text{ \AA}$, $\alpha = 108.28^\circ$, $\beta = 112.68^\circ$, $\gamma = 92.73^\circ$, and space group: $\text{P}\bar{1}[5]$. Cu(II) ions have $S = 1/2$ isotropic Heisenberg spin, but magnetic properties of this compound have not been reported yet. The lattice structure of Cu ions can be regarded as a zigzag chain consisting of eight Cu ions. Thus, a quantum Heisenberg model on a zigzag chain is targeted for a spin Hamiltonian of $\text{KCu}_4\text{P}_3\text{O}_{12}$ to be estimated. We estimate superexchange interactions between Cu

ions in this target model by a data-driven approach with susceptibility and magnetization curves experimentally measured. The estimated model parameters are $J_1 = -8.54 \text{ meV}$, $J_2 = -2.67 \text{ meV}$, $J_3 = -3.90 \text{ meV}$, and $J_4 = 6.24 \text{ meV}$, which describe the measured results well.

Once an estimated spin Hamiltonian is established, we predict, through theoretical analysis of the Hamiltonian, various magnetic properties which cannot be or have not been measured, such as magnetic specific heat, magnetic entropy, spin configuration, and spin gap. These predictions are helpful to propose a further experimental plan and design.

This work is the collaboration work with Koji Hukushima, Akira Matsuo, Koichi Kindo, and Masashi Hase.

References

- [1] R. Tamura and K. Hukushima, PLoS ONE **13**, e0193785 (2018).
- [2] H. Takenaka, K. Nagata, T. Mizokawa, and M. Okada, J. Phys. Soc. Jpn. **83**, 124706 (2014).
- [3] R. Tamura and K. Hukushima, Phys. Rev. B **95**, 064407 (2017).
- [4] H. Fujita, Y. O. Nakagawa, S. Sugiura, and M. Oshikawa, Phys. Rev. B **97**, 075114 (2018).

- [5] H. Effenberger, *Zeitschrift für Kristallographie* **180**, 43 (1987).

Establishment of new analysis method for extend X-ray absorption fine structure with sparse modeling

Hiroyuki KUMAZOE

*Institute of Industrial Nanomaterials, Kumamoto University
Kurokami, Chuo-ku, Kumamoto, 860-8555*

Measurement of extended X-ray absorption fine structure (EXAFS) is one of the primary methods to obtain local structure information around a specific element with atomic scale. We are building a new method for the analysis of EXAFS by the sparse modeling. This year, we focused on Bayes free energy as an information criteria for choosing the regularization parameter.

To perform the sparse modeling on the EXAFS signals, we employed a simplified model of the EXAFS formalism based on the single-scattering approximation [1]:

$$\begin{aligned}
 y(k) &= \chi(k) \cdot k^3 \\
 &= \sum_{j=1}^N \frac{k^2}{R_j^2} \exp[-2k^2\sigma_j^2] \exp\left[-2\frac{R_j}{\Lambda}\right] \\
 &\quad \times (a_j \sin 2kR_j + b_j \cos 2kR_j), \quad (1)
 \end{aligned}$$

where, $y(k)$ is the k^3 weighted EXAFS signal, $\chi(k)$ as a function of the photoelectron wavenumber, k . R_j is the distance from the focused atom, j . σ_j is the Debye–Waller factor for atom, j . Λ is the mean free path. To obtain the local structure information, we convert Eq. (1) to a linear regression problem and solve it with L_1 regularization.

$$\hat{\mathbf{w}} = \arg \min_{\mathbf{w}} \left[\frac{1}{2} \|\mathbf{y} - \mathbf{X}\mathbf{w}\|_2^2 + \lambda \|\mathbf{w}\|_1 \right], \quad (2)$$

where the regression coefficient is $\mathbf{w} = (\dots, a_j, b_j, \dots)^T$. The response vector, \mathbf{y} comes from the target data and the predictor

matrix, \mathbf{X} incorporates other terms in Eq. (1). In this method, some elements of the coefficient, \mathbf{w} is are suppressed to exactly zero with the moderate value of λ .

Let us consider the sparse regression problem for the LASSO estimations within Bayesian inference to choose the regression parameter, λ . In Bayesian inference, this linear regression problem is optimized by maximizing the posterior probability. Here, we introduce the Bayesian free energy [2, 3] as an information criterion to optimize a regularization parameter and to extract the physical model appropriately. As a result, we estimated the radial distribution function with fewer bases than in previous studies [1].

This work was supported by JST CREST Grant Number JPMJCR 1861, Japan.

References

- [1] I. Akai, K. Iwamitsu, Y. Igarashi, M. Okada, H. Setoyama, T. Okajima, and Y. Hirai, *J. Phys. Soc. Jpn.* **87**, 074003 (2018).
- [2] Y. Igarashi, H. Takenaka, Y. Nakanishi-Ohno, M. Uemura, S. Ikeda, and M. Okada, *J. Phys. Soc. Jpn.* **87**, 044802 (2018).
- [3] Y. Mototake, Y. Igarashi, H. Takenaka, K. Nagata, and M. Okada, *J. Phys. Soc. Jpn.* **87**, 114004 (2018).

Competition between dipolar and short-range interactions on the magnetic thin films

Hisato KOMATSU, Yoshihiko NONOMURA, and Masamichi NISHINO
National Institute for Materials Science, Namiki, Tsukuba, Ibaraki 305-0044

Magnetic thin films are known to exhibit a variety of orderings when the exchange and the dipolar interactions compete with each other [1]. These systems are described by the following Hamiltonian:

$$\begin{aligned} \mathcal{H} = & -J \sum_{\langle i,j \rangle} \mathbf{S}_i \cdot \mathbf{S}_j \\ & + D' \sum_{i < j} \left\{ \frac{\mathbf{S}_i \cdot \mathbf{S}_j}{r_{ij}^3} - \frac{3(\mathbf{S}_i \cdot \mathbf{r}_{ij})(\mathbf{S}_j \cdot \mathbf{r}_{ij})}{r_{ij}^5} \right\} \\ & - \eta \sum_i (S_i^z)^2 - H \sum_i S_i^z. \end{aligned} \quad (1)$$

Here, $\mathbf{r}_{ij} = {}^t(x_{ij}, y_{ij}, 0) \equiv \mathbf{j} - \mathbf{i}$ means the difference between the position i and j . Previous studies revealed that this system has the spin-reorientation(SR) transition between the stripe and the planar ferromagnetic phase [2, 3] driven by the anisotropy η . However, these studies are limited to the cases when the magnetic field H does not exist.

We investigate the relation between the structure of the ordered phase and the parameters η and H using the Monte-Carlo(MC) simulation. In the simulation, naive MC algorithm require $O(N^2)$ simulation time, and thus we adopt the $O(N)$ SCO algorithm [4]. The coupling constant of interactions are fixed as $J = D' = 1$. Figures 1 and 2 show the snapshots and the $\eta - T$ phase diagrams given by our investigation, respectively. These figures show that the SR transition exists no matter whether H is zero or nonzero.

The numerical calculations of this study were mainly performed on the Numerical Materials Simulator at National Institute for Ma-

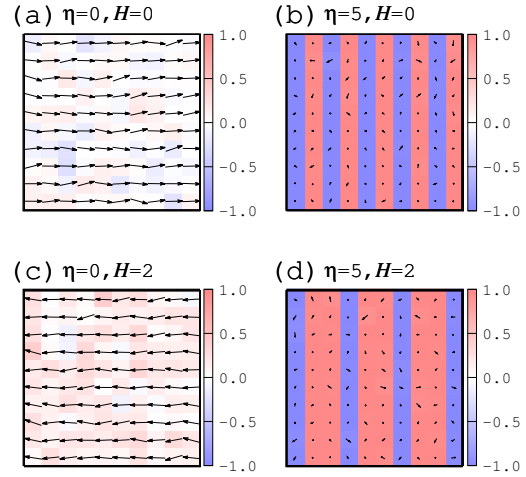


Figure 1: Snapshots of the system at several cases. The vectors and color mean the values of (S^x, S^y) and S^z , respectively. The parameters η and H are fixed at (a) $\eta = 0, H = 0$, (b) $\eta = 5, H = 0$, (c) $\eta = 0, H = 2$, and (d) $\eta = 5, H = 2$, and the temperature $T = 0.1$. Note that the widths of the stripes depend on H .

terials Science. We applied for the uage of the ISSP Supercomputer in preparation for the maintenance period of this simulator. However, we have ended this period without need for the new large-scale simulation, and do not have used the ISSP Supercomputer.

References

- [1] K. De’Bell, A. B. MacIsaac, and J. P. Whitehead, *Rev. Mod. Phys.* **72**, 225 (2000).

[2] J. P. Whitehead, A. B. MacIsaac, and K. De'Bell, Phys. Rev. B **77**, 174415 (2008)

[3] M. Carubelli, O. V. Billoni, S. A. Pighin, S. A. Cannas, D. A. Stariolo, and F. A. Tamarit, Phys. Rev. B **77**, 134417 (2008).

[4] M. Sasaki and F. Matsubara, J. Phys. Soc. Jpn. **77**, 024004 (2008).

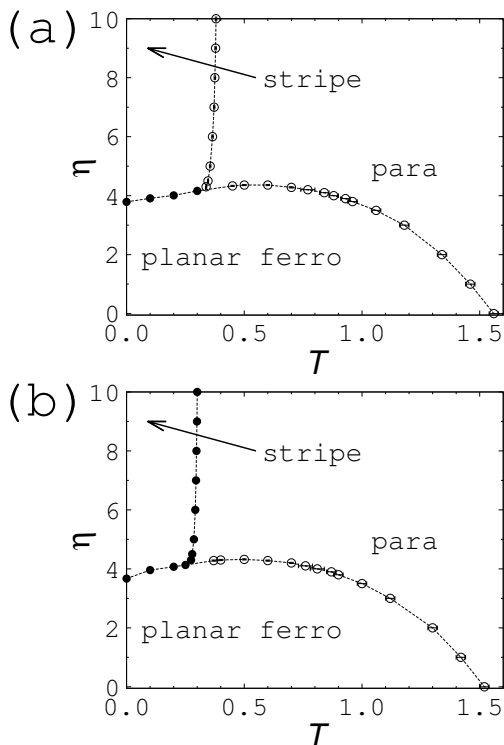


Figure 2: The $\eta - T$ phase diagrams at (a) $H = 0$ and (b) $H = 2$. The closed and open circles mean the first- and the second-order phase transition.

Competition between dipolar and Dzyaloshinskii-Moriya interactions on the magnetic thin films

Hisato KOMATSU, Yoshihiko NONOMURA, and Masamichi NISHINO
National Institute for Materials Science, Namiki, Tsukuba, Ibaraki 305-0044

Studies in recent years revealed that the spin systems with the Dzyaloshinskii-Moriya(DM) interaction have various types of magnetic structures such as the skyrmion lattice or the chiral magnetism [1]. Most of these studies does not consider the effect of the dipolar interaction between the magnetic moments of the spins, although it can not be removed. We investigate the two-dimensional square lattice where the DM, the nearest-neighbor ferromagnetic, and the dipolar interactions compete with each other, by the Monte-Carlo(MC) simulation.

The Hamiltonian we consider in this study is given as follows:

$$\begin{aligned} \mathcal{H} = & -J \sum_{\langle i,j \rangle} \mathbf{S}_i \cdot \mathbf{S}_j \\ & -D \sum_i \left\{ (\mathbf{S}_i \times \mathbf{S}_{i+e_x})_x + (\mathbf{S}_i \times \mathbf{S}_{i+e_y})_y \right\} \\ & +D' \sum_{i<j} \left\{ \frac{\mathbf{S}_i \cdot \mathbf{S}_j}{r_{ij}^3} - \frac{3(\mathbf{S}_i \cdot \mathbf{r}_{ij})(\mathbf{S}_j \cdot \mathbf{r}_{ij})}{r_{ij}^5} \right\} \\ & -\eta \sum_i (S_i^z)^2 - H \sum_i S_i^z. \end{aligned} \quad (1)$$

Here, $\mathbf{r}_{ij} = {}^t(x_{ij}, y_{ij}, 0) \equiv \mathbf{j} - \mathbf{i}$ means the difference between the position \mathbf{i} and \mathbf{j} . We fixed the coupling constant of short range interaction as $J = D = 1$. In the simulation, naive MC algorithm require $O(N^2)$ simulation time, and thus we adopt the $O(N)$ SCO algorithm [3].

As we can see in the figure 1, the skyrmion lattice changes its structure depending mainly

on the value of D' and η . It makes the triangular lattice under certain conditions, and the square lattice under the others. Furthermore, the chiral magnetic phase also shows the change of the direction of the structure depending on the parameters. We calculate the orientational order parameter of these phases, and investigated the condition under which each structure appear.

The numerical calculations of this study were mainly performed on the Numerical Materials Simulator at National Institute for Materials Science. We applied for the uage of the ISSP Supercomputer in preparation for the maintenance period of this simulator. However, we have ended this period without need for the new large-scale simulation, and do not have used the ISSP Supercomputer.

References

- [1] S. D. Yi, S. Onoda, N. Nishikawa, and J. H. Han, Phys. Rev. B **80**, 054416 (2009).
- [2] M. Sasaki and F. Matsubara, J. Phys. Soc. Jpn. **77**, 024004 (2008).

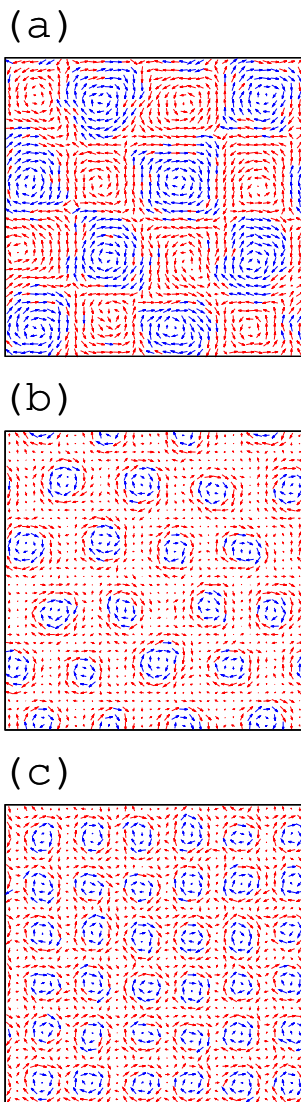


Figure 1: Snapshots of the skyrmion lattice phase at (a) $D' = 0.0$, $\eta = -1.2$, $H = 0.2$, (b) $D' = 0.0$, $\eta = 0.0$, $H = 0.5$, and (c) $D' = 0.6$, $\eta = 2.0$, $H = 1.5$. The temperature of each one is fixed at $T = 0.1$. The skyrmions make the square lattice at the cases (a) and (c), whereas they make the triangular lattice at (b). Note that direction of the square lattice is different in (a) and (c).

Investigation of Dynamics of a Supercooled Liquid and Proteins using the Free-Energy Landscape

Takashi YOSHIDOME

*Department of Applied Physics, Graduate School of Engineering, Tohoku University, Sendai
980-8579*

Free-energy landscape (FEL) picture has been used for understanding the properties of glass transition and protein folding [1,2]. The free-energy landscape is defined as a function of a particle configuration [2]. In the present study, we have investigated the dynamics of a Lennard-Jones system in a supercooled state and the dynamics of two proteins upon unfolding process from the viewpoint of the FEL.

We first computed the FEL for a crystallization process in a supercooled state. The computation of free-energy landscape was conducted using the protocol we have proposed [3]. The initial configuration was prepared using a Monte-Carlo (MC) simulation at a temperature above the freezing temperature. We have successfully obtained a FEL upon crystallization.

As for the protein dynamics upon unfolding process, we focused on the two proteins (goat alpha-lactalbumin and human lysozyme). It has experimentally shown that they have quite similar native structures but different structures at the transition state. We first performed all-atom molecular dynamics (MD) simulations of

the two proteins at 400 K to observe unfolding process. Then the trajectories were analyzed. It was found that the experimental result was successfully reproduced.

The calculations were performed using the L4cpu and F18acc in the system B, and L4cpu in the system C. We used our custom-made program [3] for computing the free-energy landscape of a Lennard-Jones system and for MC simulations. As for the study of protein unfolding, MD simulations were performed using the program GROMACS [5]. The MD trajectories were analyzed using our custom-made programs.

References

- [1] D. Wales: *Energy Landscapes: Applications to Clusters, Biomolecules and Glasses* (Cambridge University Press, 2004).
- [2] T. Odagaki: J. Phys. Soc. Jpn. **86** (2017) 082001.
- [3] T. Yoshidome, A. Yoshimori, and T. Odagaki: Phys. Rev. E **76** (2007) 021506.
- [4] H.J.C. Berendsen, D. Van der Spoel, and R. van Drunen, Comput. Phys. Commu. **91** (1995) 43.

Non-monotonic Behavior of the Binder Parameter in Potts Models

Hiroshi WATANABE

*Department of Applied Physics and Physico-Informatics, Keio University
Yokohama, Kanagawa 223-8522, Japan*

Satoshi MORITA, Yuichi MOTOYAMA, and Naoki KAWASHIMA
*Institute for Solid State Physics, University of Tokyo
Kashiwa-no-ha, Kashiwa, Chiba 277-8581*

The Binder parameter, *a.k.a.*, the forth-order cumulant, is a useful tool for analyzing the critical phenomena [1]. Since the scaling dimension of the Binder parameter is zero, its value does not depend on the system size at the criticality. While the Binder parameter usually a monotonic function for the systems involving continuous phase transition, it sometimes exhibits non-monotonic behavior. For example, a hump appears in the Binder parameter near the criticality of the Potts model. It exhibit system size dependence, and therefore, it is not trivial whether the universal scaling function itself has a hump or not. Additionally, it is known that the amplitude of the hump depends on the definition of the order parameter. However, the reason has not been clarified yet.

To study the peculiar behavior of the Binder parameter, we investigate the Fortuin-Kastelyen graph representation. We find that the graph representation of the Binder parameter consists of two parts, namely, the low- and high-temperature components, and the peculiar behavior of the Binder parameter is caused by the low-temperature one. We also find the spin representation of the high-temperature components of the Binder parameter, which is a monotonic function. We study the $J_1 - -J_2$ frustrated Ising model [2] and find that the non-monotonic behavior of the Binder parameter can be removed.

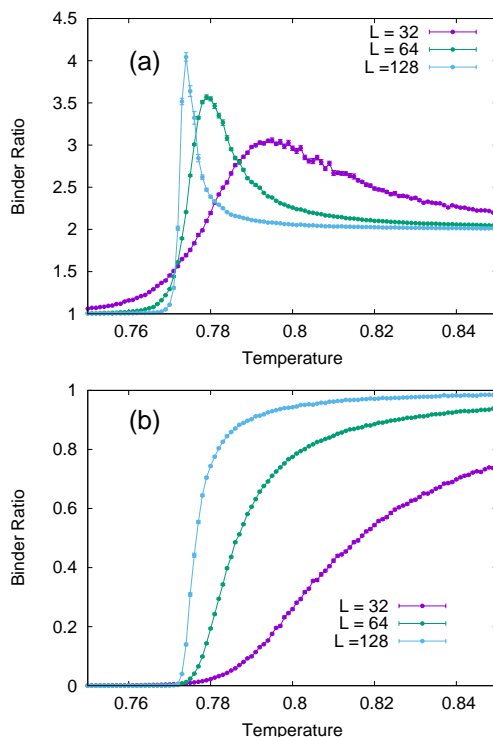


Figure 1: The Binder parameters of the $J_1 - -J_2$ frustrated Ising model with (a) the conventional and (b) the proposed definitions. The former exhibits humps while the latter does not.

[1] K. Binder, Z. Phys. B Cond. Matt. , vol. 43, pp. 119-140 (1981).

[2] S. Jin, A. Sen, and A. W. Sandvik, Phys. Rev. Lett. vol. 108, pp. 2-6 (2012).

Simulating phonon cross section using density functional theory

Naoki Murai

*Materials and Life Science Division, J-PARC Center, Japan Atomic Energy Agency
Tokai, Ibaraki 319-1195, Japan*

The studies of lattice dynamics, phonons, in crystalline materials are of fundamental importance as they provide key insights into the understanding of some relevant physical properties such as superconductivity and thermal conductivity. Historically, the direct observation of phonon dispersion using inelastic neutron scattering (INS) by Brockhouse opened the field of phonon spectroscopy as an energy- and momentum-resolved technique[1]. Since then, especially with the development of modern time-of-flight spectrometers at spallation neutron sources[2], INS has emerged as a powerful tool that allows efficient determination of phonon dispersion. Meanwhile, as an alternative method, inelastic x-ray scattering (IXS) has demonstrated its potential to precisely measure phonon dispersion[3]. Thus, the field of phonon spectroscopy has grown quickly over the past few decades, and the development of new instruments offers a unique opportunity to explore lattice dynamics in novel materials.

So far, we have been working on phonon dispersion measurements using the state-of-the-art INS spectrometers at J-PARC. The present project was carried out as a joint experimental and numerical study of lattice dynamics properties in novel materials. In particular, thanks to recent advances in density functional theory (DFT) calculations, it is now possible to perform *ab initio* phonon calculations whose only input information is the chemical composition of the materials.

In the present research project, we per-

formed *ab initio* phonon calculations, with a particular focus on unconventional superconductors and thermoelectric materials. Phonon calculations were performed using the density functional perturbation theory (DFPT)[4], as implemented in QUANTUM ESPRESSO code[5, 6]. Figure. 1 shows representative results obtained for SnS, which is predicted to be an attractive thermoelectric candidate. Here, all calculations were performed using the plane-wave pseudopotential method and the generalized gradient approximation (GGA) for the exchange correlation functional in the Perdew-Burke-Ernzerhof (PBE) parametrization[7]. Pseudopotentials and energy cutoffs of plane-wave basis were chosen according to the results of convergence tests provided in the standard solid-state pseudopotential (SSSP) library[8], in which the precision and performance of publicly available pseudopotential libraries are extensively tested to facilitate the optimal choice of pseudopotentials. In the present work, we used ultrasoft pseudopotentials from the GBRV library[9] with cutoffs of 70 Ry and 560 Ry for the expansion of the wave functions and charge densities, respectively. The Brillouin zone integration was performed over a $12 \times 12 \times 12$ \mathbf{k} mesh. Dynamical matrices were computed on $6 \times 6 \times 6$ meshes in \mathbf{q} space, which were then interpolated to determine the full phonon dispersion. Comparing the experimental phonon dispersion of SnS with DFPT calculations, we found that DFPT calculations are quite successful in

predicting the experimental phonon frequencies. From the calculated phonon eigenvalues and eigenvectors, we also computed the dynamical structure factor $S(\mathbf{Q}, \omega)$, which provides an estimation of the phonon intensity. A comparison with the neutron scattering data revealed that the experimental phonon intensities of SnS were perfectly reproduced by this simulation.

The present work thus serves to highlight the potential to use DFPT phonon calculations to simulate phonon cross sections as well as phonon frequencies. A more detailed report is now in course of preparation and will be published elsewhere.

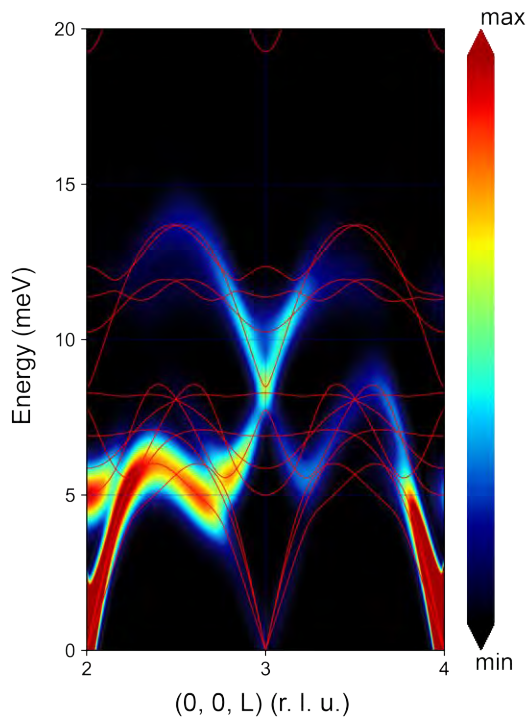


Figure 1: Calculated phonon dispersion of SnS. To facilitate the comparison between theory and experiment, the dynamical structure factor, $S(\mathbf{Q}, \omega)$, is weighted on the calculated phonon dispersion curves.

References

- [1] B. N. Brockhouse and A. T. Stewart Phys. Rev. **100**, 756 (1995).
- [2] K. Nakajima *et al.*, Quantum Beam Sci. **1**, 9 (2017).
- [3] A. Q. R. Baron, High-Resolution Inelastic X-Ray Scattering, in *Synchrotron Light Sources and Free-Electron Lasers: Accelerator Physics, Instrumentation and Science Applications*, edited by E. J. Jaeschke, S. Khan, J. R. Schneider, and J. B. Hastings (Springer International Publishing, Cham, 2016) pp. 1643–1719, (see also arXiv:1504.01098).
- [4] S. Baroni *et al.*, Rev. Mod. Phys. **73**, 515 (2001).
- [5] P. Giannozzi *et al.*, J. Phys. Condens. Matter **21**, 395502 (2009).
- [6] P. Giannozzi *et al.*, J. Phys. Condens. Matter **29**, 465901 (2017).
- [7] J. P. Perdew, K. Burke, and M. Ernzerhof, Phys. Rev. Lett. **77**, 3865 (1996).
- [8] G. Prandini *et al.*, npj Computational Materials **4**, 72 (2018).
- [9] K. F. Garrity *et al.*, Computational Materials Science **81**, 446 (2014).

Molecular dynamics simulations of water confined in carbon structures with the reactive force field

Tomoko MIZUGUCHI

*Faculty of Materials Science and Engineering, Kyoto Institute of Technology
Matsugasaki, Sakyo-ku, Kyoto 606-8585*

Many studies have been done on water in confinement by both theoretical and experimental techniques and revealed that the properties of confined water may strongly differ from that of bulk water. It is clearly important to properly evaluate the influence of confinement on water for various applications such as ion channels or drug delivery. Until last year, we had performed molecular dynamics (MD) simulations of confined water in nanoporous silica with the reactive force field (ReaxFF) using the supercomputer at ISSP. We examined the influence of hydrophilic surface on the physical properties of water, specifically, the hydrogen bond structure and dynamics [1]. This year, I embarked on MD simulations using ReaxFF for water in a carbon nanotube as a model of a hydrophobic pore to clarify the influence of interface on water.

ReaxFF allows us to incorporate bond breakage and formation, which are particularly important on interface, in MD simulations with a lower computational cost than quantum-mechanics-level calculations. I used four ReaxFF parameter sets: (i) developed by Monti *et al.* for biomolecules (protein-2013) [2], (ii) by Zhang and van Duin to improve the weak interaction between hydrocarbon and water from protein-2013 force field (CHON-2017_weak) [3], (iii) by Yeon and van Duin to simulate hydrolysis reactions at silica/water interface (Yeon2015) [4], and (iv) by Pitman and van Duin for clayzeolite com-

posites (Pitman2012) [5]. I prepared a single-walled carbon nanotube solvated in water and observed the inflow and outflow of water into the nanotube. The diameter of the carbon nanotube (CNT) was set 2.7 nm for comparison with our previous results in the silica/water system. All simulations were conducted in the NPT ensemble ($T = 300$ K and $P = 1$ atm) using the Nosé-Hoover thermostat and barostat with LAMMPS pre-installed in the supercomputer at ISSP. The ReaxFF MD simulations were carried out with a time step of 0.25 fs through the USER-REAXC package of LAMMPS.

When the protein-2013 and Pitman2012 force fields were used, water flowed into the CNT and filled it in 250 ps. In the 250-ps simulation using the Yeon2015 force field, water flowed into the CNT somewhat. It seems to need more time to fill in the CNT with water. In fact, when I started the simulation with a structure where the CNT was filled with water, the CNT remained filled with water. On the other hand, water went out of the CNT using the CHON-2017_weak force field. Some experiments show that water spontaneously flows inside the CNT, thus the CHON-2017_weak force field seems not to be suitable for the CNT/water system. But we should carefully verify the result. I am now planning to carry out DFT calculations to compare with the simulation results using ReaxFF.

References

- [1] T. Mizuguchi, K. Hagita, S. Fujiwara and T. Yamada: *Mo. Sim.* **45** (2019) 1437.
- [2] S. Monti, A. Corozzi, P. Fristrup, K. L. Joshi, Y. K. Shin, P. Oelschlager, A. C. T. van Duin, and V. Barone: *Phys. Chem. Chem. Phys.* **15** (2013) 15062.
- [3] W. Zhang and A. C. T. van Duin: *J. Phys. Chem. B* **122** (2018) 4083.
- [4] J. Yeon and A. C. T. van Duin: *J. Phys. Chem. C* **120** (2016) 305.
- [5] M. C. Pitman and A. C. T. van Duin: *J. Am. Chem. Soc.* **134** (2012) 3042.

Manipulation of electronic states with nanostructures: model construction and its application

Toshikaze KARIYADO

International Center for Materials Nanoarchitectonics,

National Institute for Materials Science, Namiki, Tsukuba, Ibaraki 305-0044

We focus on computing orbital magnetic susceptibility, which is relatively easy to measure in experiment, to characterize novel band structure such as Dirac/Weyl fermions. There are some situations in which computation of orbital magnetic susceptibility requires large computing resources. One example of such a situation is when we deal with (i) nanostructured system, which is the main topic of this project. Nanostructures lead to large number of sites in a unit cell, which in turn makes the computation hard. Another situation is when we handle with (ii) real materials. Generically, taking more orbitals into account gives better precision at the cost of computing power. Furthermore, in order to characterize singular band structures like Dirac/Weyl cones, fine sampling of k-points is inevitable.

A useful strategy to improve the efficiency of computation is applying massive parallelization on k-point sampling, which had been done in the preceding project last year. This year, we have made some corrections in memory handling to push up the maximum system size allowed in the same facility.

The improved program has been used to calculate the orbital magnetic susceptibility of Sr₃PbO, a Dirac material with antiperovskite crystalline structure. Temperature and carrier number dependence of the susceptibility is obtained using a tight-binding model derived from the ab-initio calculation. The improved program enables us to have better results in low temperature. It turned out that the susceptibility at low temperature is affected mainly by the change in the temperature dependence of the chemical potential associated with the change in the density of states.

Another topic in this project is the investigation on the bilayers of atomically thin materials with some mismatch showing moire pattern. A generic theory on the symmetry-based constraints on the interlayer coupling is proposed [1], which is inspired by data sets of the interlayer coupling in bilayer graphene obtained by systematic ab-initio calculations.

References

- [1] T. Kariyado and A. Vishwanath, Phys. Rev. Research 1 (2019) 033076.

Statistical Properties in a Branching Network

Satoshi YUKAWA, Kei TAKAYA, and Takeru WATANABE
Department of Earth and Space Science, Osaka University
Machikaneyama, Toyonaka, Osaka 560-0043

In a river network, there are many interesting statistical laws, such as Hack's law and Horton's law. Recently another statistical law was found in the distribution of bifurcation angle.[1, 2] The distribution has a universal characteristic angle depending on the aridity of the climate:[3] For the humid area, the angle is $2\pi/5 = 72^\circ$ and, on the other hand, for the highly arid area, it takes a smaller angle of almost 45° . The angle $2\pi/5$ is theoretically explained for the Laplacian growth network, but the smaller angle is not.

In this supercomputer project, we develop a theoretical model to understand the aridity dependence of the network based on the coupled map lattice model.[4] The model is constructed on a square lattice with water and soil variables. Dynamical rules are too complicated to be expressed here. The resultant networks generated by computer simulation are shown in Figs. 1.

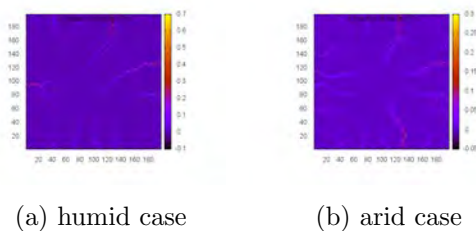


Figure 1: Simulated network structures

Distribution of the bifurcation angle can be obtained from the simulated network. The result is presented in Fig. 2. We observe slight aridity dependence in the figure. Increasing aridity index, the peak at the characteristic angle becomes much larger. Besides the lower tail

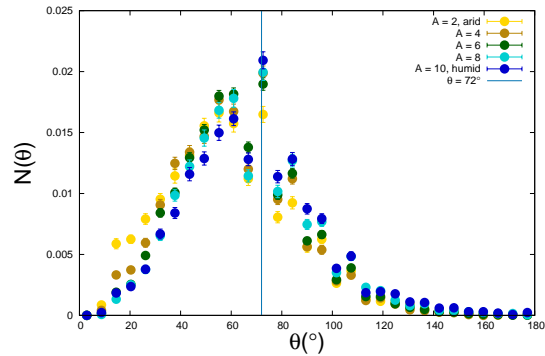


Figure 2: Bifurcation angle distribution for several aridity parameters A .

of the distribution decreases. There is, however, discontinuous behavior around the characteristic angle in the distribution. The origin of such behavior is unclear. We need additional computer simulations.

References

- [1] O. Devauchelle, A. P. Petroff, H. F. Seybold, and D. H. Rothman: *Proceedings of the National Academy of Sciences* **109** (2012) 20832.
- [2] S. Yukawa, T. Watanabe, and K. Hara: *Journal of the Physical Society of Japan* **88** (2019) 024901.
- [3] H. Seybold, D. H. Rothman, and J. W. Kirchner: *Geophysical Research Letters* **44** (2017) 2272.
- [4] B. Murray and C. Paola: *Earth Surface Processes and Landforms* **22** (1997) 1001.

Numerical Study of Cell Guiding Mechanism in Cellular Tissue

Katsuyoshi Matsushita

*Department of Biological Science, Osaka University
Toyonaka, Osaka 563-0043*

Cells have function in the organisms. In the development of organisms, cells are not always born in the suitable place which the cells function. In these cases, cell migration play a significant role to transport the cells to the suitable place. As a prominent observation, there is a case that the transport length of the cell migration reaches mm scales much larger than the cell's typical scale of $10\mu\text{m}$ [1]. In such cases, the migration should be properly guided by surrounding tissues to transport the cell for its suitable position. The guiding mechanism is still unclear and is expected to utilize chemical signals.

As a candidate of the chemical signal, the chemical cell-cell adhesion is one of most powerful candidate. The possibility of the cell-cell adhesion on the explanation of the long distance transport of cells is not sufficiently examined. In this work, we have investigated the cell migration on tissue which is guided by the cell-cell adhesion. We employed the Cellular Potts model and examine cell-cell adhesion effect on the cell migration in tissue [2].

We consider the model consists of suspended transported cells on cellular tissue on the Cellular Potts model[3] and one dimensional transport of the cells. The cells and tissue interacts with the heterophilic cell-cell adhesion, As a guiding mechanism of the cell migration direction, we consider the polarity of the cell-cell l adhesion. The polarity is a hypothetical factor for guiding collective cell migrations with long distance [4, 5] and is expected to be

effective in the case of cell transport on tissue.

We show that the migration direction of cells on the tissue aligns in the same direction even when the cells are suspended. The order in cell migration is induced as a polarity memory effect [6, 7]. The net transport velocity exhibits a non-linear transport and becomes a finite value above a threshold adhesion strength. Furthermore, the transport distance is longer than 10^2 times of the cell scale. This result show potential of the heterophilic adhesion with polarity as the guiding mechanism of cell transports.

References

- [1] C. Lois and A. Alvarez-Buylla, *Science* **264**, 1145 (1994).
- [2] K. Matsushita: submitted to PRE.
- [3] F. Graner and J. Glazier, *Phys. Rev. Lett.* **69**, 2013 (1992).
- [4] K. Matsushita: *Phys. Rev. E* **97**, 042413 (2018).
- [5] K. Matsushita: *Phys. Rev. E* **95**, 032415 (2017).
- [6] K Matsushita, K Horibe, N Kamamoto, S Yabunaka, K Fujimoto, *Proc. Sympo. Simul. Traffic Flow* **25**, 21 (2019).
- [7] Matsushita, K Horibe, N Kamamoto, K Fujimoto, *J. Phys. Soc. Jpn.* **88**, 103801 (2019).

Magnetism in the System with the Multiple-Spin Exchange Interactions

Chitoshi YASUDA

*Department of Physics and Earth Sciences, Faculty of Science,
University of the Ryukyus, Okinawa 903-0213, Japan*

Helium-3 (^3He) atoms adsorbed on graphite form the commensurate solid layer regarded as the spin-1/2 quantum spin system on a triangular lattice at certain density of ^3He . In the exchange process of ^3He atoms, there are not only an exchange between two neighbor atoms but also that among three or more neighbor atoms. The exchange integrals of three- and four-spin cyclic exchange interactions are larger than that of two-spin exchange interaction. Furthermore, the comparison between the theoretical and experimental studies shows that effects of the five- and six-spin exchange interactions are not negligible. Thus, in relation to the solid ^3He , the multiple-spin exchange (MSE) model on the triangular lattice has been extensively studied. Ground states and thermodynamic properties of the MSE model on the triangular lattice have been investigated using various methods, e.g., the mean-field approximation[1,2], the Monte Carlo simulations, the exact diagonalization, and the spin-wave theory[3,4]. In particular, the model has attracted attention owing to the existence of novel states such as the quantum spin liquid and the spin-nematic state and the effects of fluctuations on ordered phases with chirality. However, the study becomes difficult for the complexity of the system with the various interactions on the triangular lattice.

Recently, a new quantum spin liquid is experimentally observed in the solid ^3He layer. This layer is a monolayer ^3He adsorbed on graphite preplated with atomic layers of deuterium hydride. At low density of ^3He , it was suggested that there exists the quantum spin liquid with novel dependences of

the heat capacity and the magnetic susceptibility on temperature. In particular, the low-temperature heat capacity is proportional to $2/3$ power of temperature, which is an unprecedented behavior in the quantum spin system. The details of this experimental work are not yet clear, however, it is suggested that the solid ^3He layer is a honeycomb lattice.

We investigate the MSE model on the honeycomb lattice using numerical methods, which were applied in works of the MSE model on the triangular lattice. In the present project, we concentrate the classical MSE model with the two-spin interaction and the six-body ring exchange interaction. The ground state is investigated using the conjugate gradient method. In this method, we need to prepare many random spin states as the initial states because of avoidance of the trap to a metastable state. For large six-body ring exchange interactions, we found the classical ground state with the multi-sublattice structure. We also advance research on thermodynamic properties using the exchange Monte Carlo simulations.

References

- [1] C. Yasuda, Y. Uchihira, K. Kubo, J. Mag. Mag. Mater. **310**, 1285 (2007).
- [2] C. Yasuda, Y. Uchihira, S. Taira, K. Kubo, J. Phys. Soc. Jpn. **87** 104704 (2018).
- [3] C. Yasuda, D. Kinouchi, K. Kubo, J. Phys. Soc. Jpn. **75**, 104705 (2006).
- [4] S. Taira, C. Yasuda, T. Momoi, K. Kubo, J. Phys. Soc. Jpn. **88**, 014701 (2019).

Simulation Analysis of Collision of Two Filaments Driven by Protein Molecular Motors

Kazuo SASAKI

*Department of Applied Physics, Graduate School of Engineering, Tohoku University,
Sendai, 980-8579*

It is known that protein filaments driven by protein motors distributed on the glass surface form vortices when the density of filaments is high [1]. We studied this collective motion by computer simulation. In this year, we focused on the following two systems. One is the system consisting of two filaments and a lot of protein motors [2]. The other is the system in which the filaments were simplified as point particles.

In the first system, we studied the collision between two protein filaments, which is closely related to the emergence of the vortices. Four types of collisions were found experimentally [1]: parallel, anti-parallel, stop, and crossing; the probability of which type was observed strongly depended on the incident angle between two filaments. We simulated the collision of the two filaments for various incident angles. We have successfully reproduced the dependences of the probabilities on collision angle for parallel, anti-parallel, and stop of collision types.

In the second system, we simplified the model of protein filaments in accordance with the previous study [3]: The filaments were modeled as self-propelled particles; and they moved on a lattice. We performed Monte-Carlo

simulations of the particles for several particle densities and parameters of the model, and their collective motion was analyzed from the viewpoint of percolation theory [4]. A percolation transition was found to occur as the particle density was increased if the interaction between particles was weak, while a new phenomenon, the character of which is to be clarified, was observed in the case of strong interaction. Formation of vortices was not observed, probably due to the simplicity of the model.

The calculations were performed using the L4cpu in both the systems B and C. We used our custom-made program for the calculations.

References

- [1] Y. Sumino, *et al.*: *Nature* **483** (2012) 448.
- [2] Y. Ishigure and T. Nitta: *Langmuir* **30** (2014) 12089.
- [3] F. Peruani, T. Klaus, A. Deutsch, and A. Voss-Boehm: *Phys. Rev. Lett.* **106** (2011) 128101.
- [4] D. Stauffer and A. Aharony: *Introduction To Percolation Theory*, 2nd ed. (Taylor & Francis, London, 1992).

Elucidation of the coercivity mechanism by statistical physical approaches

Masamichi Nishino

*National Institute for Materials Science,
Tsukuba, Ibaraki 305-0044, Japan*

The neodymium (Nd) permanent magnet, $\text{Nd}_2\text{Fe}_{14}\text{B}$, which has strong coercivity, is an indispensable material in modern technologies, applied to information-storage devices, hybrid and electric vehicles, generators, etc. [1] This magnet has also another interesting feature. It exhibits a temperature-induced spin-reorientation (SR) transition. The spin dynamics on the SR transition in the magnet has not been clarified. The temperature dependence of the ferromagnetic resonance (FMR) frequency is an open question.

In the present work we studied the temperature dependence of the FMR frequency at zero external field. [2] The FMR spectrum $I(f)$ is calculated by the auto-correlation function of spins (power spectrum) for an atomistic model of the Nd magnet. The temperature dependence of the FMR frequency f_R is plotted by blue diamonds in Fig. 1.

We find that f_R exhibits a drastic change around T_R (SR transition temperature) and non monotonic temperature dependence. In particular, it is found that $f_R \sim 0$ below T_R .

This is totally different from the dependence of conventional magnets with a single uniaxial anisotropy energy, in which a monotonic decrease of the FMR frequency is observed. We clarified the mechanism for $f_R \sim 0$ below T_R . At zero temperature the state of the tilted spin alignment is stable, and the precession around the ground-state (GS) easy axis (parallel to the GS magnetic moments) does not occur. We also derived the formula for the FMR fre-

quency above T_R in connection to the temperature, magnetization along to the easy axis, and the fluctuation of the magnetization along to the hard axis (hard plane). We found that this formula is a good description for overall temperature region, and the last factor (fluctuation of transverse magnetization) in the formula is important for the qualitative nature of the FMR frequency.

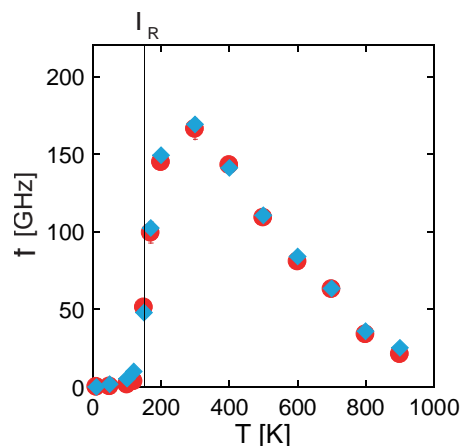


Figure 1: Temperature dependences of f_R (blue diamonds) for the atomistic Nd magnet model..

References

- [1] S. Hirosawa, M. Nishino, and S. Miyashita, *Adv. Nat. Sci: Nanosci. Nanotechnol.* **8** (2017) 013002.
- [2] M. Nishino, and S. Miyashita, *Phys. Rev. B* **100** (2019) 020403(R).

Transition in the memory effect of paste

Akio NAKAHARA

College of Science and Technology, Nihon University

7-24-1 Narashino-dai, Funabashi, Chiba 274-8501

A dense colloidal suspension, called a paste, remembers the direction of its motion, such as vibration and shear, and these memories in paste dominate the preferential direction for cracks to propagate. When a paste remembers vibration, cracks propagate in the direction perpendicular to the direction of the vibration, while, when a paste remembers shear, cracks propagate along the shear as is shown in Fig. 1 [1-2].

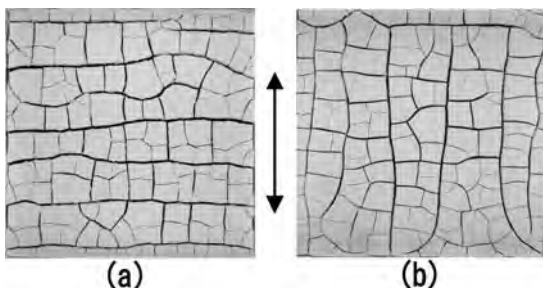


Fig. 1: Crack patterns induced by memory effect. (a) Memory of vibration (b) Memory of shear.

To explain the formation of striped crack pattern, we performed numerical simulations of shear motion of colloidal suspension using LAMMPS. Colloidal particles attract each other via Lennard-Jones potential and receives Stokes’s drag force from surrounding fluid. When we assume a simple shear as shown in Fig. 2, we obtain formation of elongated clusters along shear, as shown in Fig. 3, which dominates preferential direction for cracks to propagate. To

reproduce the transition from memory of shear to vibration, we find that we have to abandon the assumption of simple shear flow and solve more realistic flow motion under vibration.

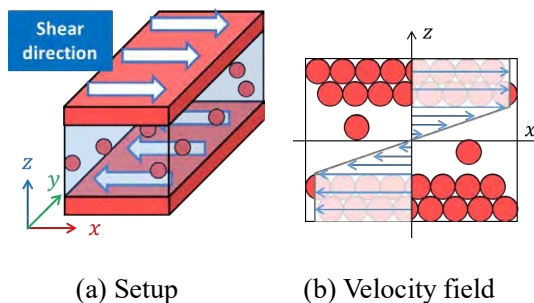


Fig. 2: Direction of a simple shear applied to a paste in numerical simulations.



Fig. 3: Elongated clusters along shear flow with its solid volume fraction of paste 3.3%.

References

[1] L. Goehring, A. Nakahara, T. Dutta, S. Kitsunezaki and S. Tarafdar, *Desiccation Cracks and their Patterns* (Wiley, 2015).
 [2] Japan patent JP 6565067, Material Mixing Method, A. Nakahara, Y. Matsuo, M. Ito and R. Yoneyama (2019)

Numerical Study of One Dimensional Frustrated Quantum Spin Systems

Kazuo HIDA

*Professor Emeritus, Division of Material Science,
Graduate School of Science and Engineering,
Saitama University, Saitama, Saitama 338-8570*

We investigate the ground-state phases of spin-1 alternating-bond diamond chains described by the following Hamiltonian [1]:

$$\begin{aligned} \mathcal{H} = & \sum_{l=1}^N \left[(1 + \delta) \mathbf{S}_l \boldsymbol{\tau}_l^{(1)} + (1 - \delta) \boldsymbol{\tau}_l^{(1)} \mathbf{S}_{l+1} \right. \\ & + (1 + \delta) \mathbf{S}_l \boldsymbol{\tau}_l^{(2)} + (1 - \delta) \boldsymbol{\tau}_l^{(2)} \mathbf{S}_{l+1} \\ & \left. + \lambda \boldsymbol{\tau}_l^{(1)} \boldsymbol{\tau}_l^{(2)} \right], \end{aligned} \quad (1)$$

where \mathbf{S}_l , $\boldsymbol{\tau}_l^{(1)}$, $\boldsymbol{\tau}_l^{(2)}$ are spin-1 operators. The lattice structure is depicted in Fig. 1.

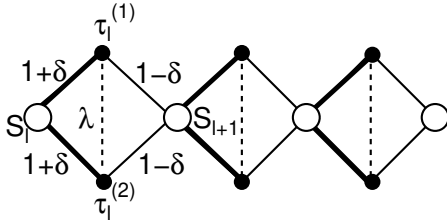


Figure 1: Structure of a spin-1 alternating-bond diamond chain. $S = \tau^{(1)} = \tau^{(2)} = 1$. The exchange parameters are denoted by λ , $1 + \delta$, and $1 - \delta$, where λ and δ control the strengths of frustration and bond alternation, respectively.

Each ground state consists of an array of spin clusters separated by singlet dimers owing to an infinite number of local conservation law,

$$\forall l \quad [\mathbf{T}_l^2, \mathcal{H}] = 0, \quad (\mathbf{T}_l \equiv \boldsymbol{\tau}_l^{(1)} + \boldsymbol{\tau}_l^{(2)}). \quad (2)$$

A pair of spins with $T_l = 0$ is a singlet dimer. For $\lambda > 2$, the state with $T_l = 2$ is not allowed.

Hence, each ground state consists of an array of n successive $T_l = 1$ pairs separated by singlet dimers. This phase is called a DC n phase. If no singlet dimers are present, the ground state is equivalent to that of a mixed spin chain,

$$\begin{aligned} \mathcal{H} = & \sum_{l=1}^N \left[(1 + \delta) \mathbf{S}_l \mathbf{T}_l + (1 - \delta) \mathbf{T}_l \mathbf{S}_{l+1} \right. \\ & \left. + \lambda (T_l (T_l + 1) - 4) \right] \quad (T_l = 1 \text{ or } 2) \end{aligned} \quad (3)$$

with infinite length. For strong frustration, we find a series of quantum phase transitions as in the case of alternating-bond mixed diamond chains with spins 1 and 1/2[2]. For intermediate frustration, we find the nonmagnetic Haldane or dimer phases according to whether the bond alternation is weak or strong. For weak frustration and weak bond alternation, we find the ferrimagnetic states with spontaneous magnetizations $m = 1/6$ ($F_{1/6}$ phase) and $1/3$ ($F_{1/3}$ phase) per site. The $F_{1/6}$ phase is accompanied by a spontaneous translational symmetry breakdown. This phase vanishes for strong bond alternation[1]. The presence of a narrow partial ferrimagnetic phase is suggested near the point $(\lambda, \delta) = (\lambda_c, \delta_c) \simeq (1.0832, 0.2598)$. The phase diagram determined by the numerical calculation for the Hamiltonian (3) using finite-size DMRG and infinite-size DMRG methods is shown in Fig. 2 except for the partial ferrimagnetic phase whose width is estimated to be so narrow that it is invisible in this scale.

References

- [1] K. Hida, J. Phys. Soc. Jpn. **89**, 024709 (2020)
 [2] K. Hida, K. Takano, and H. Suzuki, J. Phys. Soc. Jpn. **79**, 044702 (2010).

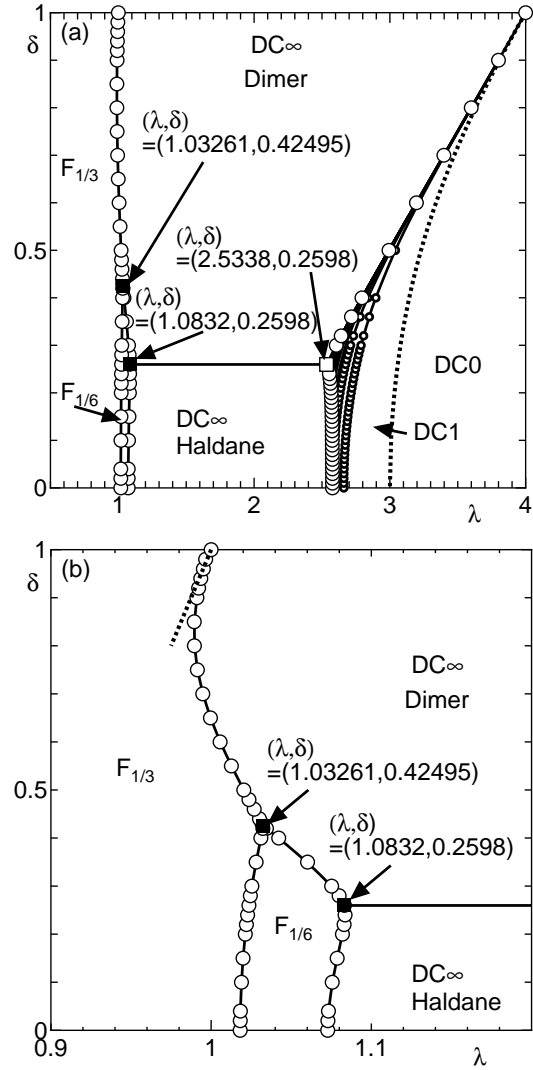


Figure 2: (a) Overall ground-state phase diagram. Small open circles are the phase boundaries between DCn and $DC(n-1)$ phases. For $n \geq 4$, these phase boundaries are only shown by solid lines to avoid complications. Other phase boundaries are shown by the large open circles and solid lines. The exact $DC0$ - $DC1$ phase boundary is shown by the thick dotted line. The open square is the accumulation point of infinite series of critical points at $\delta = \delta_c (\simeq 0.2598)$. The filled squares are triple points. (b) The enlarged phase diagram in the small λ region. The thick dotted line is the approximate relation for $\delta \simeq 1$. (from Ref. [1])

Construction of A New Method for Analysis of Crystallization Mechanism from Amorphous Precursor Using Molecular Dynamics Simulation Method and Unsupervised Machine Learning

Hiroki NADA

National Institute of Advanced Industrial Science and Technology (AIST),

16-1 Onogawa, Tsukuba, Ibaraki 305-8569

The control of crystallization from disordered systems, such as amorphous and melt, is essential to crystal engineering. However, our understanding of the mechanism of crystallization from disordered systems is still poor. This is because the structure of disordered systems can hardly be elucidated by experimental means.

Molecular dynamics (MD) are often helpful to elucidate the structure of disordered systems. A question is how to evaluate the time-evolution of the structure in disordered systems during crystallization properly.

Recently, a new methodology for evaluation of the structural similarity between different phases using the dimensional reduction, which has been developed as a method of unsupervised machine learning, is proposed [1]. The purpose of this project is to demonstrate that this methodology contributes to elucidating the mechanism of

crystallization from disordered systems in MD simulation studies.

An MD simulation of a supercooled Lennard-Jones melt was performed using ISSP supercomputer. The methodology was utilized to evaluate the structural similarity between the melt and its crystalline form, which was regarded as the geometrical similarity of the pair-distribution function between them, at each period during crystallization. An abrupt change of the structural similarity, which corresponded to crystal nucleation, was successfully detected. It is anticipated this methodology contributes to elucidation of the mechanism of crystallization, even for multicomponent systems, such as crystallization of calcium carbonate from its amorphous precursor.

References

[1] H. Nada: ACS Omega **3** (2018) 578.

The analysis of the dynamical response to the optical bistability

Tatsuhiko SHIRAI

*Green Computing Systems Research Organization, Waseda University
Waseda-chou, Shinjuku-ku, Tokyo 162-0042*

We have studied a dynamical response of an optical bistable system to a time-periodic driving field. The optical bistability has been found in cavity systems with an external driving field. As a function of laser intensity, there is a finite interval with bistability of a high transmission state (HTS) and a low transmission state (LTS). When the intensity of the input laser is time-periodically modulated beyond the bistable regime, the system shows a dynamical phase transition when the period of the modulation changes. At large period, the system stays in a different stable state depending on whether the laser intensity is increasing or decreasing. On the other hand, at small period, the system is kept in either the HTS or the LTS. Here, we show that the Floquet dissipative map is useful to characterize the dynamical phase transition. The Floquet dissipative map is given by a time-evolution operator of a quantum master equation, and it characterizes the limit cycle and the decay rate of the relaxation dynamics. We found that the decay rate exhibits qualitatively different system-size dependence before and after the phase transition, and it shows a finite-size scaling of spinodal phenomena around the transition point. This work was published to Physical Review A [1].

In this work, we develop a numerical algorithm to efficiently solve the dynamics governed by the quantum master equation consisting of many spins. To do it numerically, it is necessary to express the time evolution

operator L as a matrix. Naively, the number of elements in L increases exponentially with the number of spins N , which gives a strong restriction on N in the numerical simulation. However, we made use of the fact that the present model has a symmetry under exchange of spins. This symmetry reduces the number of non-zero elements in L to the order of N^3 [2, 3, 4]. We have used this property and performed simulations up to $N = 100$.

This research was supported by MEXT as the “Exploratory Challenge on Post-K Computer” project (Challenge of Basic Science-Exploring Extremes through Multi-Physics and Multi-Scale Simulations).

References

- [1] T. Shirai, S. Todo, and S. Miyashita: Phys. Rev. A **101** (2020) 013809.
- [2] S. Sarkar, and J. S. Satchell: EPL **3** (1987) 797.
- [3] M. Gegg, and M. Richter: New J. Phys **18** (2016) 043037.
- [4] T. Shirai, S. Todo, H. de Raedt, and S. Miyashita: Phys. Rev. A **98** (2018) 043802.

Theoretical study for superconductivity in superstructured strongly correlated materials with two-particle self-consistent approach

Kazutaka NISHIGUCHI

*Graduate School of Science, Technology, and Innovation, Kobe University
1-1 Rokkodai-cho, Nada-ku, Kobe 657-8501, Japan*

– *High- T_c superconductivity in multi-layer cuprates* –

We have theoretically studied superconductivity in multi-layer cuprate, which is a series of superstructured strongly correlated materials. Here 1–5-layer Hubbard model has been considered as an effective model for multi-layer cuprate superconductors. Then we have investigated the multi-layer superconductivity by solving the linearized Eliashberg equation for the superconducting gap function within the two-particle self-consistent (TPSC) approach. We have also developed the TPSC approach so as to treat the multi-layer systems. Many degrees of freedom arising from the multi-layer properties have been treated by the massive parallelization in ISSP Supercomputer Systems.

– *Possible superconductivity induced by spin-orbit coupling in carrier doped Sr_2IrO_4* –

Possible superconductivity in carrier-doped iridium oxide insulator Sr_2IrO_4 have studied by a weak-coupling approach[1]. We have treated t_{2g} 3-orbital Hubbard model with a large spin-orbit coupling (SOC) as an effective model for carrier-doped Sr_2IrO_4 . Numerically solving the linearized Eliashberg equation for the superconducting (SC) gap function with the random phase approximation (RPA), we have systematically examined both singlet and triplet SC gap functions with possible pairing symmetries and their parameter dependence. For the realistic SOC λ and Hund's coupling

J/U relevant to Sr_2IrO_4 , namely, for a large λ and small J/U region, we find that the intra-band antiferromagnetic (AF) pseudospin $j_{\text{eff}} = -l + s$ fluctuations favor a $d_{x^2-y^2}$ -wave pseudospin $j_{\text{eff}} = 1/2$ singlet pairing in the electron-doping (Figure 1). We also find that the $d_{x^2-y^2}$ -wave pairing is more stabilized with increasing the SOC and decreasing the Hund's coupling. Furthermore, we show for a small λ and large J/U region that an s_{\pm} -wave singlet pairing is favored in the hole-doped region (Figure 2). The origin of the s_{\pm} -wave pairing is due to the interband pair scattering arising from the intra-orbital AF spin s fluctuations. Although the possibility of a pseudospin triplet pairing is considered, we find it always unfavorable for all parameters studied here. We have also developed the multi-orbital and spin-dependent RPA so as to treat the multi-orbital systems with spin-orbit coupling. Many degrees of freedom arising from the multi-orbital and spin properties, namely, spin-orbit coupling, have been treated by the massive parallelization in ISSP Supercomputer Systems.

– *Electronic structures of doped $SrTiO_3$ as H_2 -generation semiconductor photocatalyst* –

We have performed the first-principles calculations based on the density functional theory to obtain electronic structures of doped $SrTiO_3$ as a H_2 -generation semiconductor photocatalyst. We have set the dopants to be a Rh and Sb atom and replaced the Ti sites with them in the $3 \times 3 \times 3$ $SrTiO_3$ supercell. The

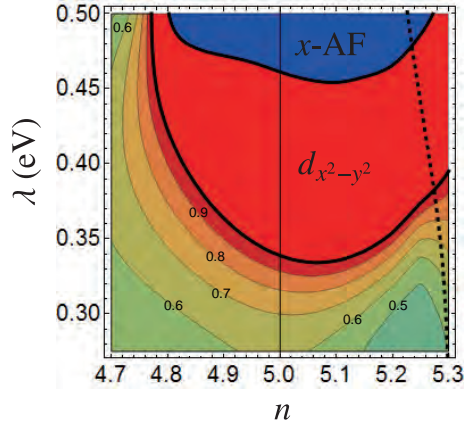


Figure 1: Contour plot of the largest eigenvalue of the linearized Eliashberg equation for the $d_{x^2-y^2}$ -wave pseudospin singlet pairing in the parameter space of the electron density n and the SOC λ for $U = 0.8$ eV, and $J/U = 0.05$. The red (blue) region represents the $d_{x^2-y^2}$ -wave pseudospin singlet SC (x -AF) phase.

O-vacancies have also been considered as the intrinsic defect in the realistic experimental situations. The first-principles calculations have been performed by using VASP (The Vienna Ab initio Simulation Package)[2], in which the hybrid functionals (HSE06) are adopted to reproduce the accurate band gap of SrTiO₃, and the massive band and k-point parallelization are used in ISSP Supercomputer Systems. The numerical calculations have shown from the density of states that the Rh-doping produces the impurity levels within the band gap as both donor and acceptor levels. We have also observed that the Sb-doping works as electron-doping and then removes the acceptors in the Rh+Sb-doping systems. In addition, the O-vacancies also works as electron-doping, which leads SrTiO₃ to the n-type semiconductors.

References

- [1] K. Nishiguchi, T. Shirakawa, H. Watanabe, R. Arita, and S. Yunoki: *J. Phys. Soc. Jpn.* **88** (2019) 094701.

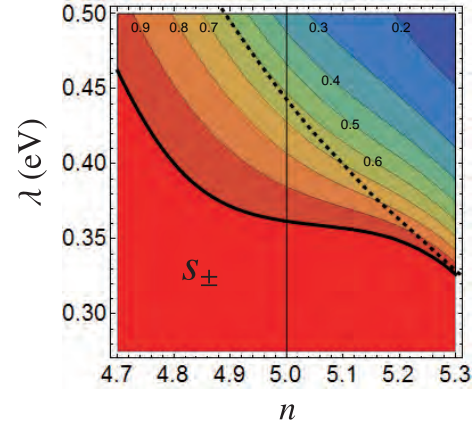


Figure 2: Contour plots of largest eigenvalue of the linearized Eliashberg equation for the s_{\pm} -wave pseudospin singlet pairing in the parameter space of n and λ for $U = 0.9$ eV and $J/U = 0.3$. The red region represents the s_{\pm} -wave pseudospin singlet SC phase.

- [2] VASP (The Vienna Ab initio Simulation Package): <https://www.vasp.at>

Study on Ising machines from a viewpoint of statistical mechanics

Shu TANAKA

*Green Computing Systems Research Organization, Waseda University
27 Wasedacho, Shinjuku, Tokyo 162-0042*

We have studied the performance of Ising machines from a viewpoint of statistical mechanics. The Ising machines have been attracting attention in recent years as a computer that has the potential to solve combinatorial optimization problems with high speed and accuracy. Very recently, quantum annealing machines, simulated annealing machines, and various other types of Ising machines have been developed. In order to draw out the potential of the Ising machine, it is more important to develop not only the hardware of the Ising machine but also the algorithm and software in accordance with the established mathematical framework. We conducted research on the following two topics on the basis of this trend.

(A) A guiding principle for embedding in simulated-annealing based Ising machines

When we use the Ising machine, the cost function and constraints of the combinatorial optimization problem are first expressed in the Hamiltonian of the Ising model or equivalent form. Herein, we refer to the Ising model as the logical Ising model. Next, we represent the logical Ising model on the limitations of the network of spins in an Ising machine. The operation is called embedding. In embedding algorithms, there are hyperparameters that should be adjusted to improve the computational performance, and how to adjust them is still unknown. In order to solve this question, we have succeeded in constructing a method of embedding algorithm based on the calculation

of the correlation function by the transfer matrix. The results suggest an improvement in the computational performance of simulated annealing-based Ising machines against typical existing embedding algorithms [1].

This work was done in collaboration with Dr. Tatsuhiko Shirai (Waseda University).

(B) The performance of black-box optimization using Ising machines from a viewpoint of statistical mechanical informatics

We have previously proposed a new method of black-box optimization using the Ising machine [2]. The results suggest that this method is superior to existing methods in the search for metamaterials with excellent thermal radiation characteristics. The theoretical basis for the superiority of this method is clarified from the perspective of statistical mechanical information.

This work was done in collaboration with Dr. Ryo Tamura (National Institute for Materials Science, The University of Tokyo).

References

- [1] T. Shirai, S. Tanaka, and N. Togawa, submitted. preprint version is available via https://www.dropbox.com/s/o8alkr8ch05ahtr/bare_jrnl_compsoc.pdf
- [2] K. Kitai, J. Guo, S. Ju, S. Tanaka, K. Tsuda, J. Shiomi, and R. Tamura: Phys. Rev. Research **2** (2020) 013319.

Nonequilibrium phase transition and slow dynamics in the dense hard sphere systems

Masaharu ISOBE

Nagoya Institute of Technology
Gokiso-cho, Showa-ku, Nagoya, 466-8555

The hard disk/sphere systems are one of the simplest models, which have been actively investigated in both equilibrium and non-equilibrium statistical physics. In this project, we investigated non-equilibrium phenomena in the hard disk/sphere model system with modern algorithms, especially for Event-Chain Monte Carlo(ECMC) [1] and Event-Driven Molecular Dynamics(EDMD) [2], where we propose the “Hybrid Scheme”, namely, ECMC for equilibration and EDMD for calculation of dynamical properties [3, 4].

Dynamic facilitation and direct evidence of void induced structural relaxations in glass formers:

On approaching glass transition, the viscosity of the supercooled liquid would be increased rapidly. It often behaves as solid with disorder structure within observation timescale. One of the challenging issues is to understand whether the essential properties of glass-forming materials are fundamentally thermodynamic or dynamic in origin. However, the microscopic origin of structural (so-called α) slow relaxation in deeply supercooled liquids at an atomic scale has remained elusive due to the limitation of both electron microscopy experiments and computer simulation. Although many theoretical models have been proposed and debated actively, one of a perspective that favors a dynamic origin is called Dynamic Facilitation (DF) theory [5, 6, 7]. DF theory was known to explain a wide range of empirically observed dynamical features of thermal super-

cooled liquids and glasses. The applicability of DF theory to athermal systems, i.e., systems of hard particles where the relevant control parameter is pressure rather than temperature, under “super-compressed” conditions was investigated by employing novel efficient algorithms [1, 2, 3]. The novel methodologies allowed studying in detail the true equilibrium dynamics of high-density systems, which is consistent with the predictions of DF theory. In such athermal molecular systems under “super-compressed” conditions — where what is facilitated is the ability of the constituent particles to structurally relax — giving rise to correlated and cooperative dynamics, in a manner predicted by theory [8].

In collaboration with the experimental group in Hong Kong, we resolve the coarse-grained trajectories obtained by colloidal experiments to confirm DF theory. The results undergo a transition from collective “creeping” to the string-like “hopping” motion on approaching the glass transition, where mobile of particles can be rearranged in string-like manners or compact geometries. Still, the compact ones decomposed into connected sequences of string-like hopping motion. Furthermore, such a string-like motion has an ultra-high returning hopping probability, which is proved to be the leading contributor to the kinetic arrest for slow relaxation. One of the paradoxical issues in DF theory is how a starter of string-like hopping has sufficient room for the first hop in highly dense packing fraction. A void as a

defect in the crystal structure can diffuse one after another on the crystal lattice positions in case of dense mono-disperse systems. However, in a dense amorphous structure, there are few voids with a size of particle diameter. Instead, we found the quasi-voids distributed within a few neighboring shells. The sufficient free volumes come from accumulated quasi-voids within a local area as a soft spot might induce the origin of string motion, where free volumes transport along to the string-like hopping motions. These hypotheses are now carefully investigated by molecular dynamics simulation, where the results would show direct evidence of the scenario based on DF theory [9].

[9] C.-T. Yip, M. Isobe et al.: in preparation.

References

- [1] E. P. Bernard, W. Krauth, and D. B. Wilson: *Phys. Rev. E* **80** (2009) 056704.
- [2] M. Isobe: *Int. J. Mod. Phys. C* **10** (1999) 1281.
- [3] M. Isobe: *Mol. Sim.* **42** (2016) 1317.
- [4] M. Isobe: “Advances in the Computational Sciences — Proceedings of the Symposium in Honor of Dr Berni Alder’s 90th Birthday”, edited by Eric Shwegerl, Brenda M. Rubenstein, and Stephen B. Libby, World Scientific, **Chapter 6** (2017) 83.
- [5] D. Chandler and J. P. Garrahan: *Annu. Rev. Phys. Chem.* **61** (2010) 191.
- [6] L. O. Hedges, R. L. Jack, J. P. Garrahan and D. Chandler: *Science* **323** (2009) 1309.
- [7] A. S. Keys, L. O. Hedges, J. P. Garrahan, S. C. Glotzer, and D. Chandler, *Phys. Rev. X*, **1** (2011) 021013.
- [8] M. Isobe, A. S. Keys, D. Chandler, and J. P. Garrahan: *Phys. Rev. Lett.* **117** (2016) 145701.

Glass phases induced by correlations

Chisa Hotta

*Department of Basic Science, University of Tokyo
Meguro-ku, Komaba, Tokyo 153-8902*

We studied the possibility of having a finite temperature glass phases driven by the correlation effect. Conventional spin glasses in realistic spatial dimensions, $d = 2, 3$ are realized in a series of Edwards-Anderson models with classical interactions between spins, J_{ij} , which distribute at around $\overline{J_{ij}} = 0$. There, the degree of disorder the only energy scale that competes with the thermal fluctuation. Even in such case the spin glass phases breaking the time reversal symmetry is allowed to exist at finite temperature only when $d \geq 3$. We studied two different types of models [1,2].

One is the classical vector spin Heisenberg model on a pyrochlore lattice with additional Ising-like lattice degrees of freedom, σ_i [1]; $\sigma_i = \pm 1$ indicate the displacement of the lattice site at each vertex, in and out of the tetrahedra, and the exchange interaction J_{σ_i, σ_j} between Heisenberg spins depends on the location of displacements of sites that the spins live on. Although there is no quenched randomness in the system, the elastic energy term $\propto \sigma_i \sigma_j$ and the spin exchange energy term $J_{\sigma_i, \sigma_j} \mathbf{S}_i \cdot \mathbf{S}_j$ are correlated with each other via J_{σ_i, σ_j} and work as dynamical randomness to each other. The two degrees of freedom finally undergo a simultaneous glass transition, which is detected by the scaling analysis on the auto-correlation functions[1].

The other one is the quantum transverse Ising model on a triangular lattice with very small quenched bond randomness[2]. This time, the transverse field first works on the spin degrees of freedom and drives the system to a KT phase, and successively to the clock-

phase, where the three-sublattice magnetic ordering appears. Introducing a very small bond randomness breaks the regular three-sublattice structure of the clock phase into pieces of domains, cooperatively with the emergent glass behavior of the spin degrees of freedom. The spins and lattices(bond order) work to each other as an emergent random fictitious field, which is the origin of the finite temperature spin glass in $d = 2$ system.

There are two common aspects between these two cases. First, the model has a finite spin coupling constant J , and energy scale representing the quenched disorder is either absent or very small, which is contradictory to the case of conventional spin glass whose energy is scaled by the quenched disorder. However, since these J 's are defined on frustrated lattices, the interactions themselves are not enough to stabilize any kind of magnetic orderings. This allows the emergent energy scale of disorder to dominate the low energy properties of the system. Second point is that the interplay of the two different species of degrees of freedom can stabilize the glass phase much more easily than had been considered before. Each of the degrees of freedom have a tendency to order and are on the verge of transition. The correlation with other degrees of freedom would not allow them to have a regular order, and both cooperatively goes into the glass phase.

References

- [1] K. Mitsumoto, C. Hotta, and H. Yoshino, Phys. Rev. Lett. **124**, 087201, (2020).
- [2] C. Hotta, K. Ueda and M. Imada, in preparation.

Magnetic structures of multiple-Q states in frustrated itinerant magnets

Takashi UCHIDA

Hokkaido University of Science

4-1, 7-15, Maeda, Teine-ku, Sapporo 006-8585

Recently, the magnetic structures of multiple-Q states have attracted attention since the topologically protected vortex-like magnetic structures such as magnetic skyrmions emerge as 3Q multiple helical spin density waves in the Dzyaloshinskii-Moriya (DM) interaction driven systems under magnetic field. In addition to these systems, the frustrated systems without the DM interaction have been found to reveal magnetic skyrmions [1, 2]. In the present work, we have applied the molecular spin dynamics (MSD) method [3] to the triangular-lattice single-band Hubbard model without the DM interaction to investigate the magnetic structures of multiple-Q states realized around the antiferromagnetic-ferromagnetic phase boundary.

The MSD method is based on the functional integral method with the static approximation for the spin fluctuation theories and the isothermal molecular dynamics method. The method allows us to find automatically the magnetic structures of a large system with thousands of atoms in a unit cell at finite temperatures.

In the numerical calculations the most time-consuming process is the magnetic force calculation at each time step, where the local electronic structures are calculated in real space by means of the recursion method. We have adopted the automatic parallel calculation scheme and found it to be effective in saving both computing time and CPU resources.

We have performed the magnetic structure calculations on the supercell with 20×20 triangular lattice, which is embedded in a large cluster consisting of 3×3 supercells, each of which are connected by the periodic boundary condition and are subject to the self-consistent uniform effective medium. Under zero magnetic field and the fixed value of the temperature $T/t = 0.0005$, we have changed the Coulomb interaction strength $U/t = 5 \sim 8$ and the electron number $n = 1.29 \sim 1.36$. The various multiple-Q states such as 2Q, 4Q, 2Q+1Q were found to be realized near the ferromagnetic boundary. Of these, the 2Q states are accompanied by small spontaneous magnetization. It is not clear, however, whether the calculated multiple-Q states are topologically protected structures or not. This is partly because that the main Q state is often accompanied by small satellite components, which make the whole magnetic structure complex. In order to make clear the magnetic structures of the multiple-Q states, the magnetic structure calculations with the site-dependent self-consistent effective medium are now in progress.

References

- [1] T. Okubo, S. Chung, and H. Kawamura: Phys. Rev. Lett. **108** (2012) 017206
- [2] Y. Takehashi, D. Kojima, T. Otonari, and H. Miyagi: J. Phys. Soc. Jpn. **87** (2018) 094712.
- [3] Y. Takehashi, S. Akbar, and N. Kimura: Phys. Rev. B **57** (1998) 8354.

Magnetization reversal process in classical spin systems

Taichi Hinokihara

Institute for Solid State Physics,

The University of Tokyo, Kashiwa-no-ha, Kashiwa, Chiba 277-8581

We studied and reveal the magnetization reversal process by using the classical spin Heisenberg model with the dipole-dipole interactions (DDI).

Recently, theoretical studies for the coercivity based on the atomistic-scale spin model are increasing due to the development of the first-principles calculations.

While these studies enable us to obtain material-dependent properties, the computational cost also increases to simulate such the model.

The problem becomes severe for studying the coercivity of magnet because it strongly depends on the long-range interaction, DDI [1,2].

In this project, we focused on the following two subjects: (i) develop efficient methods to simulate this system. (ii) propose a coarse-graining method to construct a macro spin model from the atomistic scale system obtained from the first-principles calculations.

For the subject (i), we recently developed the novel efficient method for the simulation of the dynamics of spins, called time quantified Monte Carlo with the stochastic cutoff method (TQMC+SCO).

As an example, the computational cost for the spin update is for the three-dimensional DDI system even when the system consists of the complicated lattice structure.

We analytically prove that the TQMC+SCO gives the same Fokker-Planck equation with the stochastic Landau-Lifshitz-Gilbert (s-LLG) equation, which is widely used for the simulation of spin dynamics.

Namely, the ensemble average of the magnetization trajectory calculated by the TQMC+SCO is the same as that by the s-LLG.

We also evaluated the validity of the present method by demonstrating the magnetization reversal process and comparing it to the result obtained by the s-LLG.

Figure 1 shows three magnetization-trajectories of the total magnetization along z-axis: s-LLG without DDI, s-LLG with DDI, and TQMC+SCO with DDI.

This simulation is performed in the $10 \times 10 \times 10$ spin system with exchange coupling J , the

anisotropy $K = 0.1J$, the DDI $D = 0.05J$, and the temperature $T = 0.2J$.

We performed the magnetic field $= 0.085J$ to drive the magnetization reversal process.

This figure clearly shows two results: (a) the DDI plays an essential role in the system with DDI, and (b) both s-LLG and TQMC+SCO gives the almost same magnetization trajectory.

We have submitted our paper, and it is now under review [3].

Besides, we recently found the other way of the bond-update process, which is suitable for the GPU calculation.

We are now preparing this paper.

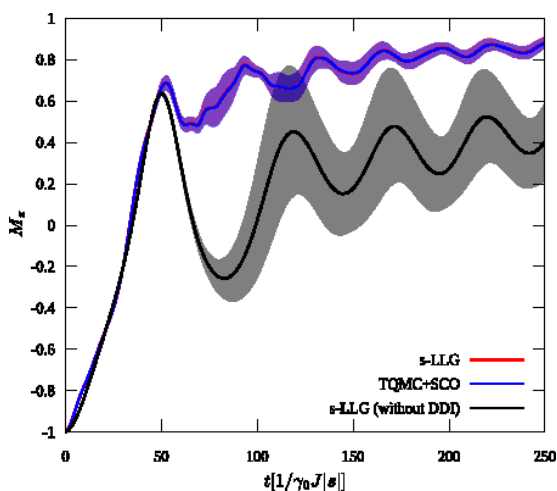


Fig. 1: Magnetization reversal process calculated by s-LLG without DDI (black), s-LLG with DDI (red), and TQMC+SCO with DDI (blue).

For the subject (ii), we constructed the macro-spin Hamiltonian from the atomistic-scale spin model of Nd₂Fe₁₄B in the following procedure. First, we construct the free-energy landscape for the single macro spin from the atomistic-scale spin model.

Each macro spin motion follows this landscape.

Next, the exchange coupling between the macro spins is selected to optimize the physical properties such as domain-all width.

We study the validity of our model by comparing it to other physical properties such as the total-magnetization and the susceptibility.

We are now preparing this paper.

References

- [1] Taichi Hinokihara, Masamichi Nishino, Yuta Toga, and Seiji Miyashita: Phys. Rev. B **97** 104427 (2018).
- [2] Yuta Toga, Masamichi Nihino, Seiji Miyashita, Takashi Miyake, and Akimasa Sakuma: Phys. Rev. B **98** 054418 (2018)
- [3] Taichi Hinokihara, Yuta Okuyama, Munetaka Sasaki, and Seiji Miyashita, arXiv: 1811.00237v2 (2019)

Quantum simulation for quantum many body systems using noisy-intermediate-scale quantum computers

Keisuke Fujii

Graduate School of Engineering Science,

Osaka University, 1-3 Machikaneyama, Toyonaka, Osaka 560-8531

Noisy Intermediate-Scale Quantum (NISQ) devices, or medium-scale quantum computers whose qubits are not fault-tolerant, are expected to be realized within a few years. As Google showed in 2019 [1], NISQ devices may be able to perform some tasks faster than the state-of-the-art classical computer. Such tasks should be sufficiently simple and suitable for a quantum computer, because of its incapability to remove errors in the computation process. Particularly, calculations for quantum many-body systems and quantum chemical systems are expected to be promising applications of NISQ devices.

In this project, we have developed a method to compute properties of quantum many-body systems, especially molecules in quantum chemistry, with NISQ devices and performed numerical simulations of them by using the ISSP supercomputer. Concretely, we invented a perturbative approach based on the variational quantum eigensolver (VQE) algorithm [2], which is a quantum-classical hybrid algorithm to compute the ground state energy of a system. One of the obstacles to utilize NISQ devices in quantum chemistry is that the number of available qubits is limited and often not enough

to describe molecular electronic wavefunctions quantitatively. Our method mitigates the problem by decomposing VQE calculation for a large system into a lot of VQE calculations for small systems. We applied this method to various molecules to verify accuracy and efficiency by numerically simulating the outputs of quantum circuits. The largest system we investigated was the Benzene molecule with the cc-pVDZ basis sets. We note that it is unfeasible to perform the simulation of the original VQE algorithm on classical computers as it requires 228 qubits for this system.

Our numerical simulation is based on the following programs: a fast quantum circuit simulator Qulacs [3] developed by our group; OpenFermion library [4] which can handle mapping fermionic Hamiltonians to qubit Hamiltonian; a quantum chemistry library PySCF [5]. Our code was highly parallelized using MPI, as our perturbative VQE method can be performed in an embarrassingly parallel fashion owing to its additive scheme.

K.F. would like to thank Wataru Mizukami for his help and collaboration throughout this project.

References

- [1] F. Arute et al., Nature **574**, 505-510 (2019).
- [2] A. Peruzzo et al., Nat. Commun. **5**, 4213 (2014).
- [3] Qulacs, <https://github.com/qulacs/qulacs>
- [4] J. McClean et al., arXiv:1710.07629
- [5] Q. Sun et al., WIREs Comput. Mol. Sci. **8**, e1340 (2017).

Study on Complex Systems by Generalized-Ensemble Algorithms

Takuya HAYASHI, Daiki MATSUBARA, and Yuko OKAMOTO

Department of Physics, Graduate School of Science, Nagoya University

Furo-cho, Chikusa-ku, Nagoya, Aichi 464-8602

We had two projects regarding generalized-ensemble algorithms applied to complex systems.

The density of states (DOS) is one of the most important physical values in statistical mechanics. Recently, we proposed a simulation protocol, REWL-MUCAREM [1], in order to obtain the DOS with high accuracy even in large systems by combining the *Replica-Exchange Wang-Landau* (REWL) method [2] and the *Multicanonical Replica-Exchange Method* (MUCAREM) [3]. The effectiveness of REWL-MUCAREM was demonstrated by using the 2-dimensional Ising model in [1].

We also applied the REWL-MUCAREM protocol to the ice Ih system in order to estimate the residual entropy with high accuracy. The residual entropy of ice has become one of good examples to test the efficiency of sampling algorithms. However, it seems that there is slight disagreement among the estimates by various calculation methods (see Fig.1). In this work, we give our latest estimate of the residual entropy by REWL-MUCAREM protocol.

Our latest estimate of residual entropy

per one water molecule [4] is

$$S = 0.815533 \pm 0.000066.$$

This estimate is in good agreement with the results of several other research groups. The results also imply that we need to develop a new simulation model in order to estimate the residual entropy with more accuracy.

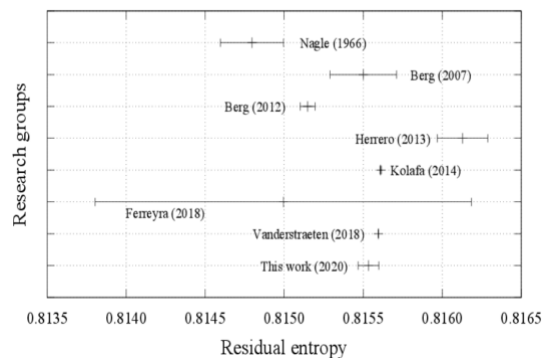


Figure 1: The estimates of residual entropy of ice Ih by several research groups.

In the second project, we have proposed the Grand Canonical Replica-Exchange Method (GCREM) [5], which is one of the multidimensional replica-exchange methods [6]. This method achieves a random walk in the temperature and chemical potential space, i.e., variables of grand canonical ensemble, in one simulation. In this study, we applied GCREM to the LJ potential system and succeeded in drawing a phase diagram

including gas-liquid first-order phase transition, second-order phase transition, and supercritical fluid (see Fig.2). We also calculated the critical point as $(T_c^*, \mu_c^*) = (1.18 \pm 0.01, -3.34 \pm 0.01)$. This is in good agreement with the results of previous study [7].

GCREM could sample various structural phases in one simulation run (see Fig.3): It was possible to sample the states of different numbers of particles such as gas, liquid, supercritical fluid, because the number of particles in the grand canonical ensemble varies. By using the structure that defines each of these states, structural analysis based on, e.g., radial distribution functions and cluster formation, became possible.

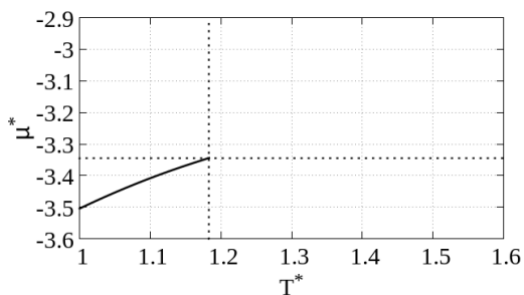


Figure 2: The phase diagram on reduced temperature and chemical potential space. The black line indicate 1st order phase transition points and the edge is the 2nd order phase transition point, i.e., critical point. Dotted lines indicate the critical temperature and chemical potential.

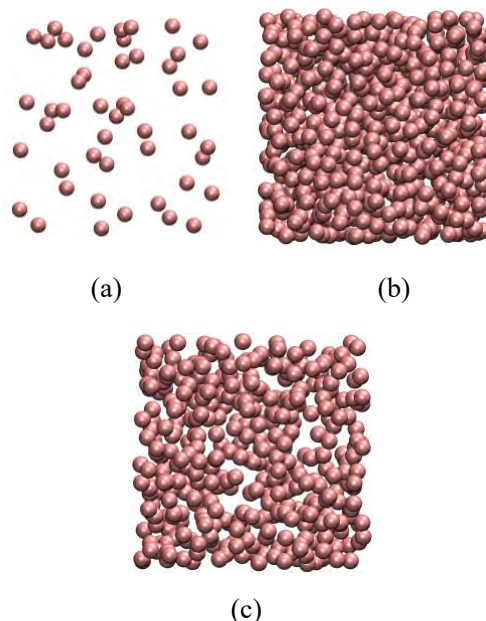


Figure 3: Snapshots of the LJ particle system obtained from a single GCREM run. Fig.3 (a) corresponds to Gas phase, (b) corresponds to Liquid phase, and (c) corresponds to supercritical phase.

References

- [1] T. Hayashi and Y. Okamoto, Phys. Rev. E. **100**, 043304 (2019).
- [2] T. Vogel, Y. W. Li, T. Wüst and D. P. Landau, Phys. Rev. Lett. **110**, 210603 (2013).
- [3] Y. Sugita and Y. Okamoto, Chem. Phys. Lett. **329**, 261 (2000).
- [4] T. Hayashi, C. Muguruma, and Y. Okamoto, in preparation.
- [5] D. Matsubara and Y. Okamoto, J. Chem. Phys. **152**, 194108 (2020).
- [6] Y. Sugita, A. Kitao, and Y. Okamoto, J. Chem. Phys. **113**, 6042–6051 (2000).
- [7] N. B. Wilding, Am. J. Phys. **69**, 1147-1155 (2001).

Development of a Coarse-Grained Force Field Designed with a Polar Water Model

Wataru Shinoda

*Department of Materials Chemistry, Nagoya University
Furo-cho, Chikusa-ku, Nagoya 464-8653*

Coarse-grained (CG) approaches have been adopted to investigate biological events relevant to the mesoscale. Many models have been proposed and used for various target systems, depending on the level of accuracy required in the CG description. One of the promising CG FFs, recently renamed as SPICA FF [1, 2, 3], accurately reproduces the experimental thermodynamic properties and structure (distribution function) obtained from AA-MD simulations using the CHARMM FF [4]. However, the ability of the SPICA FF to predict the morphology of highly charged molecular complexes in aqueous solution is still limited due to the lack of the polarity with the CG water model and to the assumption of a high (background) dielectric constant. To overcome this problem, we developed a CG FF, pSPICA, that is based on a polar CG water model in order to precisely describe the molecular events that are difficult to simulate using the SPICA FF with non-polar water in lipid membrane systems, such as water defects, membrane electroporation, and morphological changes in the charged lipid self-assemblies. We follow the parameter-optimization scheme used in the SPICA FF, namely, the parameters are optimized to reproduce several thermodynamic quantities measured experimentally [1, 2, 3].

In this study, we used the LAMMPS for CG-MD simulations, and the simulations were significantly accelerated by GPU. In the pSPICA FF, the polar CG water particle is composed of a pair of interacting sites, WO and WH

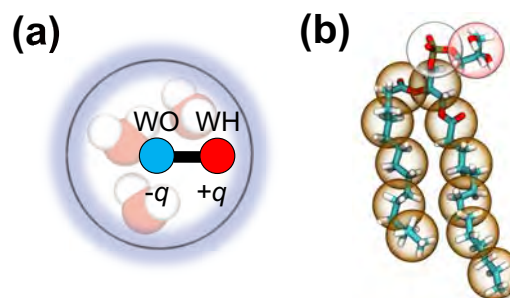


Figure 1: (a) Polar CG water, representing three water molecules, developed in this study. The blue bead, WO, has a van der Waals radius shown with a black circle. The red bead, WH, is connected to WO via a rigid bond and is positioned within the van der Waals radius of WO. (b) The CG mapping of a DMPG lipid. All-atom representation is given in stick and CG representation is given in transparent particle.

(Fig. 1 (a)), and was designed to represent three neighboring water molecules in aqueous solution. The two sites, WO and WH, are connected by a rigid bond, and have positive and negative partial charges, respectively. The choice of the CG sites for lipid molecules is the same as that in SPICA FF (Fig. 1). The parameters of the CG sites were systematically optimized to reproduce surface/interfacial tension, density, solvation or transfer free energy, as well as distribution functions obtained from all-atom molecular dynamics trajectory generated with the CHARMM FF, following the

scheme used in the SPICA FF. Lipid membranes simulated using the present CG FF demonstrate reasonable membrane area and thickness, elasticity, and line tension, which ensure that the simulated lipid membranes exhibit proper mesoscopic morphology. Using the pSPICA FF with the supercomputer at ISSP, we performed a large scale simulation to investigate the morphology of aggregates of the lipids dimyristoylphosphatidylglycerol (DMPG) in dilute solution. Thanks to the reasonable variation of line tension and elastic moduli of the lipid membranes depending on salt concentrations in the pSPICA FF, the morphological changes in the lipid aggregates showed good agreement with those observed in experiments (Fig. 2 (a)). CG-MD simulations of the membrane electroporation processes of flat lipid bilayers and vesicles were successfully performed by the pSPICA FF. A water channel bridging the lipid bilayer was formed spontaneously in the presence of an electric field generated by an imbalanced NaCl salt distribution, allowing ion transport across the lipid bilayer (Fig. 2 (b)). The results were similar to the pore opening process observed using AA-MD. Thus, the new CG FF enabled us to quantitatively investigate biological events, especially those involving water strings and defects in lipid membranes and ionic molecules.

References

- [1] W. Shinoda, R. DeVane, and M. L. Klein: *Mol. Simul.* **33** (2007) 27.
- [2] W. Shinoda, R. DeVane, and M. L. Klein: *J. Phys. Chem. B* **114** (2010) 6836.
- [3] S. Seo, W. Shinoda: *J. Chem. Theory Comput.* **15** (2019) 762.
- [4] J. B. Klauda, R. M. Venable, J. A. Freites, J. W. O' Connor, D. J. Tobias, C. Mondragon-Ramirez, I. Vorobyov, A. D. MacKerell, R. W. Pastor: *J. Chem. Phys. B* **114** (2010) 7830.

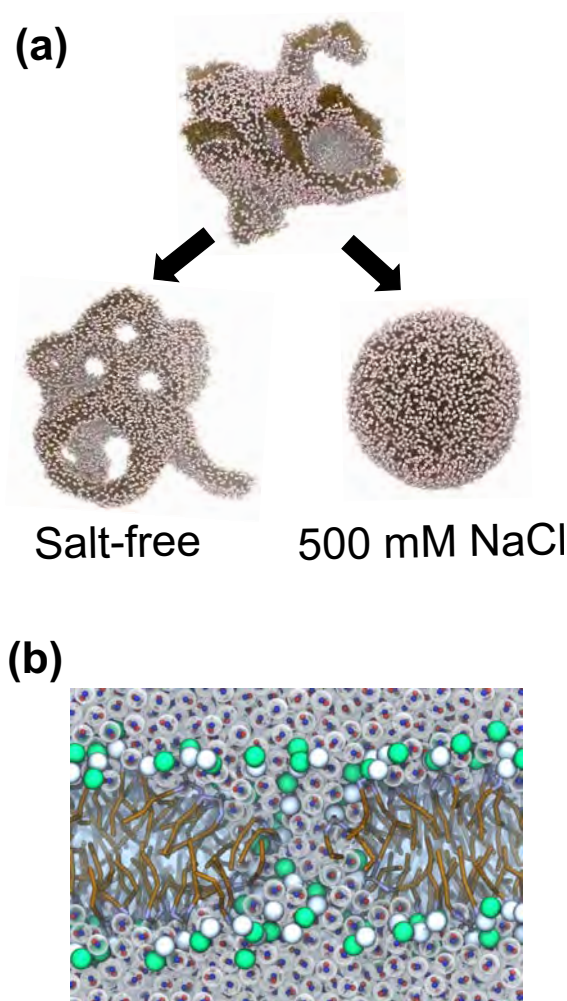


Figure 2: (a) Snapshots of the initial aggregate composed of 5000 DMPG units and the finally obtained aggregate in salt-free and 500 mM NaCl solution. (b) Snapshot of the electroporation process found in the simulation for a planar membrane system.

Screening of Substitutable Element in Rare-earth Inter-metallic Compounds

Riki KOBAYASHI

*Department of Physics and Earth Sciences, Faculty of Science
University of the Ryukyus, Nakagami, Okinawa 903-0213, Japan*

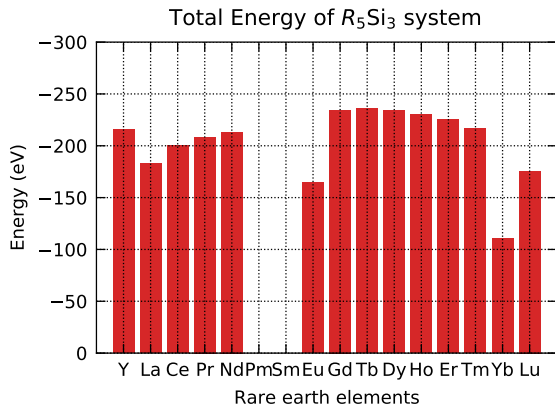


Figure 1: Total energy of R_5Si_3 ($R = \text{REEs}$) system after structure relaxation.

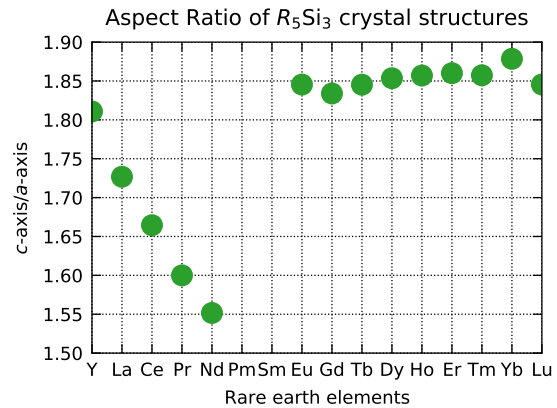


Figure 2: Aspect ratio of R_5Si_3 ($R = \text{REEs}$) crystal structures.

Recently, we have succeeded in growing single crystals of Ce_5Si_3 and Ce_5Ga_2Ge with the tetragonal Cr_5B_3 -type crystal structure and found that the Cr2-sites in the Cr_5B_3 -type crystal structure form the Shastry-Sutherland-Tetrahedral-Lattice (SSTL). SSTL has four geometrically frustrated two-dimensional layers in a unit cell, called orthogonal-dimer systems, and the ground state of Ce2-sites in Ce_5Si_3 and Ce_5Ga_2Ge is a spin-dimer due to this geometric frustration. There are no other Ce compounds showing spin-dimers at the ground state other than Ce_5Si_3 and Ce_5Ga_2Ge , which are important targets for the study of heavy fermion systems with geometric frustration. However, few rare-earth compounds with the Cr_5B_3 -type crystal structure have been reported, and this lack of targets is a bottle-

neck for the above research. In this study, the structural stability of R_5Si_3 ($R = \text{Rare earth elements}$) is investigated by comparing the total energy of R_5Si_3 obtained by first-principles calculations to find new Cr_5B_3 -type materials.

The calculations were performed using the Vienna Ab-initio Simulation Package (VASP), which is capable of generalized gradient density approximation (GGA), and the K-points and energy cut-off values were based on the $8 \times 8 \times 4$ mesh and VASP recommendations, respectively[1]. In this study, both quasi-Newtonian and conjugate gradient algorithms are used to calculate the structural relaxation, and it is confirmed that there is no significant difference in the results between the two algorithms.

Figure 1 shows the total energy of R_5Si_3

from first-principles calculations. Pm_5Si_3 and Sm_5Si_3 were excluded from the graphs because Pm is a radioactive isotope with a short half-life, and Sm_5Si_3 did not converge in the SCF calculation. The present calculations revealed that the total energy is lower in the compounds containing Eu and Yb elements than in the others, and it may be difficult to obtain a Cr_5B_3 -type crystal structure in these compounds.

Figure 2 shows the aspect ratio of the lattice parameter of $R_5\text{Si}_3$. Systematic changes in the aspect ratios were observed for compounds containing light REE from Y to Nd. This indicates that a specific axis of the unit cell may shrink due to lanthanide contraction.

References

- [1] G. Kresse and J. Furthmuller, Phys. Rev. B **54**, 11 169 (1996).